NASA Technical Memorandum 4238

Candidate Control Design Metrics for an Agile Fighter

Lorman A. Murphy, Melvin L. Bailey,
and Aaron J. Ostroff

MARCH 1991

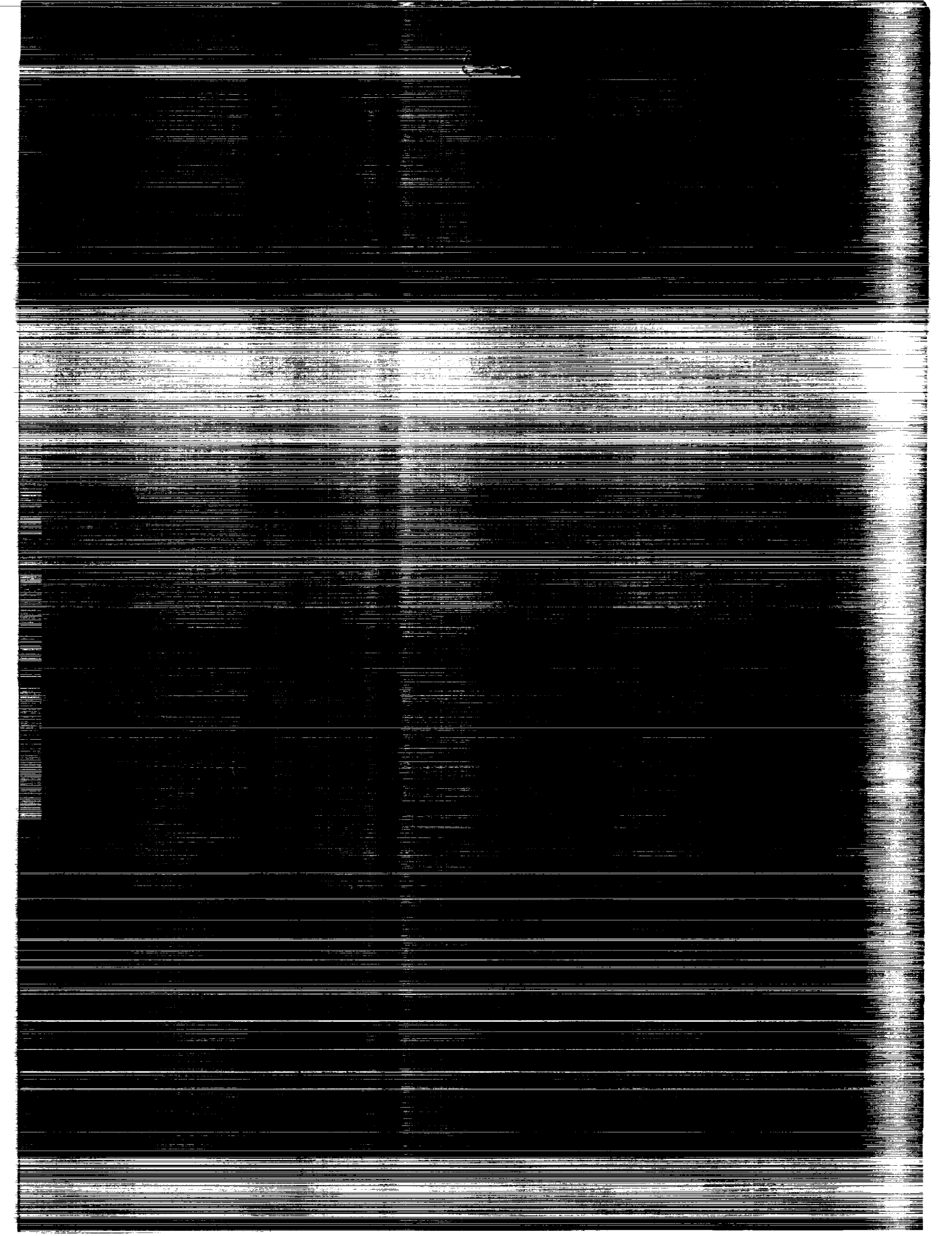

NASA Technical Memorandum 4238

Candidate Control Design Metrics for an Agile Fighter

Patrick C. Murphy
Langley Research Center
Hampton, Virginia

Melvin L. Bailey
Lockheed Engineering & Sciences Company
Hampton, Virginia

Aaron J. Ostroff
Langley Research Center
Hampton, Virginia

National Aeronautics and
Space Administration
Office of Management
Scientific and Technical
Information Division

1991

Summary

Success in fighter combat of the future will require increased capabilities from aircraft technology. These advanced capabilities, in the form of superagility and supermaneuverability, will require special design techniques that translate advanced air combat maneuvering requirements into design criteria. Control design metrics can provide some of these techniques for the control designer.

This study presents an overview of control design metrics and specifically investigates metrics for advanced fighter agility. The objectives of various agility metric users, such as airframe designers and pilots, are differentiated from the objectives of the control designer. With the use of an advanced fighter model, metric values are documented for a portion of the flight envelope through piloted simulation. These metric values provide a baseline against which future control system improvements can be compared and against which a control design methodology can be developed. For this study, agility is analyzed independently of flying qualities to separate pilot-in-the-loop effects from aircraft and flight control system effects. Separating these effects should provide designers with a "building block" capability through which trade-offs between agility and flying qualities can be more easily made.

Agility is measured for axial, pitch, and roll axes. Axial metrics highlight acceleration and deceleration capabilities under different flight loads and include specific excess power measurements to characterize energy maneuverability. Pitch metrics apply to both body-axis and wind-axis pitch rates and accelerations. Included in body-axis pitch metrics are nose pointing metrics that highlight displacement capabilities between the nose and the velocity vector. Roll metrics (or torsional metrics) focus on rotational capability about the wind axis. Only wind-axis (coordinated) rolls are considered since relatively large angles of attack are likely for an agile fighter. At these angles of attack, uncoordinated rolls may cause loss of control or unacceptable flight loads.

Introduction

Success in the fighter combat environment of the future will certainly require increased capabilities from aircraft technology. Future fighters may have to operate in environments where having enhanced maneuverability and controllability, throughout a greatly expanded flight envelope, is a requirement or is at least a significant advantage. This enhanced capability is referred to as superagility. Designing for this capability represents a serious challenge to the flight controls engineer. Fighter airframe designs and their control systems are the result of many opposing trade-offs; for example, high-speed efficiency requires a very low drag profile and low-speed maneuverability is enhanced by straight, thick wings and large control effectors. Agility and low observability may create other design conflicts. With the development of agile-fighter technology, future designers may make much more advantageous trade-offs. These advanced capabilities will require specialized design techniques that translate advanced air combat maneuvering requirements into design criteria. Agility metrics provide a measure of merit that can be an integral part of these specialized design techniques. Control design metrics (CDM's) provide this measure of merit specifically for the flight controls engineer.

The concept of a design metric is not new; it is simply a measure of merit (usually quantitative) for evaluating design trade-offs or system performance. Common examples of metrics can be found in MIL-STD-1797A (ref. 1); these provide guidelines for achieving good flying qualities. One example metric is roll-mode time constant, which is recommended to be less than 1 sec for high performance fighters. This specification provides level 1 flying qualities. The notable characteristic of these metrics is that they translate important operational requirements into engineering quantities that can be used by a control designer. These engineering quantities provide guidance to the designer as the system is changed and overall performance is optimized.

From a control design point of view, the fighter agility area has very few metrics specifically defined for control designers. This is in contrast to the flying qualities area, which has the majority of its metrics in a form directly usable by control designers. Although many agility metrics exist (see refs. 2 to 9), their primary purpose is for assessing combat capability and therefore they do not readily lend themselves to being used in the control design process. Metrics for combat capability are often given in terms that reflect a contest, such as kill ratio. Clearly, measures of merit such as kill ratio are not helpful in determining the size of a feedback gain. As indicated in reference 3, current studies by combat analysts have emphasized the benefits of high-transient-response capability without sufficient consideration for flying qualities. And, conversely, flying qualities analysts have always assumed good transient response, as defined in reference 1, provided good combat capability. The net result is that a very limited set of agility metrics can be used directly by control designers. The contribution of this study is to begin development of CDM's for agility and to establish a baseline set of metric values (of a simulation aircraft) as a bench-

mark for future comparison. Future comparisons of metric values produced by control system variations would allow determination of the most sensitive metrics and how best to use them.

These CDM's provide the following two capabilities: (1) quantitative measures of specific system capabilities that translate desirable operational agility characteristics into useful engineering terms for control design and (2) guides for an optimization process that enhances the control system contribution to a particular system capability. In the CDM methodology, this optimization process occurs in either an active or a passive form. A passive metric is computed or measured after the design is specified or tested. This is the conventional form of metrics, and peak rate values are typical examples of this form. Active forms are continuous functions of system dynamics or continuous time functions of states and controls and can be used directly as parameters in an optimization process. Active metrics are usually summarized in this report by presenting peak values and time to peak values (passive form) even though the utility of the active metrics is in their complete description of a specified transient response. It is more convenient and efficient to summarize the metric values for many different flight conditions in passive form.

Associated with the CDM's are benchmark maneuvers (BKM's) that specify techniques and flight conditions for testing (in flight or simulation) of a particular capability. Each CDM and BKM pair characterizes a particular desired capability. In some cases, the BKM may require the subject aircraft to perform outside its practical flight envelope. This is done to anticipate future comparisons with more agile and more maneuverable (high-angle-of-attack agility) versions of the aircraft under study.

The payoffs for a well-constructed set of CDM's occur in design, production, and operations. In the design phase, guidelines are established for incorporating specific capabilities such as agility. Certain capabilities can be optimized relative to other requirements; for example, multiply redundant control effectors can be optimally blended for effective nose pointing or loaded roll capability. The result is efficient, integrated designs. In the production phase, desired capabilities are achieved with the prototype and this gives lower final product cost. In operational phases, agile performance with good flying qualities is obtained. This should ultimately result in higher kill ratios.

This study is a first step toward developing CDM methodology. The philosophy for this development has been to collect a set of potential metrics that can be evaluated for their utility in the control design process. Not all the metrics and BKM's considered will survive as useful CDM's. Follow-on studies will show the advantages and disadvantages of each as applied to fighter control design problems. Because of strong interest in agility by the fighter design community and a practical need to limit the scope for the first step, only agility metrics are considered in this study. However, as designs are synthesized in follow-on studies, flying qualities requirements will be incorporated to ensure pilot acceptability. This study provides values of candidate agility metrics for a modern fighter. The values are determined for only a portion of the flight envelope. Later studies will be required to extend the scope of CDM's to include advanced aircraft with high-angle-of-attack capability.

Symbols and Abbreviations

C_L	lift coefficient
F_{ped}	pedal force, lbf
g	acceleration due to gravity, 32.174 ft/sec^2
h	altitude, ft
K	transfer function gain
M	Mach number
m	functional agility parameter, $m = K/\tau$
N_y	lateral acceleration, positive toward right wing, g units
N_z	normal acceleration, positive down, g units
$N_{z,w}$	wind-axis normal acceleration, positive down, g units
PN	loaded roll metric, product of p_w and $N_{z,w}$, deg-g units/sec
P_s	specific excess power, ft/sec
p	body-axis roll rate, deg/sec
p_w	wind-axis roll rate, deg/sec
q	body-axis pitch rate, deg/sec
q_w	wind-axis pitch rate, deg/sec
r	body-axis yaw rate, deg/sec
S	wing area, ft^2
s	Laplace independent variable
T	thrust, lb
t	time, sec
V	total velocity, ft/sec

W	weight, lb
α	angle of attack, deg
β	sideslip angle, deg
γ	flight path angle, deg
$\dot{\gamma}$	flight path angular rate, deg/sec
Δ	incremental value
$\Delta\delta_s$	differential stabilator deflection, in.
δ_a	aileron deflection, in.
δ_{ap}	pilot lateral stick deflection, in.
δ_f	trailing-edge flap deflection, in.
δ_n	leading-edge flap deflection, in.
δ_r	rudder deflection, in.
δ_s	stabilator deflection, in.
δ_{sp}	pilot longitudinal stick deflection, in.
δt	metric of time to achieve, sec
δt_{pk}	metric of time to peak, sec
θ	pitch angle, deg
τ	transfer function time constant, sec
τ_d	transfer function time-delay constant, sec
ϕ	roll angle, deg
$\dot{\psi}$	body-axis turn rate, deg/sec
$\dot{\psi}_w$	wind-axis turn rate, deg/sec

Subscripts:

c	corner
max	maximum
w	wind axis
x	along longitudinal axis
y	along lateral axis
z	along vertical axis

Abbreviations:

AB	afterburner
AFU	auto flap-up mode
accel	acceleration maneuver
decel	deceleration maneuver
accel-decel	acceleration and deceleration maneuver
BKM	benchmark maneuver
CAS	control augmentation system
CDM	control design metric
DMS	Differential Maneuvering Simulator
EM	energy maneuverability
FA	functional agility
FLXTRM	computer program for solving equations of motion
PLA	power lever angle
POR	power onset rate, ft/sec^2
RSRI	rolling-surfaces-to-rudder interconnection
SB	speed brake
TF	transfer function

A dot over a symbol indicates derivative with respect to time. A bar over a symbol indicates time average of variable.

Control Design Metrics

Definitions

For convenience, control design metrics (CDM's) are separated into five categories. The categories are not absolute boundaries. Some metrics may logically fall into more than one area; however, the discussion is more tractable with this breakdown. The first category of CDM's is agility. Agility metrics characterize the capability of the aircraft flight control system to change aircraft states rapidly and precisely. Since agility is the focus of this study, it is discussed more thoroughly in the following paragraphs. The second category is made up of flying qualities metrics. These metrics identify requirements for the control system that reflect the fact that a human must be able to fly the aircraft and perform a mission effectively. The third category is control power metrics. These metrics represent the limits or desirable levels of capability for specific control effectors or combinations of effectors. The fourth category is a large group including many conventional control metrics. This group contains typical control design specifications such as time to rise, bandwidth, robustness tests, and gain and phase margins. The fifth category is pilot models. This category has been studied with respect to flying qualities with some success. Current efforts at NASA Langley Research Center are aimed at "cooperative control design" (ref. 10), wherein pilot models are used in the control design process.

Agility is not a new concept in fighter design (ref. 4). However, a new effort is being made in

the research community to improve agile capabilities of fighters (refs. 2 to 9). Although some controversy exists over the precise definition of agility, a very broad definition is used in this study to allow unrestricted development. Agility is defined as a combination of maneuverability and controllability allowing rapid and precise changes of state. Maneuverability refers to an ability to rapidly change states and is usually characterized by rates and accelerations. This aspect of agility is usually divided into transient and functional agility, with transient agility applying to short-term responses such as peak accelerations and functional agility applying to somewhat long-term responses such as peak angular rates (ref. 11). Controllability, for this study, implies the existence of a control sequence that can regulate aircraft states. This is a conventional control theory definition and is intentionally different from a commonly used, broader concept that includes the pilot's ability to fly the aircraft with good Cooper-Harper ratings. Flying qualities metrics apply for the pilot-in-the-loop case and should provide limits on the aircraft agility. This differentiation produces metrics that allow separate treatment of agility and flying qualities, and thus control designers have a building block methodology that facilitates making design trade-offs.

A logical breakdown of agility is into the axial, pitch, and roll degrees of freedom. These are the primary degrees of freedom controlled by the pilot using throttle, longitudinal stick, and lateral stick, respectively. The pitch axis requires further breakdown to separate fdjust or pointing the nose relative to the flight path. For analysis it is convenient to further subdivide pitch maneuvers for bending of the flight path into longitudinal and lateral components corresponding to the vertical and horizontal planes of maneuvering. Using metrics for vertical pitch maneuvers highlights longitudinal system dynamics and using horizontal pitch maneuvers (i.e., turning) includes lateral-directional system dynamics. Separate consideration of these dynamics does not limit the analysis, even though bending of the flight path can occur in any plane. For convenience, pitch agility is divided into pitching motions in the vertical plane, turning motions in the horizontal plane, and pointing motion where the nose is displaced relative to the velocity vector. With this breakdown structure, five functional areas of agility are defined for this study: (1) axial, (2) pitch (vertical-plane maneuvers), (3) turning (horizontal-plane maneuvers), (4) nose pointing, and (5) roll (or torsion). Figure 1 gives a breakdown of the categories of CDM down to the five functional areas of agility discussed in this report.

The first area of agility considered in this study is axial agility. These metrics characterize the aircraft system ability to accelerate or decelerate under various flight conditions. Energy maneuverability relations are often used in connection with these metrics and have been a principal tool for comparing aircraft for the past 10 to 15 years (ref. 9). The second area considered is vertical-plane, flight path bending maneuvers, which are discussed under the heading *Pitch Agility*. The airframe and flight control system capability to pitch both the nose and the velocity vector up and down under various flight conditions can have significant impact on shot opportunities. The capability to pitch down may also have significant impact on axial agility, as indicated by reference 3. Although emphasis is usually placed on nose pitch capability, in this study both body-axis and wind-axis maneuvering are considered for pitch agility. The third area of interest is turning (horizontal-plane maneuvers). This area is considered separately because of the fundamental importance it has to the fighter aircraft mission and because it is complementary to the vertical-plane pitch area. Again, special attention is given to differentiate between turning the velocity vector and turning the nose. Closely related to the pitch agility area is the fourth area, nose pointing agility. Nose pointing agility can be measured in terms of the speed and precision of displacing the nose relative to the velocity vector (i.e., α and β control). For this study, only α control is considered since the test aircraft was not designed to perform large sideslip maneuvers. The fifth area of agility is referred to as torsional, or roll, agility. This area characterizes the aircraft capability to rotate the lift vector about the flight path while under various flight loads. Rotations about the body longitudinal axis are not really of interest since this type of maneuvering is very limited and usually undesirable. At high angles of attack, body-axis rotations can produce large β because of kinematic coupling.

Associated with each CDM is a benchmark maneuver (BKM). The BKM's are generic flight tasks, such as loaded rolls, that characterize a particular required capability. They are specifically designed to aid the flight controls engineer in assessing airframe and flight control system performance. Consequently, they may only be indirectly useful in assessing overall combat capability. The idea behind a BKM is to dissect the complex maneuvers required in combat into more basic, structured maneuvers that place specific demands on the aircraft and flight control system. For example, a split-S is a basic fighter maneuver composed of a half-roll and a half-loop. The split-S would not be a good BKM; however, a half-roll or a half-loop might be a useful BKM. The

BKM (along with matching CDM) must translate the particular required capability of the fighter into demands on the flight control system and it must be in terms that the flight controls engineer can use.

The CDM methodology is applied through one of two approaches that depend on the type of metric being utilized; these approaches are referred to as active and passive. For those metrics that require simulation for evaluation and therefore can only be used after a design has been created and simulated, the approach is referred to as passive. In this case, the designer must manually adjust design parameters after a simulation has shown undesirable metric values. The passive design approach is the traditional approach used in most cases today. The active approach, on the other hand, requires metrics that can be used directly in the design optimization calculations. The type of metrics used must be either functions of system dynamics or continuous functions of time, such as functions of system states and controls. In the active design process, metrics provide functions for optimization that reflect desired characteristics to be incorporated into the design. Eigenvalue specifications, which characterize desired system dynamics, are one form of active metrics.

Design Perspective

The CDM's and BKM's are best understood by considering the design perspective of the flight controls engineer. There exists a hierarchy, shown as a pyramid in figure 2, that explains how the requirements of the fighter mission translate into the specifications for the control system. At the top of the pyramid are the mission requirements. This is the highest level where strategists consider whether an intercept or ground attack mission is required. To perform the intercept mission, for example, certain tasks are required for the fighters. One task that might be given to an intercept flight of three is to find the best weapons solution when two enemy fighters appear 90° off the nose, closing fast. At this point, continuing down the hierarchy, certain specific maneuvers are required to accomplish this task. These maneuvers are basic fighter maneuvers (ref. 12) such as high-speed yo-yo's and split-S's. Finally, at the bottom of the pyramid are the base capabilities from which all maneuvers are made. Any combat maneuver is created by a fighter pilot commanding various combinations of acceleration, pitching, rolling, or turning. These base capabilities are defined by state and control transfer functions that control designers can significantly modify. At this base level, agile performance is determined for any level above.

The challenge for metric designers is to translate agile performance as defined at task and maneuver levels of the pyramid into control specifications for the base capabilities. Control systems are goal-oriented systems, and these goals need to be defined in terms that the control designer can implement. Control design metrics are a device for translating goals defined at levels high up the pyramid into control system specifications.

Each level of the pyramid has metrics that are best suited for defining goals and measuring success at that particular level. Differentiating metric types for each level will clarify the purpose and application of control design metrics. At the top of the hierarchical pyramid metrics are tied to quantities such as kill ratio. At the tasks and maneuvers levels, "contest" or "combat" metrics are best. These metrics characterize the effectiveness of a fighter by quantifying the advantage one fighter can attain over another. For example, one contest metric that has been recommended is pointing margin (ref. 6). This is the angular advantage of one fighter over another after one achieves a weapon solution. At the base capabilities level, where the control designer works, overall system goals such as increased pointing margin must be translated into control design metrics. In light of the objectives in combat and the constraints of the dynamic system, greater pointing margin may translate into specific bandwidth requirements for wind-axis pitch rate and angle-of-attack control (i.e., pointing on demand by the pilot). Clearly, each level of the pyramid has metrics that are best suited to that level. Pointing margin is effective at the tasks level; however, it cannot be used directly at the base capabilities level. Contest metrics are optimal for comparing combat capability of fighters, and control design metrics are best for designing control systems.

Description of Simulation Aircraft

Aircraft

The simulation aircraft is a high-performance, single-place fighter-attack airplane powered by two turbofan engines. Each engine provides 10 700 lb of thrust at sea level with military power and 16 000 lb of thrust with maximum afterburner. Gross takeoff weight is 45 000 lb; the weight used during simulation was 32 366 lb, which produced a maximum thrust-to-weight ratio close to 1.0 at sea level and 0.5 at 15 000 ft. The aircraft features a variable camber wing through scheduled leading- and trailing-edge flaps. Leading-edge extensions are mounted on each side of the fuselage from the wing roots to just forward of the canopy. The twin vertical stabilizers are angled outboard 20° from the vertical. Ailerons, rudders, differential stabilators, and leading- and trailing-edge flaps are hydraulically actuated. A

speed brake is mounted on the top side of the aft fuselage between the vertical stabilizers. Aircraft dimensions for length, span, and height are 56 ft, 37.5 ft, and 15.25 ft, respectively. Wing area is 400 ft^2.

The aircraft simulation is a real-time simulation in the Langley Differential Maneuvering Simulator. The simulation is based on the data in references 13 and 14.

Control Augmentation System

This section presents a summary of the fly-by-wire control augmentation system (CAS) used for the various maneuvers described herein. (See refs. 15 and 16 for more detail.) The CAS is composed of three controllers: (1) longitudinal, (2) lateral, and (3) directional. There is very little coupling between the longitudinal (pitch) controller and the other two controllers. However, the lateral and directional controllers are coupled through various interconnections and are described together. The flight phase of interest for the research described herein is up and away flights using the auto flap-up (AFU) mode. Figures 3 and 4 show abbreviated block diagrams for the longitudinal and lateral-directional controllers.

Longitudinal controller. The longitudinal controller uses a symmetric deflection of the stabilators plus the leading- and trailing-edge flaps. Feedback measurements are pitch rate q, normal acceleration N_z, and angle of attack α. The controller is mainly comprised of nonlinear functions such as dead bands and gain schedules. The main signal flow is an error created between the pilot longitudinal stick command (where stick command has been g limited) and a blend of the feedback signals. This error is first processed along proportional plus integral paths and then passed through a notch filter tuned to a structural bending frequency. The forward-loop integrator gain is air data scheduled and activated for $\alpha < 33°$. This provides increased stick force cues for mid- to low-speed flight conditions. The pitch rate feedback is dynamically shaped by a lead-lag filter that may vary with dynamic pressure during supersonic flight. Angle-of-attack feedback is only applicable above $\alpha = 22°$ in order to help provide a proportional nose-down command; this command provides an increase in stick force cues for high-angle-of-attack maneuvering. Both angle of attack and Mach number are used to schedule leading- and trailing-edge flap deflections. A speed-brake-to-stabilator interconnection is used to alleviate g transients for speed-brake extension or retraction. Speed-brake extension is inhibited at high load factors ($>5g$) or at high angles of attack ($>28°$). The brake is simulated with an actuation rate of 1 deg/sec both in extension and in retraction. An inertial coupling term, proportional to the product of roll rate and yaw rate, is fed back to the stabilator to offset pitching moments generated at high roll rates. This coupling term is the only input from the lateral-directional controller.

Lateral-directional controller. The lateral controller uses differential deflection of the ailerons, stabilators, leading-edge flaps, and trailing-edge flaps, whereas the directional controller uses synchronous (antisymmetric) rudder deflections. Interconnections from the rolling surfaces (ailerons and differential stabilators) to the rudder (RSRI) and from the rudder pedal command to the rolling surfaces result in a coordinated lateral-directional controller. Feedback measurements to the lateral-directional controller are roll rate p, yaw rate r, and lateral acceleration N_y. The lateral-directional controller is mainly composed of limiters, gain schedules, and various structural filters. Maximum roll rate is limited to 220 deg/sec when normal loads are less than $5g$ and 150 deg/sec for normal loads greater than $5g$.

Other features of the lateral controller include notch filters tuned to aeroelastic bending frequencies to prevent structural mode coupling. These are located in the roll rate feedback path and in the lateral stick signal path. A rudder-pedal-to-roll interconnection is used to drive the ailerons and differential stabilators. This reduces sideslip and angle-of-attack changes due to rudder deflections at high α. Rate limiters are located in the differential stabilator path to reduce coupling between the roll and pitch axes at high dynamic pressures. Differential stabilator command is also limited by stabilator pitch command (pitch priority) and by an angle-of-attack schedule. Differential leading- and trailing-edge flaps are driven by an error signal created by the difference between the lateral stick command and p. Differential leading-edge flaps are only used in the low- to mid-altitude transonic region.

Feedback signals for the directional controller are a blend of lateral acceleration, stability-axis yaw rate, and an inertial coupling term that is the product of p and q. Stability-axis yaw rate is created by summing $p \sin \alpha$ and $r \cos \alpha$. A washout filter is used to eliminate steady-state yaw rate signals to the rudder. A third-order low-pass filter, created to prevent structural feedback coupling, is used to process the blend of feedback signals. Finally, the filtered sum of feedback signals is summed with the rudder pedal command and the RSRI signal, after being passed through a lead-lag function. This error signal drives the rudders.

Description of Simulation Equipment

The Langley Differential Maneuvering Simulator (DMS), shown in figure 5, provides the capability of simulating two piloted aircraft with a realistic cockpit environment and a wide-angle external visual scene for each of the pilots. The system consists of two identical, fixed-base cockpits and projection systems, each based in a 40-ft-diameter projection sphere. At the time of this study, each projection system consisted of a sky-Earth projector to provide a horizon reference and a system for target image generation and projection. The internal sky-Earth scene provided reference in all three rotational degrees of freedom in a manner that allowed unrestricted aircraft motions. The sky-Earth scene provided no translational motion cues. This part of the projection system has since been upgraded. The internal visual scene also provides continuous rotational and bounded (300 to 45 000 ft) translational reference to a second vehicle (i.e., the target) in 6 degrees of freedom. The target image presented to each pilot represents the aircraft being flown by the other pilot if the dual simulator mode is used. This study used only one sphere without a target aircraft. The cockpit contains three color CRT displays on the instrument panel, each with a 6.5-in.-square viewing area and a wide-angle head-up display. Kinesthetic cues for this study, in the form of a g-seat system and programmable control forces, are provided to the pilots consistent with the motions of their aircraft. Pilot controls include a center stick controller with longitudinal and lateral trim button, rudder pedals, and dual throttles with speed-brake switch. The controls were programmed and configured to be consistent with those of an advanced fighter.

Results and Discussion of Control Design Metrics for Agility

This section presents a group of agility metrics that are candidates for testing in a CDM methodology. These metrics provide both a design tool and a measure of base capabilities of the test aircraft. This measure of base capabilites provides a datum against which any improvements in agile response can be observed or metric sensitivity can be tested. The format for presenting metrics is to first describe the flight condition and BKM along with the basic metric. Response time histories, transfer function (TF) metrics, and applicable functional agility (FA) metrics are provided when appropriate. The metric peak value and the time to peak value, denoted by δt_{pk}, are also presented for various flight conditions over which Mach number or normal load factor have been varied. For efficient presentation of the metrics, peak values and time to peak values (passive metric forms) are usually presented rather than time histories of the metric.

The results reported herein were obtained primarily through real-time, piloted simulation in the DMS. Some results were computed with an optimization program called FLXTRM. This code essentially solves equations of motion with the same aerodynamic model as was used in the DMS. The FLXTRM program solves the equations of motion for aircraft states at a specified flight condition and control setting, but does not provide simulation capability. The FLXTRM program was produced by extending the capability of the code in reference 17. Body-axis or wind-axis equations of motion used in this study can be obtained or derived from reference 18.

Classic Measures

Classic measures of maneuverability, used since World War I, provide valuable insight into aircraft capabilities. Table I lists some of these values for the test aircraft primarily at $h = 15\,000$ ft and fuel weight of 60 percent. These measures only characterize point performance, but a few have been tied to modern concepts of agility. Wing loading, thrust-to-weight ratio, and instantaneous turn rate have been found to have some importance in agility calculations. Wing loading W/S has traditionally only been considered as a turning capability measure. In general, as wing loading is decreased, turn radius is decreased. In more recent studies, wing loading has been studied parametrically with combat agility measures such as pointing margin and combat cycle time (ref. 6). Thrust-to-weight ratio T/W is shown for the aircraft at both sea level and $h = 15\,000$ ft. This is a basic performance measure of acceleration, but it has a significant impact on overall fighter agility too. In reference 19, for example, T/W is tied to maneuver capability and combat success. Maximum horizontal turn rates are sustainable turn rate, which reflects the capability to maintain turn rate and energy, and instantaneous turn rate, which reflects the capability for rapid nose movement. Maximum instantaneous turn rate is especially important as the duration of air combat engagements is reduced. In this situation the need to maneuver for very short periods of time becomes important (ref. 9); consequently, measures of rapid nose movement can be significant.

Axial Agility

Axial agility metrics, for this study, are specific excess power and specific excess power rate as well as acceleration and deceleration measures. All are tested at various points in the flight envelope. These

candidate metrics serve as agility measures and energy monitors indicating power utilization for various candidate control designs applied to specific BKM's. Axial agility metrics are important for assessing tactical situations, such as accelerating after a low-speed, high-α condition or for assessing new tactical aircraft, such as thrust-vectored aircraft, which use engine thrust for control moments as well as axial force. Comparing thrust-vectored control schemes with conventional aerodynamics approaches may indicate the same or greater levels of pitch or pointing agility but substantially different engine power requirements; axial agility metrics should highlight the difference.

The experiments or BKM's discussed in this section are accelerations (accels), decelerations (decels), and a continuous acceleration-deceleration maneuver (accel-decel). These BKM's were performed for symmetric flight and for turning flight to obtain various normal loads during the maneuvers. Each BKM is described below. Data were determined in the DMS with a pilot in the loop except where indicated.

Accels. Acceleration $\dot{V}(t)$ is the first metric considered for axial agility. Accel experiments were performed to determine peak acceleration level and time to peak acceleration for Mach numbers up to 1.2 and flight loads between 0 and $8g$. A constant-load, level-turn accel was the BKM used to generate data for flight loads greater than $1g$. Data for $1g$ accels were obtained by pilots maintaining straight and level flight during the acceleration. The $0g$ accels (push-overs) were studied with FLXTRM. Constant-load symmetric pull-ups were also analyzed with FLXTRM; however, the maximum accelerations were virtually identical to that obtained with turning accels, so symmetrical pull-up maneuvers were not studied as an axial BKM. The procedure for each BKM was to obtain a steady flight condition, apply full throttle, and then allow the aircraft to accelerate while a constant flight load was maintained. For $1g$ straight and level flight and for turning flight, the pilot also held altitude constant. For pull-ups and push-overs the FLXTRM program was used, since it provided an easy method to obtain maximum acceleration data rather than the pilots trying to fly a steady pull-up or push-over, capture a target altitude, and perform an accel maneuver. The FLXTRM program solved the equations of motion for a steady pull-up or push-over with full throttle at the instant the velocity vector was on the horizon.

Peak acceleration envelopes for several flight loads at $h = 15\,000$ ft are shown in figure 6. The solid curves were computed with the FLXTRM program and the symbols represent corresponding DMS data, which confirm the FLXTRM calculations. For flight loads above $6g$ positive accelerations are not possible. Also, the same level of acceleration is achieved for both $0g$ and $1g$ flight over a large range of Mach numbers. At very low speeds or high angles of attack, drag is significant, so the accelerations for each flight load are quite different. The DMS data were primarily collected at flight conditions where positive accelerations occur.

Time to peak acceleration (starting from trim) δt_{pk} for various flight loads is plotted against Mach number in figure 7. For speeds above corner velocity, shorter times to reach peak acceleration occur for higher flight loads or higher Mach numbers since much less excess power is available at these conditions (i.e., power settings are approaching maximum). For example, only between Mach 0.80 to 0.85 is positive acceleration observed for the $6g$ case. (See fig. 6.) Closely related to δt_{pk} is δt, time to achieve a certain velocity or change in velocity. This metric does not characterize transient agility, but it does show important maneuvering capability or functional agility. It is presented in the appendix as supplementary information.

Another candidate active metric can be defined with specific excess power P_s, which is closely related to acceleration. Specific excess power is defined as

$$P_s = \dot{h} + (V/g)\dot{V} \tag{1}$$

where $\dot{h}$ is altitude, V is total velocity, and g is the acceleration due to gravity constant. With the accels BKM and with the same passive metrics used to describe acceleration (i.e., peak value and δt_{pk}), P_s can be quantified as shown in figures 8 and 9. Figure 8 shows peak P_s as a function of Mach number for various flight loads. Simulation data are indicated by discrete data point symbols. Figure 9 shows the times to peak P_s as a function of initial Mach number for several flight loads. These values indicate times to go from a trim initial condition to maximum P_s. Decel data corresponding to the accel data discussed above are presented in the appendix as supplementary information.

Accel-decel. The next BKM used for axial agility involved cycling between peak acceleration and peak deceleration under various normal flight loads. The maneuver consisted of pilots applying maximum throttle while maintaining a level turning load (or symmetrical $1g$ load) and accelerating sufficiently long to allow the maximum acceleration envelope to be reached. Then the throttle was cut to idle until the peak deceleration envelope was achieved. The maneuver was continued over the op-

erating Mach number range, and during the maneuver load and altitude were maintained.

Figure 10 shows the peak acceleration and peak deceleration boundaries, with and without speed brake, for a range of normal flight loads. These boundaries are plotted as a function of the Mach number at which the maximum was achieved. The solid lines show peak accel, dotted lines show peak decel, and dashed lines indicate peak decel with speed brake. Dashed lines are shown only for flight loads of $1g$, $2g$, and $4g$ since speed brake use is limited to flight conditions with normal loads less than $5g$. The time to go from minimum to peak accel and the time to go from peak accel to peak decel are shown in figure 11. These times are plotted as a function of initial Mach number. Initial Mach number is the Mach number at which the throttle was changed. This graph shows a dotted line through the data for $1g$. Scatter in the experimental data is less than ± 1 sec. Within the accuracy of these data it appears that the flight load and the speed brake do not affect the times, although there is a measurable difference between accel and decel times. This seems reasonable since the times primarily reflect engine spool-up time. To complete the data set, figures 12 and 13 provide the corresponding P_s data. These data for figure 12 were computed with FLXTRM. Figure 13 gives the time to peak P_s for all cases considered. The plot for the time to peak P_s for accel-decel has the same character as that for the acceleration time measurements. As shown in figure 13, to within experimental measurements, only times for accel and decel appear to be appreciably different, while they are relatively independent of flight load and speed brake. Thus, engine response time is primarily reflected by this metric, although it is not a direct measurement of engine spool-up time.

The accel-decel BKM defines the acceleration and P_s limits as well as the time between limits for the test aircraft. These limits are the same envelopes of performance obtained through the separate accel and decel BKM's. Although the same acceleration and P_s envelopes are obtained more efficiently with the accel-decel BKM, the separate accel and decel BKM's may be more readily accomplished in a batch analysis.

The accel-decel data are also useful for defining the power onset rate (POR), a metric introduced in reference 9. This passive metric and its BKM may be useful as both a CDM and a measure of combat capability. The POR is the difference between the maximum P_s and the minimum P_s at a given Mach number and altitude divided by the time it takes to go between the two P_s values. This time is fairly independent of flight load, so time between maxima associated with the $1g$ case can be used for any flight load of interest. For this study, however, the actual measured values of time between maxima are used. Also, the actual values of P_s found at the start and the end of the cycle of acceleration or deceleration are used.

Figure 14 shows values of POR for $1g$ level flight and for $2g$ and $4g$ turning flight. Data are given for both accel and decel with the speed brake. The results for $6g$ and $7.5g$ decel with speed brake are not presented since speed brake is not available at these flight loads. Figure 14 shows that POR, for either accel or decel, is independent of flight load and dependent on speed brake and Mach number. More comparisons of POR are given in the appendix.

The POR has been shown to be useful for assessing aircraft agility (ref. 9), but it must be evaluated after the aircraft system is specified and a simulation is performed. It falls into the category of passive metrics. Of interest in this study are active metrics that may have utility within the control design process. In order to have an active POR metric, which would be a continuous function of aircraft states, it may be useful to consider the time derivative of P_s. This function is closely related to POR since POR is simply an approximation of the derivative of P_s. It is clear from the definition of POR that it represents the average value over time of the derivative of P_s, as in

$$\mathrm{POR} = \frac{\Delta P_s}{\Delta t} \approx \int_{t_1}^{t_2} \frac{\dot{P}_s}{t_2 - t_1}\, \delta t = \overline{\dot{P}}_s \qquad (2)$$

The term $\dot{P}_s$ may have some utility as an optimization parameter for control design when axial agility is important.

The relationship between POR and $\dot{P}_s$ can be shown graphically. Figure 15 shows $\dot{P}_s$ as a function of time during the accel-decel BKM. Positive peaks occur when a step to maximum throttle is applied, and negative peaks occur when a step to minimum (idle) throttle is made. Figure 16 shows these values of $\dot{P}_s$ replotted as a function of the corresponding Mach number at which they occur. Superimposed on this graph are the values of POR. A clear picture is thus shown of the averaging relationship POR has with $\dot{P}_s$.

Pitch Agility

Candidate pitch agility CDM's characterize body-axis and wind-axis pitch displacements, rates, and accelerations in both positive and negative directions. Excess power and power rate measurements are also used to characterize energy maneuverability (EM) associated with the BKM's. Wind-axis metrics, which

have not been commonly used, are evaluated in this study because directing the flight path of the aircraft to achieve an orientation in space can be equally important to and part of pointing the nose at a target. Since some maneuvering may involve a large relative displacement between wind and body axes of the aircraft (e.g., α and β generation), characterizing and controlling the relative displacement so that it occurs when desired are important for agile performance.

Pitch agility can be conveniently divided according to the motions involved. For this study, pitch agility is separated into pitching, turning, and pointing motions. Since it is advantageous for a control designer to consider longitudinal and lateral dynamics separately when possible, the BKM's are divided into vertical and horizontal motions. The vertical pitching motion from straight flight is used for assessing longitudinal pitch agility dynamics. Level, horizontal turning that involves lateral-directional dynamics, but still has a large pitching motion component, is also treated separately under pitch agility. Pointing motion is the last division considered under pitch agility; these metrics provide more functional agility rather than transient agility information. Unlike pitching and turning motion metrics, for which rotational rates and accelerations of each axis system are primary concerns, pointing motion metrics characterize rotational displacements of the nose and velocity vector as the primary commanded motion. Included in pointing is relative motion of the nose and velocity vector in the form of α displacements and rates.

Pitching motion. The test procedure for pitching motion metrics involved simple BKM's. Starting from a series of trim conditions at $h = 15\,000$ ft and extending from high speed (Mach 1.2) to very low speed (Mach 0.2), maximum stick deflections were applied after maximum throttle. The metric values are plotted against the initial trim Mach numbers, which cover the practical operating range (at $h = 15\,000$ ft) for the aircraft and extend up to an angle of attack of approximately 35°. Although the test aircraft is capable of achieving higher angles of attack, the higher range was not considered since there is a substantial loss of control power for maneuvering at this condition. Also, pitch motion with the aircraft initially under load ($N_z > 1$) was not considered, although the metrics in this study could be used to assess that capability. In a general evaluation of the agility envelope these accelerated initial conditions should be considered.

Pitch accelerations $\dot{q}$ and $\dot{q}_w$ and pitch rates q and q_w are the primary metrics of interest for pitching motion. Figure 17(a) shows typical responses for these parameters for the pitching motion BKM performed at Mach 0.6. One method used to characterize the agility of these responses is to develop transfer function (TF) approximations. Ziegler and Nichols (ref. 20) recognized that step responses of most systems have an S-shaped curve, as shown for q in figure 17(b). This response is characteristic of higher order systems but can be reasonably approximated by

$$\frac{q(s)}{\delta_{sp}(s)} = \frac{K \exp(-\tau_d s)}{\tau s + 1}$$

where K, τ_d, and τ are defined for pitch rate response in figure 17(b). This graphic approach offers a simple and repeatable method to quickly characterize a time-domain response. Of course higher order approximations, which more accurately model the response, can be obtained. Also, system identification techniques can be used to obtain a model with substantial fidelity, but these approaches require much more computational effort. The basic information necessary to characterize and compare aircraft transient agility (to the first order) should be amply contained in this approximation. This also provides one path between the time domain and frequency domain in the CDM methodology.

Additional metrics, which characterize the functional agility of the response, can also be obtained from figure 17(b). These metrics are peak, time to peak δt_{pk}, and slope of the response $m = K/\tau$, and they represent either long-term or average response metrics. The peak response occurs relatively quickly in this example (fig. 17(b)), but it can occur after the flight condition has substantially changed from the initial condition. The TF and FA metrics are summarized in table II for the pitch rates and accelerations shown in figure 17(a). The TF and FA metrics offer another means to describe agility.

For presentation of results over a range of Mach numbers, the passive form of the metrics, which gives a key instantaneous value, is more practical. Figures 18 and 19 show peak and time to peak body-axis and wind-axis pitch accelerations for maximum aft stick of 5 in. (nose up) and maximum forward stick of 2.5 in. (nose down). Time to peak acceleration gives a measure of the onset of acceleration (jerk) that is similar to the agility metrics recommended by Herbst (ref. 19). Maneuvers were performed only at the initial trim Mach numbers indicated, although dotted lines connect the data points in the figures to indicate trend. An important concern when performing a step input maneuver is to ensure the stick is moved rapidly. The full deflection should occur within 0.5 sec. Any slower movement of the stick can substantially reduce the pitch acceleration.

A fairly large difference in pitch acceleration capability exists for the two axis systems. Within the conventional flight envelope, better flight path control is achieved if the flight control system prevents the angle of attack from going beyond maximum lift during "flight path priority" maneuvering. It may be worthwhile for the flight control system of an agile aircraft to provide more flight path control and give the pilot the ability to choose between flight path and nose pointing. Pitch accelerations provide a possible metric (active or passive) for evaluating pitch control power or designing for systems with multiply redundant pitch controllers.

The corresponding peak and time to peak body-axis and wind-axis pitch rates are given in figures 20 and 21. At high speeds, body- and wind-axis pitch rates come together, an indication the nose and flight path move together. At low speeds and near the corner velocity, $\dot{\alpha}$ grows and causes a substantial difference between nose and flight path rates in the nose-up direction. The δt_{pk} is fairly large for high speeds, so the initial flight condition has changed significantly by the time peak rate occurs. Near the corner velocity and below, δt_{pk} is small so peak rates are achieved quickly, although δt_{pk} for q_w down grows at low speeds. A large δt_{pk} for q_w down combined with a greatly reduced q_w (both nose up and down) at low speeds indicates there is virtually no flight path control for conventional low-speed flight. Pitch-down rates are relatively small compared with pitch-up rates and reflect normal design practices. This may not be desirable for a more agile aircraft since pitch-down rates may be critical for pointing the nose or achieving rapid acceleration to regain energy (ref. 3).

Pitch motion maneuvers produce a peak pitch rate that may occur several seconds after the input. In some cases, a response without a peak or with a very flat peak may be produced, the result being a time to peak occurring very late in the maneuver and, therefore, at very different flight conditions than the initial condition. Since the aircraft can change its flight conditions fairly rapidly, it can be misleading if rates late in the maneuver are assumed to have occurred at the initial trim conditions. However, because the responses are very repeatable, it is assumed the peak values chosen reflect an agility characteristic that can be associated with the initial conditions of the BKM. Figure 21 shows large values of δt_{pk} for some of the peak rates.

Since long time periods to peak values may reduce the utility of the δt_{pk} and peak rate metrics, an earlier measurement may have more utility. One candidate metric to eliminate this problem is to mark time at 50 percent of peak. These metrics have the advantage of giving a measurement early in the response and, consequently, characterize more of the initial transient rather than the long-term response. Values for these metrics are given in figures 22 and 23. The results are similar to those found for the long-term response. Using these metrics in conjunction with the peak metrics in figures 20 and 21 should give an adequate picture of the response for both short and long terms.

Another candidate metric for pitching motion is wind-axis normal load factor $N_{z,w}$, which approximately reflects flight path bending capability. Also, the maximum rate at which the load is increased or decreased gives transient agility information. Unloading is important for agility since it has a major impact on drag and thus acceleration capability. The BKM used for loading is similar to that described above for pitching motion. The BKM used for unloading is to pull to roughly level flight and maximum flight load from a dive, obtain a target Mach number and altitude, and then rapidly unload to less than $1g$. Figure 24 shows the maximum flight load and the time to pull to or unload from this load. This figure indicates that at about the corner velocity the load or unload time is roughly 1.5 sec. Below that speed a steadily growing time to unload is indicated as speed is reduced.

Pitching motion EM. The total energy of a fighter, both kinetic and potential, is always of concern to the pilot in combat. Lack of energy can be fatal, leaving the pilot and aircraft as a slow moving, easy target. Unfortunately, any maneuvering performed by the pilot requires use of available energy. It seems likely that in an agile aircraft, which may often have redundant control effectors, that certain combinations of controls may increase efficient use of the control power and help maintain a higher level of overall aircraft energy. A simple example is the use of spoilers versus ailerons for lateral control. Both effectors can achieve the same goal but in a very different manner with respect to energy. Depending on whether the pilot desires to loose energy or gain it at that instant, one choice of controls may be better than another.

In light of the above discussion, it seems useful to include in the control design process metrics that reflect the energy efficiency of the aircraft-flight control system in maneuvering. The proposed metrics (active and passive) for this study are specific excess power P_s, specific excess power rate $\dot{P}_s$, and peak change in P_s during the maneuver ΔP_s. Specific excess power P_s has been a commonly used metric for many years; however, it has traditionally been used with respect to turning capability. For this study, P_s and its rate may serve as measures of merit to

assess EM capability in pitch. The term ΔP_s, which reflects the change of excess power during the BKM, may prove useful as a passive design metric.

Figure 25 shows the P_s and $\dot{P}_s$ responses to the same BKM used for pitching motion metrics. The initial increase in P_s is caused by application of full throttle from the initial level flight trim condition at Mach 0.6. After full throttle is applied, the pitch-up maneuver is performed and the "cost" of maneuvering, or loss of P_s, is indicated by a large negative value for P_s. Figure 26 shows the ΔP_s metric evaluated at several initial Mach numbers and $h = 15\,000$ ft for both pitch-up and pitch-down maneuvers. This metric is computed as the difference between the peak P_s and the initial value of P_s. An increase in cost for the maneuver as speed is increased is shown. This cost increase reflects both the availability and the use of greater control power and maneuvering ability. Interpreting how this curve compares with curves for different control design strategies (or with curves for different aircraft) at the same level of maneuvering may prove useful for improving agility. Figure 27 shows the $\dot{P}_s$ metric as the maximum value that occurs during the pitch-up or pitch-down maneuver with respect to the initial Mach number. For the $\dot{P}_s$ metric a large negative number indicates a large rate of loss of specific excess power. This rate may reflect the relative efficiencies of an agile maneuver between two aircraft or of two control systems for one aircraft. The negative value of $\dot{P}_s$ near Mach 1.0 reflects performance losses in the transonic regime. At slower speeds, the loss of power rate is much reduced, but so is pitch performance. For the Mach numbers above 0.6 there is a steady decline in the body-axis peak pitch rate and a leveling off for the wind-axis pitch rate (see fig. 20), but the power rate indicates a reduced pitch rate at Mach 0.8. From a power availability point of view, Mach 0.8 is attractive for a rapid pitch-up maneuver.

Turning motion. Turning motion metrics characterize rotation of the aircraft nose and flight path in a horizontal turn. Candidate metrics for this motion are turn rate of the flight path $\dot{\psi}_w$, turn rate of the nose $\dot{\psi}$, and corresponding P_s for EM evaluations. Turning motion involves both longitudinal and lateral dynamics; however, for a fighter performing rapid instantaneous or sustained turns, significant demand is placed on pitching motion capability. For this reason, turning is treated as a subset of pitch agility.

The first metric considered is sustainable turn rate and it is presented in passive form as peak values of sustainable turn rate over a range of Mach numbers. This does not characterize transient agility but it does characterize basic maneuverability in turning. The BKM for these data was performed by finding the greatest bank angle that could be sustained in a level turn at a specified Mach number and altitude.

Figure 28 presents sustained turn rates versus Mach number for four different altitudes. For the sustainable turn, P_s is zero and wind-axis and body-axis turn rates are equal. The distinctive dip at the top of the curves between Mach 0.6 and Mach 0.8 apparently corresponds to breaks in the trailing-edge flap schedule as a function of Mach number. At 5000 ft a limit of $7.5g$ is reached approximately between Mach 0.75 and 0.95. Reduced power is required to trim at $7.5g$. With a g override capability, a slightly greater sustained turn rate is possible with full power. This result is shown as a dashed line for the $7.5g$ limit and a solid line with g override engaged. The dip and g override effects are a result of design choices. In both cases a reduction in turn rate results from the design choice. This may or may not be a desirable trade-off for a specific agile fighter. In any case it should be beneficial to include these metrics in the design optimization process to ensure good design trade-offs.

Instantaneous turn rates for $\dot{\psi}_w$ and $\dot{\psi}$ offer a metric for characterizing transient turning agility. The body-axis metric should help optimization of rapid nose movement as used to achieve a "first shot," and the wind-axis metric should help the design process for rapid flight path change as might be used when a "break" turn or a rapid evasive maneuver is needed. These metrics would be used in conjunction with other pitching motion metrics to achieve the best overall design trade-off.

The BKM for instantaneous turn rates was produced with a level turn requiring maximum turn rate. Starting at maximum speed and diving to the target altitude if necessary to gain speed, a maximum loaded turn was initiated. Altitude was held while speed bled off. Figure 29 shows measurements of the wind-axis instantaneous turn rate plotted against the corresponding Mach number at which the turn rate occurred. Figure 30 shows a similar plot for body-axis instantaneous turn rate. Three runs are shown in each figure to indicate the spread on these data. The peak in both figures, at roughly Mach 0.6, is the corner velocity of the aircraft at $h = 15\,000$ ft. This is the point where the aircraft is flying at maximum C_L and maximum normal flight load. From corner velocity to maximum velocity the aircraft turning is limited by structural load capability; thus, little can be done through the control system unless energy maneuverability considerations are included in the

optimization of the control system. Below the corner velocity, turning is a function of how angle of attack is controlled; therefore, more opportunities for design trade-offs are possible. The EM metrics or other general CDM's may be useful in this area too.

Figure 31 presents a comparison of wind- and body-axis instantaneous turn rates. This figure highlights the difference in turn rates, which reflects the rate of change of angle of attack. From Mach 0.8 down to the corner velocity, $\dot{\alpha}$ is becoming larger. Below the corner velocity, $\dot{\alpha}$ is getting smaller but α is still becoming larger, and consequently lift (and therefore turn rate) is rapidly falling off. Close to Mach 0.2 a rapid loss of turning ability occurs, angle of attack has become very large, and the flight path has become virtually ballistic. At this point, level turning is no longer possible. These candidate metrics may prove useful for optimizing the relationship between wind- and body-axis turn rates.

One conventional method of considering energy maneuverability is through plots of P_s versus turn rate. This presentation of P_s is not new and has been commonly used. Skow et al. (ref. 9) have suggested extensions to this conventional plot by extending into the high-angle-of-attack range and including a P_s value at $0g$ as a separate point beside the graph. A further extension for metric presentation is to show the relationships of P_s, pitch-axis rotations, and turning rotations for both the wind and the body axis. The difference between angular rates of the nose and the flight path gives some idea of how much additional angular rate is possible against the cost of P_s losses. Besides comparisons of wind- and body-axis angular rates, comparisons of pitch motion and turning motion are also easily made.

An example comparing wind-axis angular rates at $h = 15\,000$ ft and Mach 0.4 is shown in figure 32, in which P_s is plotted against flight-path angular rate $\dot{\gamma}$ and wind-axis turn rate $\dot{\psi}_w$. A few points on these curves highlight agility information. The $\dot{\gamma}$ curve has a peak that occurs in $0g$ flight, an indication of the maximum P_s possible in unloaded flight (occurring at an angular rate of −4 deg/sec). The $0g$ angular rate point is the $1g$ maximum P_s value for straight and level flight. The $P_s = 0$ line gives the maximum sustainable angular rate points. The $\dot{\psi}_w$ curve gives the maximum instantaneous turn rate at the largest angular rate point. Finally, the high-angle-of-attack condition is at the end of the graphs on the positive angular rate side. These data were primarily produced with the FLXTRM program by specifying the flight condition and angular rate. Some DMS data are shown in figure 32 to correlate the FLXTRM approach with piloted simulation.

Pointing motion. Pointing motion metrics focus on the ability of the aircraft to displace the nose or flight path. Displacing the nose relative to the flight path is also of interest; however, only displacements in the aircraft vertical plane are considered in this study. Displacing the nose relative to the flight path in yaw (sideslip) is not considered since the test aircraft characteristics are not suited for large sideslips. Other important metrics assessing flying qualities for pitch angle captures are not considered in this study.

The primary BKM's for pointing were started from $1g$ trim conditions. A maximum stick back or forward step command was used while the throttle was simultaneously pushed to maximum, minimum, or minimum with speed brake. Although test conditions can change significantly from initial conditions as the time of the maneuver increases, the experiment is repeatable and demonstrates important system characteristics. The step command is easily produced in both batch and real-time experiments. These data in this section were provided by a pilot performing a full stick deflection within 0.5 sec. This minimum time for deflecting the stick was considered acceptable for pointing measurements.

The first metrics considered for pointing motion are $\theta(t)$, slope m, peak value δt_{pk}, and the three transfer function approximation metrics, K, τ_d, and τ, introduced previously. Figure 33 presents these metric values and a time history of θ produced at Mach 0.6 and $h = 15\,000$ ft. The value θ provides a readily measured state that can be optimized in the design process. The three transfer function approximation metrics provide characteristic information for the transient response. The other metrics help to characterize the total response in terms of functional agility.

The time to peak metric provides a useful passive design metric as well as a useful means to present θ characteristics. Closely related to the time to peak metric is a measure of the time to achieve a specified displacement. This passive metric, written as δt, provides more detailed information about the θ response than a time to peak metric by quantifying the time to achieve certain changes in θ. Figure 34 shows δt for pitch angles from 30° to 90° with the BKM initiated at Mach 0.6. Both up and down displacements are indicated. Up displacements were performed only with maximum throttle since less throttle substantially reduced performance. Down displacements were performed with maximum throttle (with afterburner), with minimum throttle or idle, and with idle throttle with speed brake. The best pitch rates are possible at Mach 0.6; as a result, the best pointing in terms of δt generally occurs at this flight condition too.

Comparisons of δt at other Mach numbers are given in the appendix. At Mach 0.6, there is virtually no difference in nose down performance for the different throttle and speed brake settings. Figure 35 shows a summary of pointing performance for the Mach range considered and with the BKM performed at maximum throttle only. Negative values of δt indicate the nose-down BKM. Nose-up performance is clearly best near the corner velocity and is dramatically reduced below that speed. Nose-down performance improves with speed reduction down to Mach 0.4, where best performance occurs.

Best pitch-up performance, in terms of minimum time to achieve a θ displacement, is not necessarily obtained with the "stick snatch" maneuver described above. Through experience a pilot can learn to pull the stick back so that better performance is obtained, but this type of control interface is not ideal. A better situation may be to have a control system that gives agile performance in proportion to the pilot's demand, that is, in proportion to stick deflection. In light of this, pointing performance is considered in relation to stick deflection.

To assess pointing performance in relation to stick deflections, results were obtained with the same BKM as before except the stick was only deflected to calibrated marks on a template beside the stick. Figure 36 presents δt for time to achieve $\theta = 90°$ with various stick deflections. A desirable relationship is that more stick deflection leads to smaller δt. Figure 36 shows decreasing δt for increasing stick deflection for all Mach numbers of 0.6 and above. At Mach 0.2, the BKM is only possible at maximum stick deflection. At Mach 0.4, there is a minimum δt at less than maximum stick deflection. This indicates the pilot must search for the optimal stick deflection at low speeds. An agile aircraft probably should have a control system that eliminates this requirement.

Metrics that involve long-term response reflect nonlinear effects in the response due to changing flight conditions and, in particular, changing angles of attack. Another candidate metric for comparing relatively short-term response is the 1-sec metric. This metric gives the value of an initial response 1 sec after the commanded input. Since it is limited to a 1-sec time frame, it gives an indication of initial response rate close to the initial flight condition. This measure is a passive metric that provides information similar to the time to achieve metrics, except values are only obtained for initial responses. Although this metric does not capture system characteristics as well as measures such as eigenvalues, it is readily measured and applicable to linear or nonlinear systems.

Figure 37 gives a summary representation of the system nose pointing capability. This figure shows trim θ, maximum θ displacement, maximum change in θ (indicated by $\Delta\theta$), and $\Delta\theta$ in 1 sec for both up and down displacements from trim. The maximum θ displacement is limited to 90° in this figure so that a value of 90° indicates that the aircraft is capable of a complete loop. The value $\Delta\theta$ is the difference between the maximum displacement in pitch and the trim pitch angle; it represents the pointing capacity of the aircraft over a range of Mach numbers for the specified BKM. Besides capacity for angular displacement, the rate of angular displacement is of interest; one candidate for this measurement is $\Delta\theta$ in 1 sec. The value of this metric represents an average rate for the first 1 sec of motion. Considering rate measurements over longer periods, as done with the peak pitch rates, gives the rate capacity, but it includes nonlinear effects to a greater extent since it includes the effect of a change in flight condition from the initial test point.

Flight path control in addition to nose pointing control is important for agile performance. Stick forward or aft will command the nose up or down, but at certain times it may be desirable that this also commands the flight path up or down. How this response is obtained should be the subject of future studies. How this response occurs in the current aircraft is presented in this study.

For the representative aircraft model in this study pointing occurs in varying degrees of two extreme cases: (1) pitch displacements of the nose with almost equal flight path displacements (high-speed case) and (2) pitch displacements of the nose with virtually no movement or opposite movement of the flight path (low-speed case). For this aircraft, it is possible for the flight path to fall when the nose is commanded up at certain low-speed conditions. These limiting characteristics highlight how improved controllability over an expanded angle-of-attack range would enhance pointing capability at higher speeds and flight path response at lower speeds.

Figure 38 shows $\gamma(t)$, associated transfer function metrics, and corresponding functional agility metrics as a result of the pointing BKM at Mach 0.6 and $h = 15\,000$ ft. At these flight conditions, the $\gamma(t)$ response does not follow the S-shaped response that the metrics are based on; consequently, only τ_d and m can be determined for this case. Figure 39 presents values of the δt metric for Mach 0.6 and $h = 15\,000$ ft. At these flight conditions, $\Delta\gamma$ up through 90° is possible and $\Delta\gamma$ for the nose-down case has the same performance regardless of throttle and speed brake combinations. Values of this metric at other Mach numbers are summarized in the appendix.

Figure 40 shows a summary of pointing performance in γ for the Mach range considered and with the BKM performed at maximum throttle only. Somewhat similar trends are shown for flight path pointing (fig. 40) as are shown for θ pointing (fig. 35). The γ up response is improved with reductions in speed down to Mach 0.8 and down to the corner velocity for small displacement angles. Corner velocity provides best performance for the initial 30° of $\Delta\gamma$ up. Performance for flight path down follows the same trend as the nose-down performance, except below Mach 0.4 much worse performance results for γ. It should be noted that the Mach numbers indicated are only initial Mach numbers. For large displacement angles, Mach number is not held at the initial value during the BKM.

Figure 41 gives the trim γ, maximum $\Delta\gamma$ up, and $\Delta\gamma$ in 1 sec for both up and down at various Mach numbers. Since initial conditions were set for level flight, trim γ is zero and maximum γ equals maximum $\Delta\gamma$. Maximum γ values are limited to 90° in this figure, so a value of 90° indicates the aircraft is capable of a complete loop. Long-term maximum down displacements are trivial since the nose can always be commanded to -90°.

The ability to displace the nose relative to the velocity vector on command and under control may prove to be a desirable characteristic of agility. Focusing only in the aircraft vertical plane, $\alpha(t)$ is the primary metric of interest for assessing nose and flight path relative displacements; $\alpha(t)$ displacements and rates are assumed to provide the necessary metric information. The three transfer function approximation metrics are used to describe transient agility characteristics of the $\alpha(t)$ displacement and rate responses. The peak displacement or rate, time to peak displacement or rate δt_{pk}, corresponding slopes m, and time to achieve a specified displacement δt should provide adequate functional agility information. A time history of $\dot{\alpha}(t)$ and the control inputs for the pointing BKM are shown in figure 42. The corresponding TF and FA metrics are shown as well. The metric values for $\alpha(t)$ are shown in figure 43 for the same test run.

To give some indication of the response of $\alpha(t)$ and $\dot{\alpha}(t)$ as a function of Mach number, the peak and time to peak metrics were evaluated at several Mach numbers. Figures 44 and 45 show both peak rate and time to peak rate for nose-up and nose-down commands over a range of Mach numbers. Figures 46 and 47 show both maximum change in α and time to maximum change for nose-up and nose-down commands over a range of Mach numbers. As shown, the maximum achievable nose-up $\Delta\alpha$ for this aircraft, using the specified BKM, is 55° and it is only possible above Mach 0.4. The times to achieve the maximum are fairly long, consequently, a substantial change between initial and final flight conditions has occurred. However, this is a repeatable maneuver and so is useful in characterizing the system response.

Figure 48 provides time to achieve $\Delta\alpha$ of 5°, 10°, 15°, 30°, and 45° for a range of initial Mach numbers. As would be expected, much greater values of δt occur for the highest Mach numbers. For high-speed initial conditions a period of time is required to bleed off speed before large values of α are achievable without over loading. For lower speeds, a short time to reach α for maximum lift may be desirable, but some limiting mechanism should prevent going beyond maximum lift (unless commanded by the pilot).

Besides controlling pointing, this measurement may be useful for defining how angle of attack should be controlled for optimal flight path bending. Obtaining the best turning rate requires maximum lift, which occurs at 36° for this aircraft. However, best turning may be defined with energy maneuverability constraints so that optimum turning is a compromise between energy loss and maximum instantaneous turn rate. The rate at which angle of attack is brought to the optimum value has potential as a metric.

A summary of angle-of-attack pointing performance over the normal range of Mach numbers is shown in figure 49. This figure gives trim α, α displacement in 1 sec, maximum change in α (indicated as $\Delta\alpha$), and maximum α.

Torsional Agility

With the broad definition of agility used for this study, torsional, or roll, agility is the capability to rapidly and precisely rotate the aircraft about the velocity vector. The control design metrics for torsion focus on wind-axis roll rate and acceleration for transient agility and wind-axis roll displacement metrics for functional agility. Wind-axis rolls are the only rotations of interest since the metrics apply to the entire range of α. Body-axis rolls are only desirable at very small α as they produce undesirable, uncoordinated rolls at high α. Metrics for this section are determined over a range of Mach numbers and flight loads.

Straight flight, 1g rolls. The first group of torsional agility metrics characterize roll capability in straight and level flight. The benchmark maneuver for this group required a step lateral stick input immediately after applying maximum throttle from trim level flight. During the roll an attempt

was made to maintain constant load factor and the control system maintained coordination.

The first torsional metric for straight and level flight is wind-axis roll acceleration $\dot{p}_w$. The value of this metric and corresponding TF and FA metric values in response to a step command are shown in figure 50. The next metric considered is wind-axis roll rate p_w. The response for this metric and the resulting TF and FA metric values are shown in figure 51. The roll acceleration and rate in these figures characterize the aircraft roll agility at Mach 0.8 in $1g$ flight. These values show the full-order, coupled response of the system with nonlinearities present. Within the limits of a first-order approximation, the TF and FA metric values effectively characterize agility and provide an easily computed measure.

Peak values of $\dot{p}_w$ over a range of Mach numbers are shown in figure 52 along with times to peak versus the initial Mach number. These metric values indicate a significant loss of control power below Mach 0.4 and a smaller loss at transonic speeds. For all Mach numbers the maximum power is achieved in about 0.5 sec; this is about the time it takes a pilot to move the stick.

Figure 53 presents peak values of p_w with the corresponding δt_{pk} metric. Wind-axis roll rate, unsurprisingly, follows a trend similar to wind-axis control power; both fall off quickly below Mach 0.4. The corresponding δt_{pk} metric for p_w is relatively flat except below Mach 0.4, where it increases rapidly. Since metric values are plotted against initial flight conditions, it is important to note magnitude of the δt_{pk} metric. For large δt_{pk} the maneuver has progressed far from the initial flight conditions. For the rolling maneuver at low speeds (high angle of attack) the rotation speed is so slow that the flight path is approaching vertical when the maneuver is completed. This does not invalidate the experiment, since it is still a repeatable test and represents the actual system response. It does indicate, however, that the initial Mach number is only an initial condition and is not the Mach number at which the peak value of the metric occurs.

Another useful metric, commonly used to characterize roll capability, is the time to roll through a certain angle of bank. In this study, the CDM is specifically defined as time to roll through a wind-axis bank angle starting at an initial Mach number. Labelled as δt, the metric is presented over a set of wind-axis bank angles and trim Mach numbers. Figure 54 shows the δt metric for a set of initial trim conditions at $1g$. Mach number ranges from 1.2 to 0.2; at Mach 0.2 the trim α is approximately 35°. Below Mach 0.4 the initial trim conditions are given in terms of α. At and above $\alpha = 15°$ the δt values are very large for a tactical fighter. The best times occur for Mach 0.6 and 0.8 at each angle of rotational displacement.

In addition, figure 54 shows that using a rudder input command alone improves the roll time modestly. A slightly better (i.e., more rapid) time is obtained by using the rudder pedal only at $\alpha = 35°$. This reflects the requirement for larger body-axis yaw rates as α increases. It should be noted that the δt is so large that only a small part of the roll occurs in relatively level flight.

Turning flight, loaded rolls holding N_z. The second group of torsional agility metrics are based on loaded rolls. The BKM for these metrics was initiated from a level turn to establish the desired Mach number and flight load. A step lateral stick was applied, without rudder pedal, after maximum throttle was commanded. In some cases a descent from above target altitude was necessary to achieve the desired Mach number and flight load combination. This was necessary to get maximum flight loads at the higher Mach numbers since these are instantaneous conditions only. Normal loads up to $7.5g$ were considered, which is the maximum allowed by the control system g limiter.

Table III summarizes the TF and FA metrics for $\dot{p}_w$ and p_w responses over a specified set of flight loads, all obtained at a Mach number of 0.8. This Mach number is generally where peak loaded roll performance occurs. Roll rates are limited by the control system depending on flight load, angle of attack, and the presence of wing stores. Above $5g$ the roll rate is limited to 150 deg/sec to reduce vertical tail loads and inertial coupling moments. Table III indicates a reduction in peak loaded roll capability with increasing flight load, a reflection of the roll limitations.

Loaded roll capability at a $2g$ normal load over a range of Mach numbers is presented in figure 55. The figure shows $\dot{p}_w$, p_w, and δt metrics. A reduction in roll control power and roll performance in the transonic regime is shown as well as a substantial reduction below Mach 0.4. At Mach 0.4 the average roll rate through 360° is only 55 deg/sec. A similar situation is demonstrated for higher normal loads, as shown in the appendix.

The next candidate metric for loaded rolls is PN. It is defined as

$$PN = p_w N_{z,w}$$

where p_w is the wind-axis roll rate and $N_{z,w}$ is the wind-axis normal acceleration in g units. This metric reflects the objective of a loaded roll, which is

to rotate the aircraft about the velocity vector (p_w) while turning or rotating the flight path ($N_{z,w}$). It is tactically desirable to be able to do these two rotations simultaneously, with the pilot commanding any level of each rotation in combination. Most aircraft have the capability to bend the flight path (command N_z) up to human and structural limits, but the level of wind-axis roll rates possible deteriorates greatly as load factor increases. This metric should be useful for optimizing loaded roll capability in a fighter since it is a continuous function of the state variables and characterizes the objective. If desired, each term in the definition of PN could be normalized and weighted to reflect a specified relationship between rolling and flight path bending.

Figure 56 shows a sample of PN plotted as a function of time for a maximum loaded roll ($N_z = 7.5g$) at Mach 0.8 and $h = 15\,000$ ft. Included with the figure are TF and FA metrics. Figure 57(a) shows maximum PN over a range of Mach numbers. The PN metric clearly reflects the loss of roll capability below Mach 0.75 and in the transonic regime, confirming the results indicated by the other metrics. Figure 57(b) shows maximum PN over a range of Mach numbers and load factors. A fairly large change in the family of PN curves occurs for load factors less than $4g$.

A design point that might be considered for agile fighters is the relationship of corner velocity to PN and $\dot{p}_w$. Wind-axis instantaneous turn rate $\dot{\psi}_w$ quantifies the ability of the aircraft to bend the flight path in a horizontal, Earth reference frame. Plotting it as a function of Mach number clearly shows a peak at the speed for best instantaneous turning, or corner velocity. Figures 58 and 59 show $\dot{\psi}_w$ plotted with peak values of PN and $\dot{p}_w$ as a function of Mach number for the maximum flight load. These two plots show a loss of loaded roll capability and a loss of roll control power above the corner velocity. This may not be optimal for agile fighter design. Ideally an agile fighter would retain loaded roll capability in the corner velocity region. The design trade-off between departure resistance and torsional agility might be made differently for this system using agility metrics.

Turning flight, loaded rolls holding α. In this study, the BKM for torsional agility defined a maneuver in which the pilot attempted to hold flight load constant. The rationale for holding flight load during the BKM and for using maximum throttle is to more accurately reflect the conditions under which fighter agility is likely to be used. Using full throttle and holding flight load attempts to maintain flight path bending during the roll. This is a desirable capability to a fighter pilot and therefore a test condition of interest to a designer concerned with agility. However, while flight load is held in a loaded roll, speed can bleed off and cause a demand for greater angle of attack to maintain the flight load. Angle of attack is a primary measure on which aerodynamic models for design are formulated. A Taylor series expansion about trim α is the conventional formulation. At high α, the aerodynamic model for an aircraft is generally a strong nonlinear function of α. Consequently, holding α during a loaded roll would fix those aerodynamic terms that are dependent on α and reduce nonlinearities from one source; this is also a desirable situation for the designer. The result of this apparently conflicting requirement by the designer is that for initial linear design and analysis a constant α test maneuver is preferred, but for final evaluation a realistic, fully nonlinear maneuver is necessary.

To partially assess the degree to which the hold-α or hold-flight-load BKM's affect the metrics, loaded rolls were repeated with the task requirement to hold α constant during the maneuver. The initial conditions were the same as the hold-flight-load BKM performed with a $4g$ load factor. The only feedback to the pilot was a digital display of α and N_z on the head-up display. Generally, the pilot was able to hold α within 1° of the desired value during the maneuver. Figures 60(a), 60(b), and 60(c) show $\dot{p}_w$, p_w, and δt metrics for the hold-α BKM performed at an initial $4g$ load over a feasible range of Mach numbers. For this load factor and Mach numbers from 1.20 to 0.55, the corresponding angle of attack varies from 3° to 14°, respectively. Below Mach 0.55, rolls are not really feasible at $4g$.

Figures 61 and 62 present wind-axis roll accelerations and rates as a function of Mach number for both the hold-flight-load and the hold-α BKM. Within experimental accuracy attainable, without computer-controlled inputs, the difference in roll rates between hold-α and hold-flight-load BKM's is negligible. Therefore, for a $4g$ load factor and α up to about 15°, the two BKM's produce no significant difference in measured agility. At higher α the expectation is that the hold-α BKM will produce higher roll rates than the hold-flight-load BKM, since it requires unloading the aircraft as speed is lost during the roll. On the other hand, maintaining flight load during a roll at lower airspeeds will require more α, thus reducing roll rate capability.

Concluding Remarks

This study represents a first step toward developing a control design metric methodology. Two tasks have been accomplished in this study. The first task

was to provide an overview of control design metrics (CDM's) and highlighted the requirement that metrics need to be developed with the end user's perspective in mind. In this case, the end user is the control designer interested in improving fighter agility. The second task was to illustrate a candidate set of CDM's for fighter agility. This set of metrics is not all encompassing for agility, but it does cover a broad range of aircraft capabilities and the primarily time-domain nature of the metrics allows for the straightforward evaluation of agility. The main value of this second task is that it provides a baseline against which CDM's and control system modifications can be compared. Against these comparisons, metrics can be tuned and developed to suit the requirements of the control designer.

Flying qualities issues or pilot-in-the-loop requirements were not addressed in this study, although these issues need to be addressed to develop a complete set of CDM's. Pilot-in-the-loop constraints represent real limits on the level of agility allowed and represent requirements that must be incorporated in the design. In this study, agility was studied independently of flying qualities issues to separate pilot-in-the-loop effects from aircraft and flight control system effects. Separating these effects provides designers with a "building block" capability for which trade-offs between agility and flying qualities can be more easily made. The CDM's characterize agility levels and may be useful to a designer in assessing changes in agility with respect to different flying qualities levels. This approach should allow the CDM's to have a complementary role with flying qualities metrics and guidelines as found in MIL-STD-1797A.

NASA Langley Research Center
Hampton, VA 23665-5225
January 17, 1991

Appendix

Metric Values for Additional Test Points

This appendix provides metric values for the simulated aircraft at additional test points. The test points cover flight conditions that extend the example flight conditions discussed in the main text. The metrics and the corresponding BKM's are described in the appropriate sections of this paper.

Accels

A candidate metric related to δt_{pk} is time δt to achieve a certain velocity or change in velocity. This metric does not characterize transient agility, but it does show important maneuvering capability or functional axial agility. Figures A1 and A2 show the time to achieve a velocity starting from trim Mach number and starting from corner velocity, both for various flight loads. It is notable that virtually the same Mach number is achieved in the same time for either a $1g$ straight and level condition or a $2g$ turning load starting from the same initial Mach number.

Decels

The next series of figures shows the maximum deceleration $\dot{V}$ achievable by the aircraft. The BKM performed for these data is identical to the accel maneuver except the throttle is reduced to a minimum from an initial trim condition. One variation, used in this test, includes maximum speed brake command simultaneous with cutting the throttle.

Figure A3 shows a family of maximum decel envelopes for various flight loads. The $1g$ graph is clearly for straight and level flight and the other graphs are for the indicated normal loads produced by level turns. The corresponding times to peak deceleration δt_{pk} are given in figure A4. It is notable that the times are fairly independent of the flight load, an indication that these times really only reflect engine activity. Figures A5 and A6 provide data on decels with the speed brake. Since the speed brake cannot be commanded out above $5g$ or above $\alpha = 28°$, the curves shown do not include values for $5g$ or above. Figure A7 emphasizes the point that the time to peak decel from trim is independent of flight load or application of the speed brake to within experimental accuracy. Of course application of the speed brake or high flight loads increases the level of maximum deceleration. To complete the data set for decels, figures A8 to A11 provide the corresponding P_s data.

Accel-decel data, with and without the speed brake, over a range of normal loads are presented in figure A12 in the form of the power onset rate (POR). The accel POR and decel POR for the $1g$ load are fit with a dashed line to highlight the nominal POR values. The POR is primarily a reflection of engine spool-up capability and, consequently, is fairly independent of the normal load. The decel POR is distinctly more negative with the use of the speed brake.

Pointing

Figure A13 shows δt metric values for pitch angles ranging from 30° to 90° with the BKM initiated at Mach 0.2. Both up and down displacements are indicated. Up displacements are performed only with maximum throttle since less throttle substantially reduces performance. Down displacements are performed with maximum throttle (with afterburner), with idle or minimum throttle, and at idle with speed brake. As shown in the figure, nose-up pointing from trim is limited at this Mach to about 35°. Nose-down performance, when minimum throttle is used, is virtually the same for the case with or without speed brake. Maximum throttle reduces nose-down performance for this flight condition.

Figure A14 gives the δt metric values for the Mach 0.4 case. In this case nose-up performance is improved, with a maximum change of 80° achieved from trim. Nose-down performance is still reduced when maximum throttle is used, but by a much smaller amount compared with that of the Mach 0.2 case. Figure 34 shows this trend continuing at Mach 0.6. That is, nose-up performance is substantially improved and nose-down performance is actually slightly improved with maximum throttle except for 90° displacements. The small differences in nose-down times are probably close to the measurement errors of the experiment. Therefore, at Mach 0.6 there is virtually no difference in nose-down performance for the different throttle and speed brake settings. Displacements greater than 90° are not considered.

Figures A15, A16, and A17, representing Mach 0.8, 1.0, and 1.2, show a reverse in the above trends described for Mach 0.2, 0.4, and 0.6. This is not surprising since Mach 0.6 is very close to the corner velocity at $h = 15\,000$ ft and is the speed at which best performance should occur. The trends indicated for speeds greater than the corner velocity are a small reduction in nose-up performance and reduced nose-down performance with maximum throttle. A small difference between nose-down performance with minimum throttle and with minimum throttle with speed brake occurs for the Mach 1.0 case.

Figure A18, which shows δt metric values for the flight path angle, indicates that at Mach 0.2 only a few degrees increase in flight path occurs during the

BKM. For the flight path commanded down, δt is recorded for a range of 30° to 90°. These results are similar to nose-down results in that maximum throttle causes the poorest performance and minimum throttle, with or without speed brake, causes the best performance. Figure A19 indicates that at Mach 0.4, performance for flight path down is the same for any throttle and speed brake combination. Performance for flight path up improves to the point that 30° of increased γ was possible. At Mach 0.8, shown in figure A20, nose-up performance has reached 90° and nose-down performance is reduced for maximum throttle. Figures A21 and A22 show small increases in time for Mach 1.0 and 1.2 compared with time for Mach 0.8.

Torsion

Loaded roll capability over a range of Mach numbers and flight loads is presented in figures A23 to A25 for $4g$ to $7.5g$ normal loads. Each figure shows $\dot{p}_w$, p_w, and δt metrics for various Mach numbers. Figure A23, for a normal load of $4g$, indicates reduced roll control power and roll performance in the transonic regime, and these values fall off more substantially by Mach 0.5. At $6g$ (fig. A24), the loss of roll control power is still present in the transonic regime and now falls off below Mach 0.7. Figure A25 shows the trend of reduced roll capability continuing at maximum load of $7.5g$. At this load the roll performance is slightly reduced from that at $6g$ and the decrease in performance occurs at a slightly higher Mach number.

Maximum loaded rolls ($7.5g$) represent the aircraft limits in terms of maximum bending of the flight path while rolling. For this system, when maximum roll rate is commanded the flight load is reduced to $6g$; immediately upon removal of the roll command the flight load returns to the maximum of $7.5g$. Figure A25 shows $\dot{p}_w$ over the range of Mach numbers that rolls are successfully performed. Below approximately Mach 0.75, rolling under maximum flight load is virtually impossible. The corresponding δt metric indicates consistent response times up until it is impossible to roll. This striking loss of roll control power is caused by a control system limit on control deflection as well as some loss of aerodynamic effectiveness at this flight condition. Above $\alpha = 20°$ the ailerons are substantially limited.

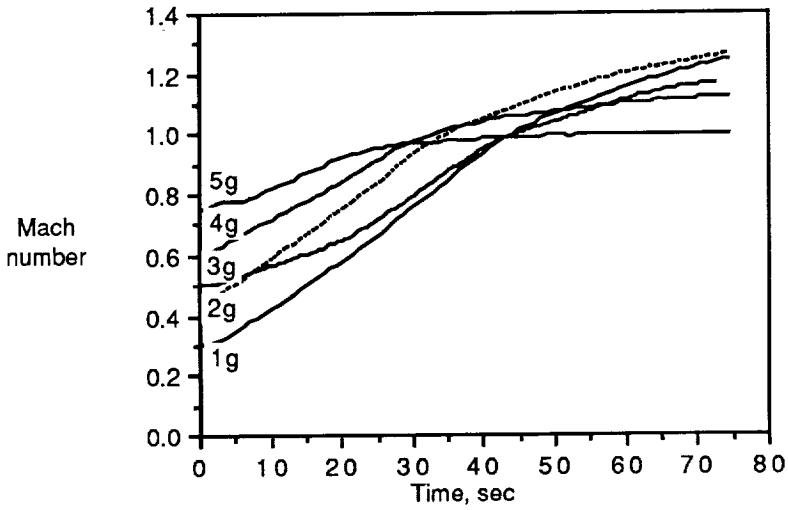

Figure A1. Accels from minimum Mach number.

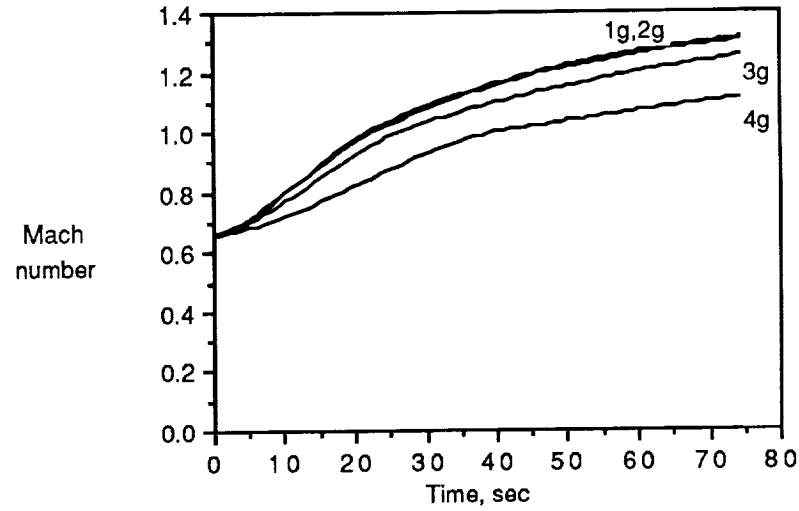

Figure A2. Accels from corner velocity.

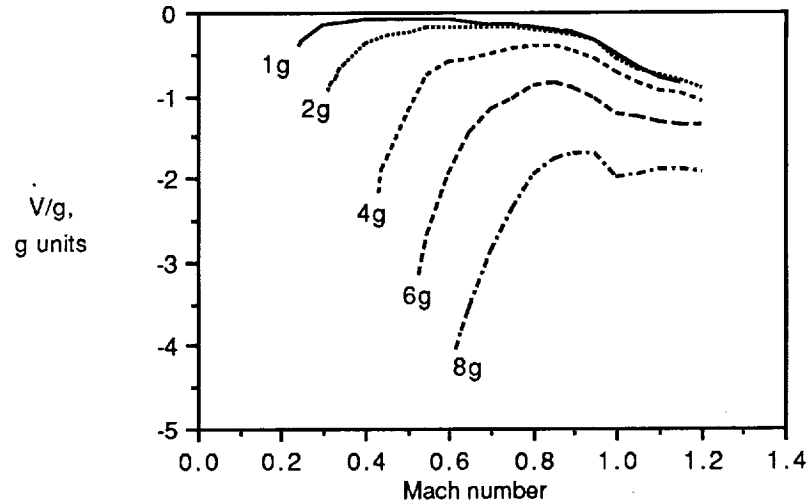

Figure A3. Maximum decels at $h = 15\,000$ ft from FLXTRM.

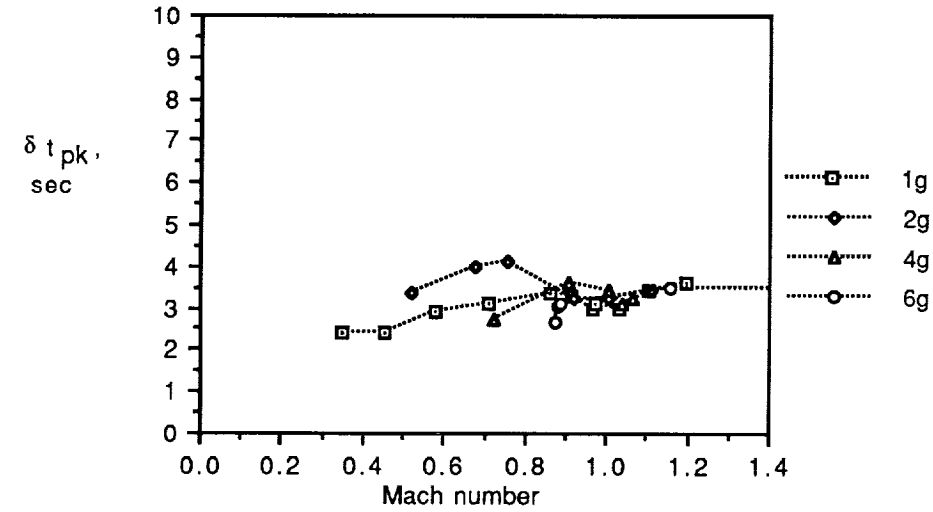

Figure A4. Time to peak decel (DMS data).

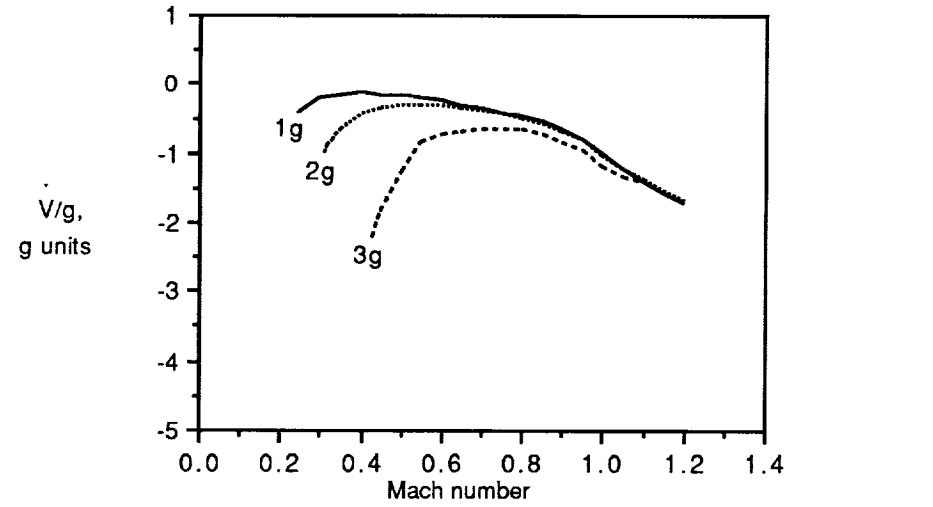

Figure A5. Decels at $h = 15\,000$ ft with speed brake (FLXTRM data).

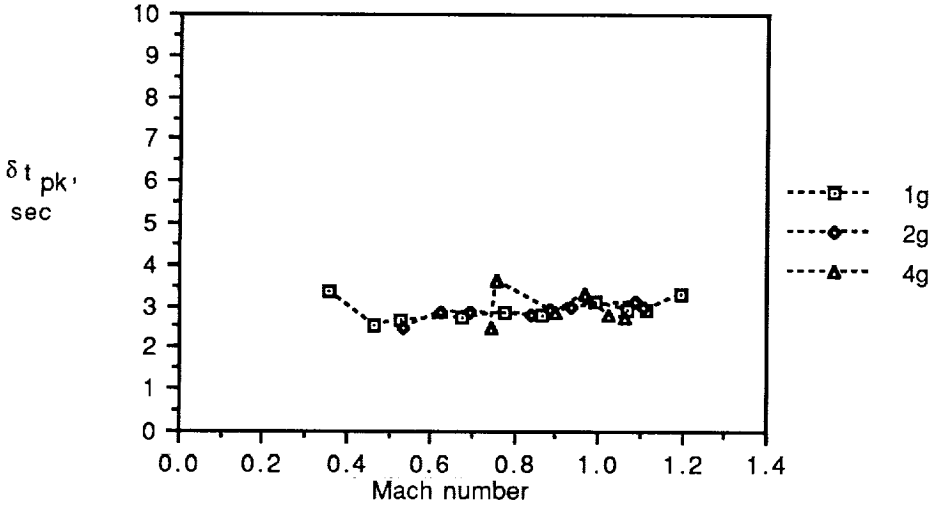

Figure A6. Time to decel with speed brake (DMS data).

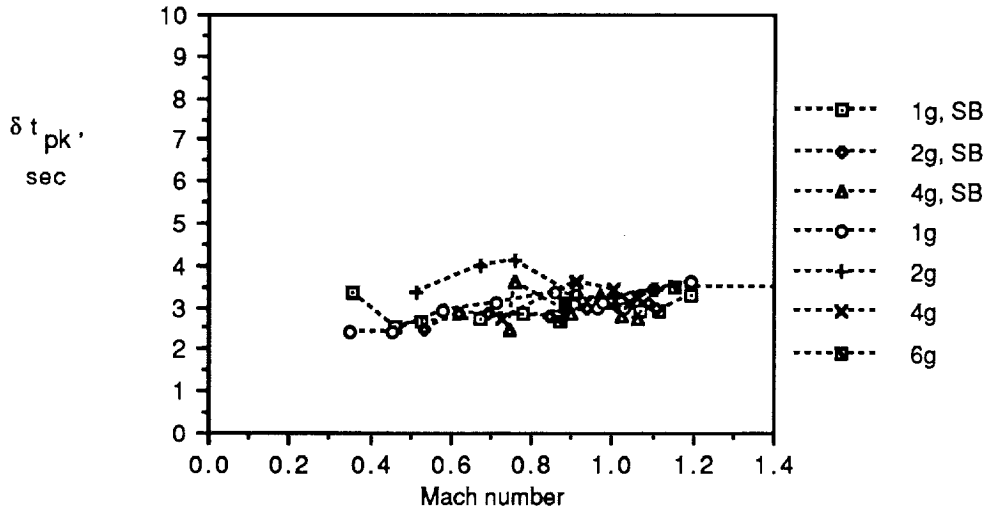

Figure A7. Time to peak decel (DMS data).

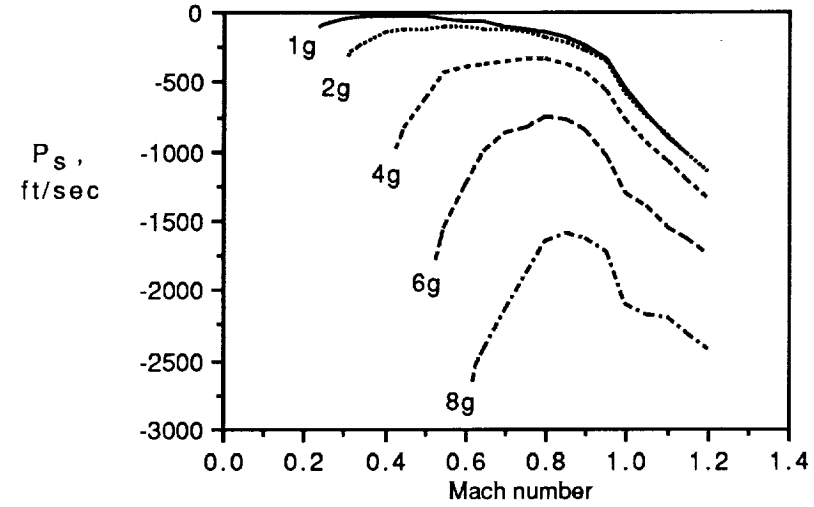

Figure A8. Specific excess power for decels.

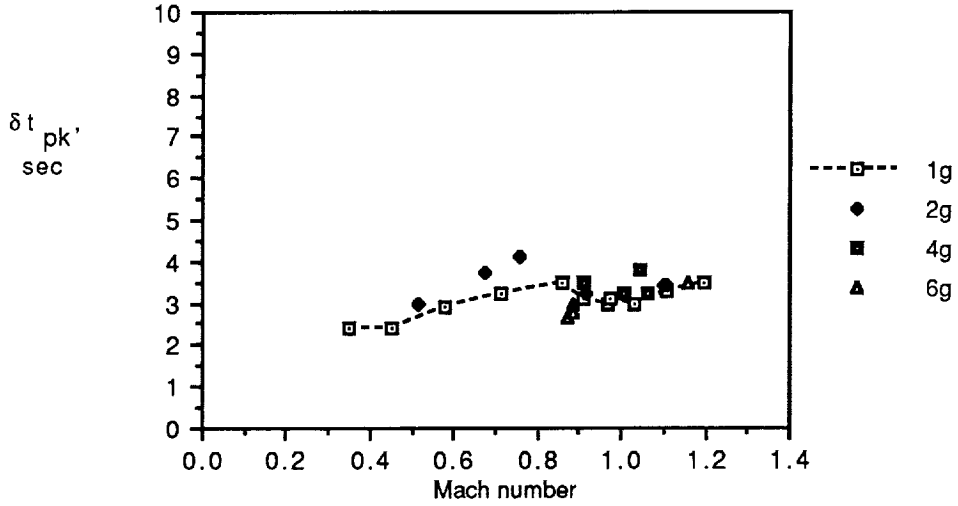

Figure A9. Time to peak P_s for decels.

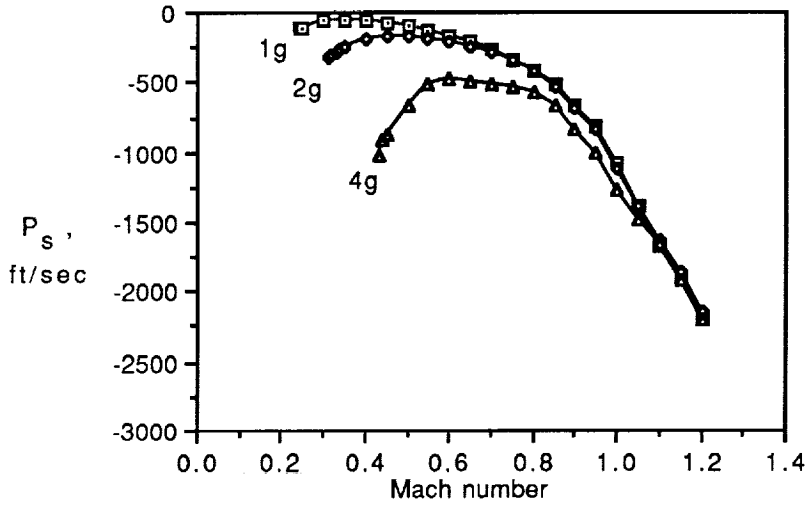

Figure A10. Specific excess power for decels with speed brake.

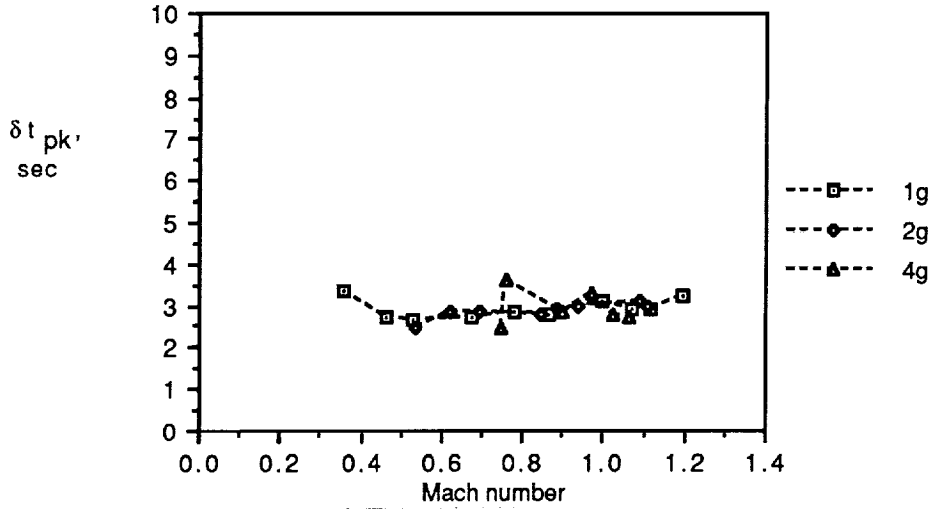

Figure A11. Time to peak P_s for decels with speed brake.

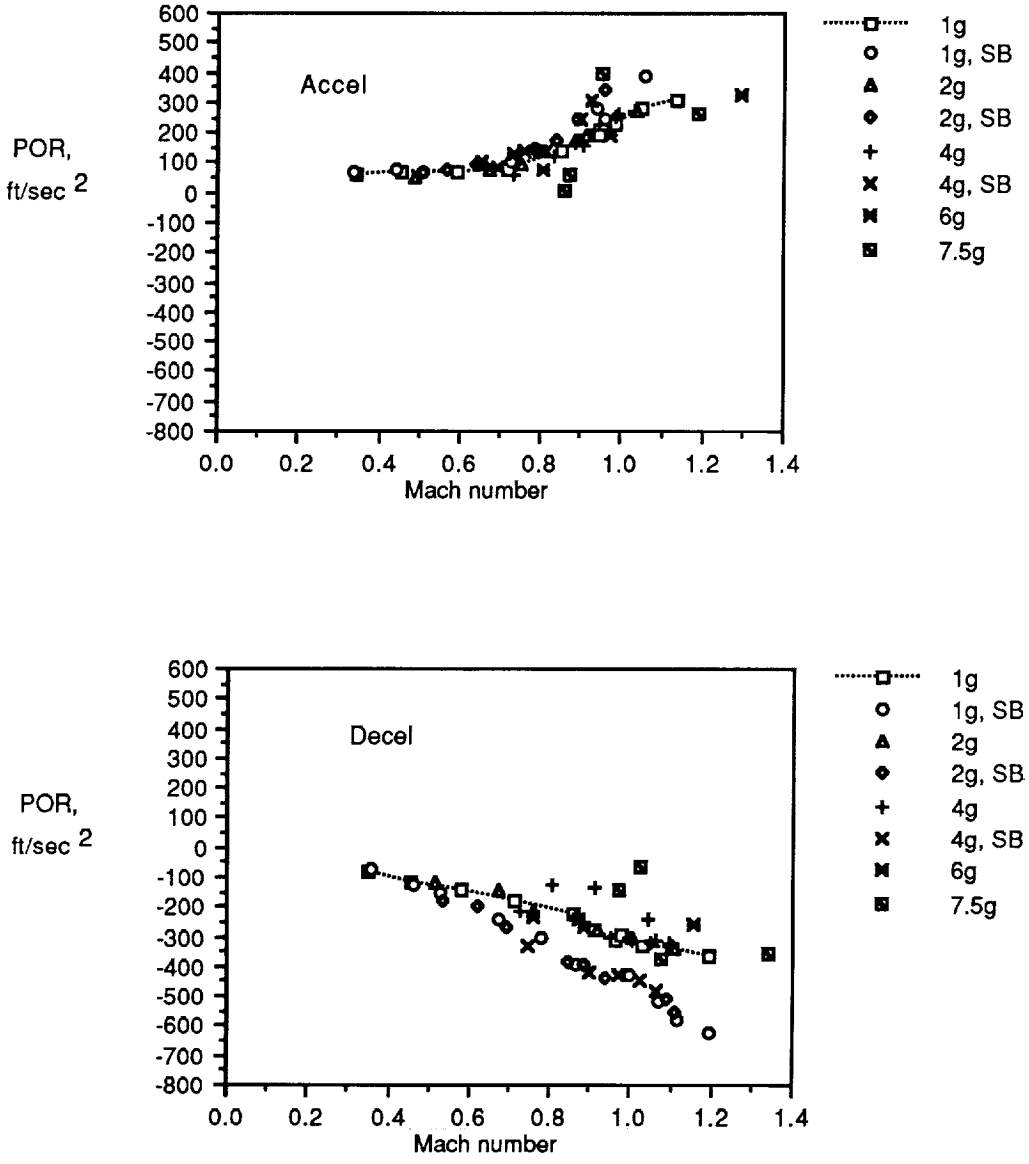

Figure A12. Power onset rate for accel-decel.

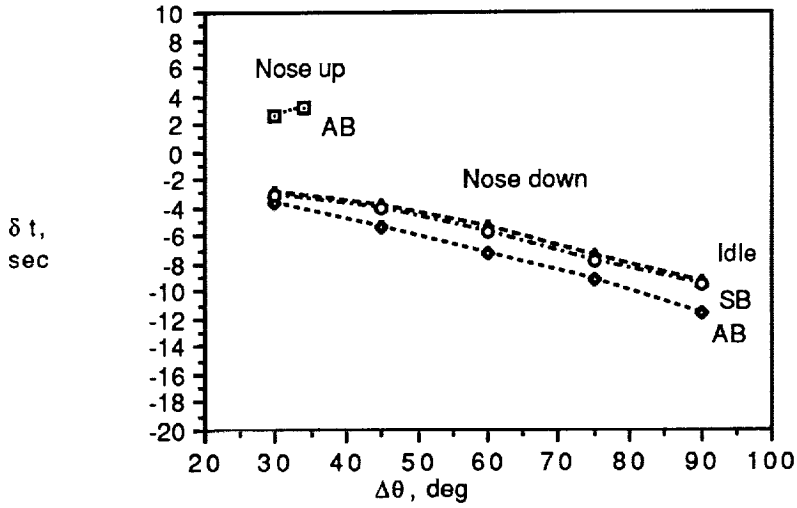

Figure A13. Time to achieve $\Delta\theta$ at Mach 0.2 and $h = 15\,000$ ft.

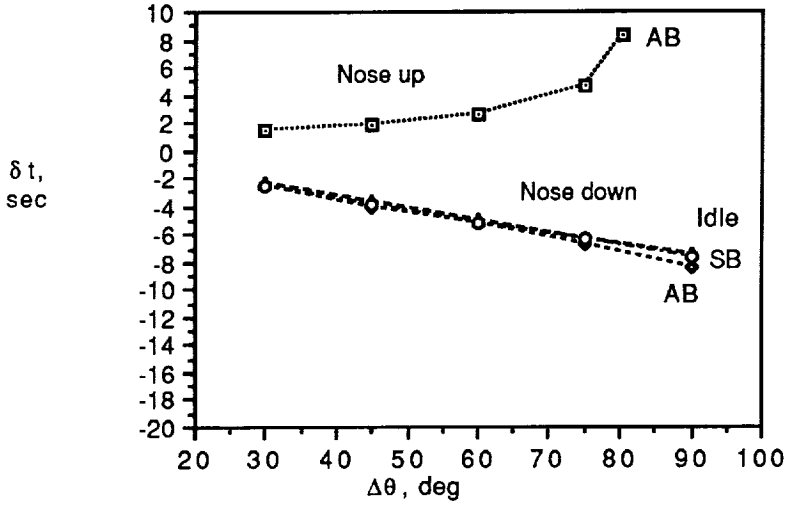

Figure A14. Time to achieve $\Delta\theta$ at Mach 0.4 and $h = 15\,000$ ft.

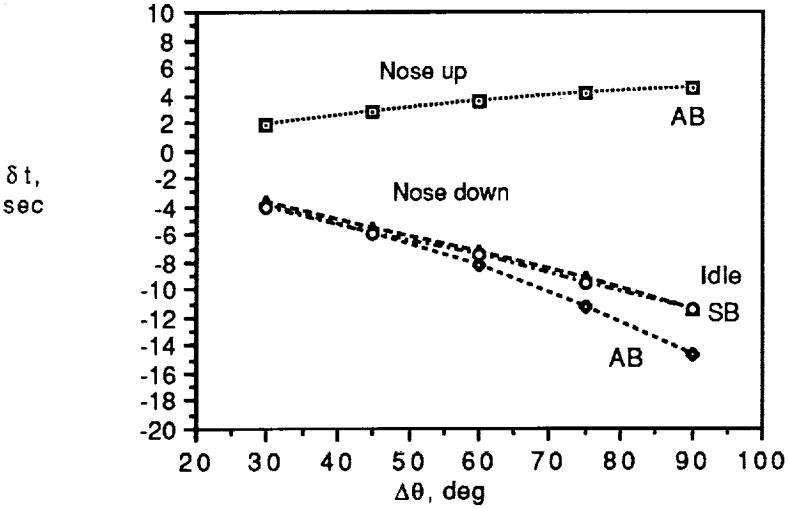

Figure A15. Time to achieve $\Delta\theta$ at Mach 0.8 and $h = 15\,000$ ft.

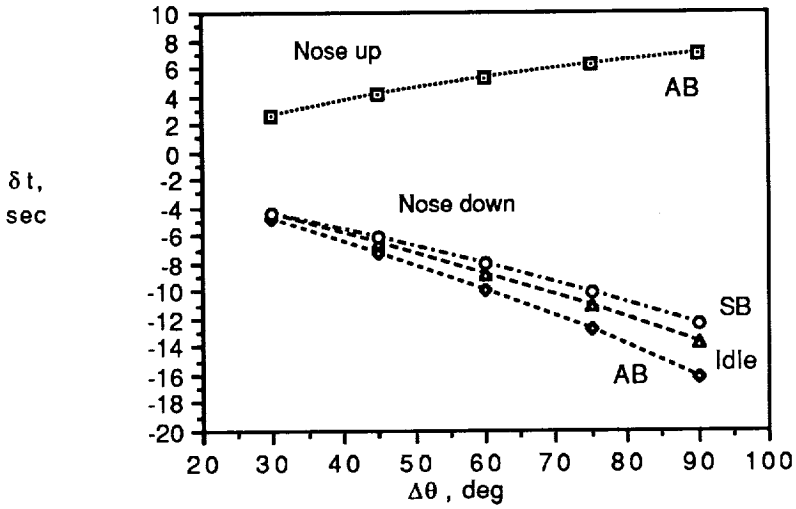

Figure A16. Time to achieve $\Delta\theta$ at Mach 1.0 and $h = 15\,000$ ft.

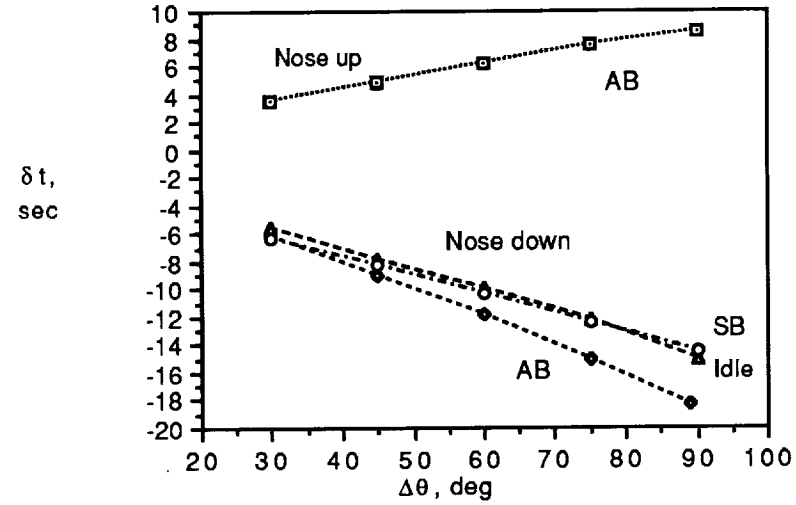

Figure A17. Time to achieve $\Delta\theta$ at Mach 1.2 and $h = 15\,000$ ft.

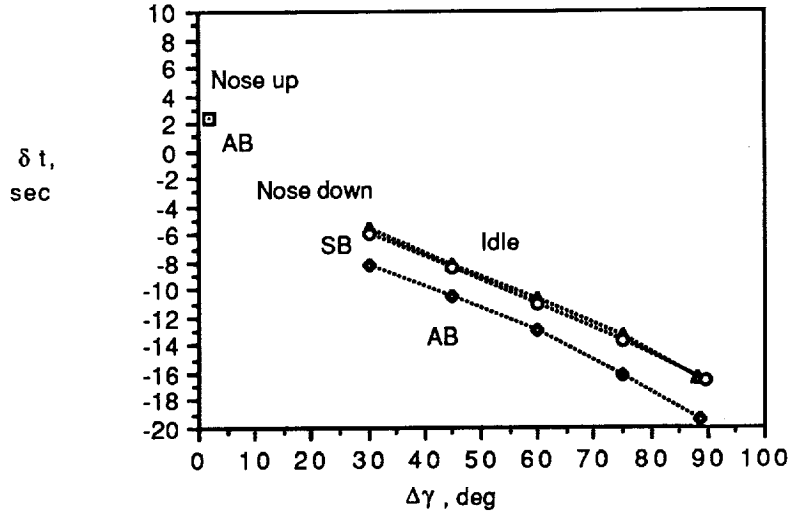

Figure A18. Time to achieve $\Delta\gamma$ at Mach 0.2 and $h = 15\,000$ ft.

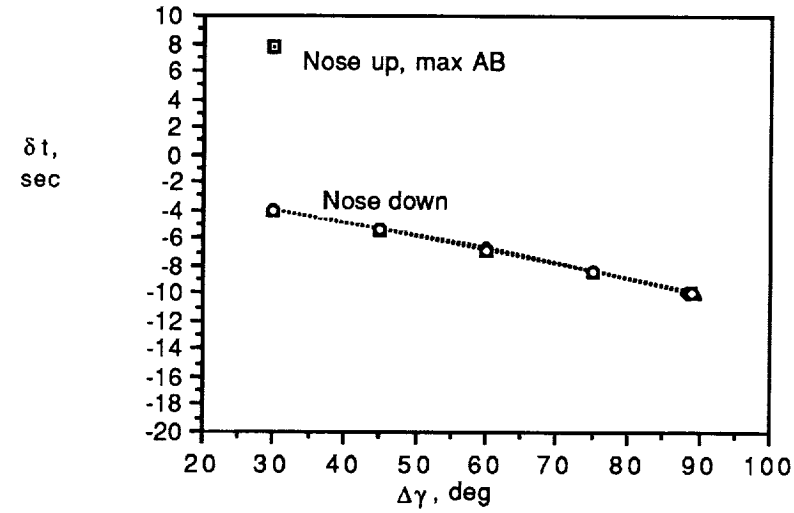

Figure A19. Time to achieve $\Delta\gamma$ at Mach 0.4 and $h = 15\,000$ ft.

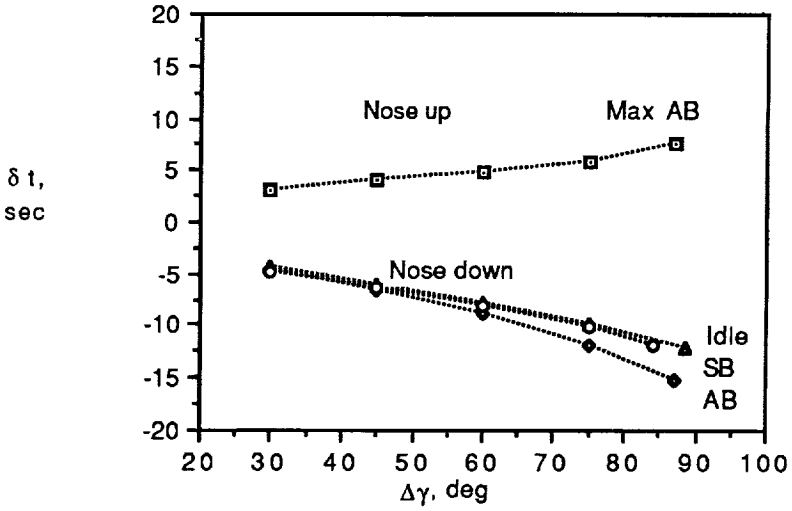

Figure A20. Time to achieve $\Delta\gamma$ at Mach 0.8 and $h = 15\,000$ ft.

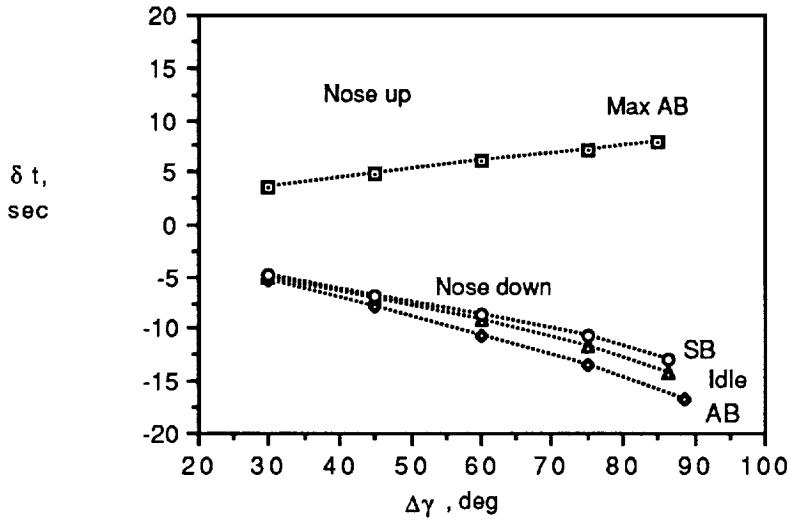

Figure A21. Time to achieve $\Delta\gamma$ at Mach 1.0 and $h = 15\,000$ ft.

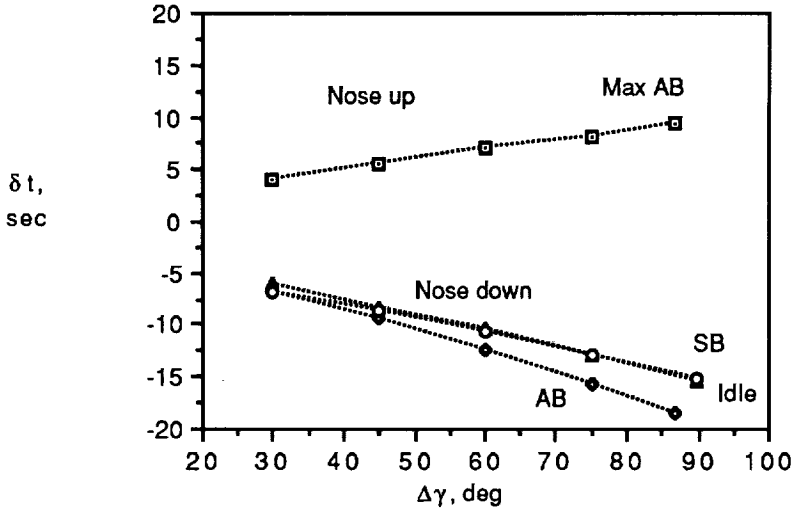

Figure A22. Time to achieve $\Delta\gamma$ at Mach 1.2 and $h = 15\,000$ ft.

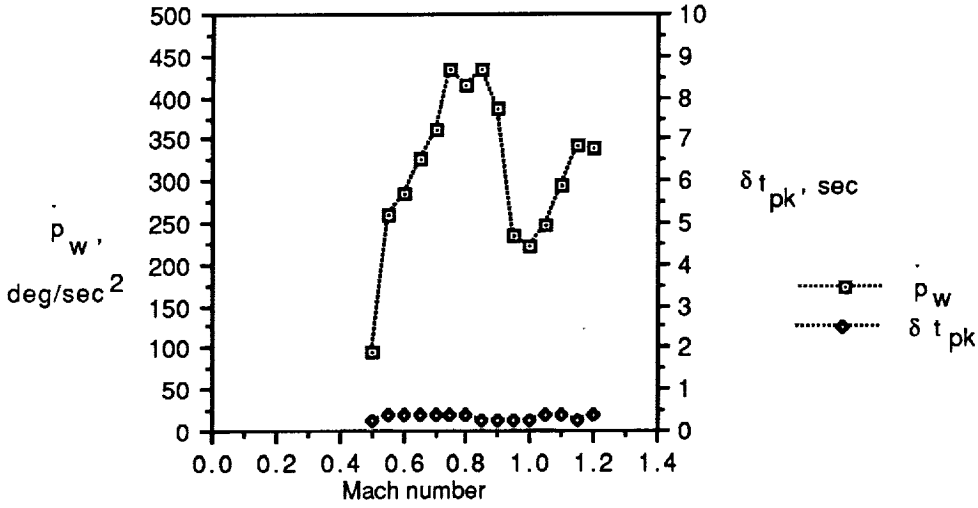

(a) Peak roll accel and time to peak.

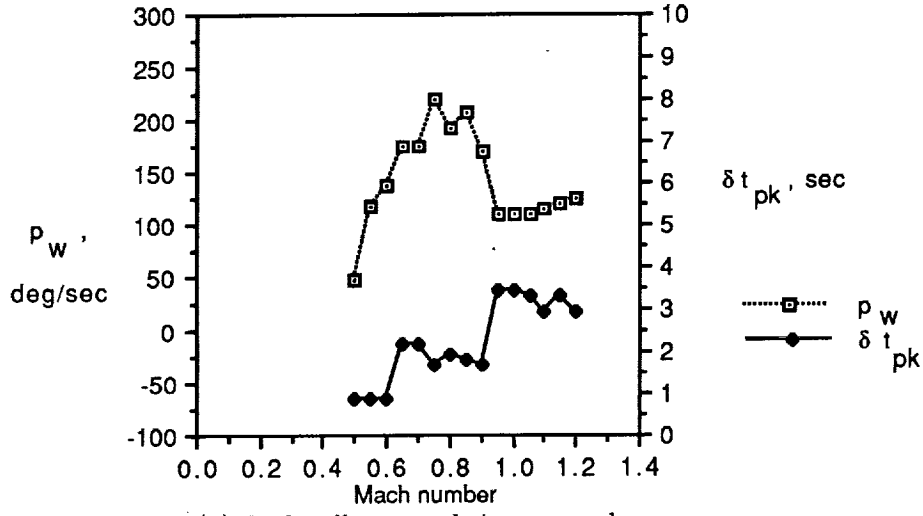

(b) Peak roll rate and time to peak.

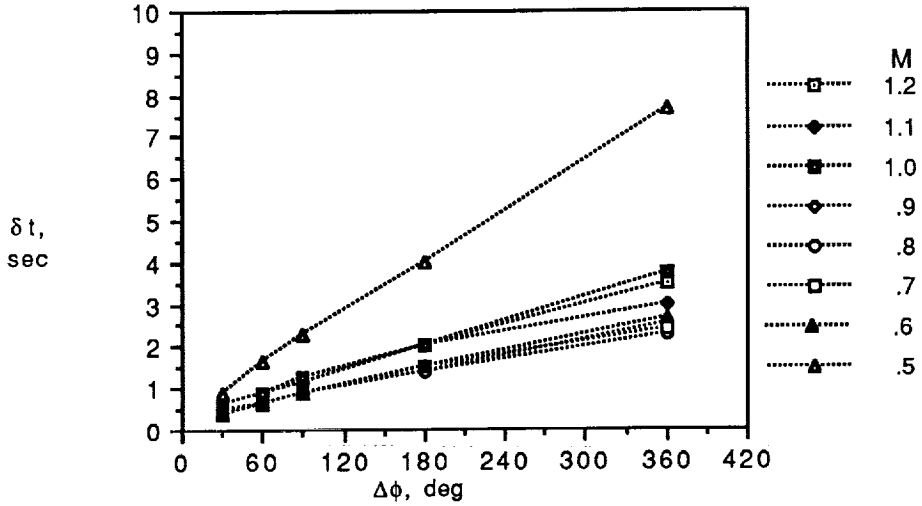

(c) Time to roll through $\Delta\phi$.

Figure A23. Wind-axis roll capability for flight load of $4g$ and $h = 15\,000$ ft.

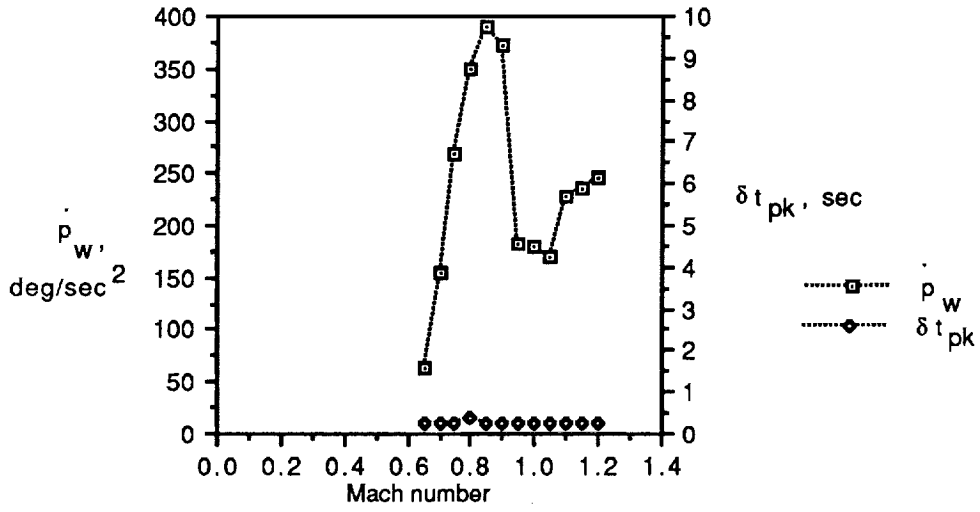

(a) Peak roll accel and time to peak.

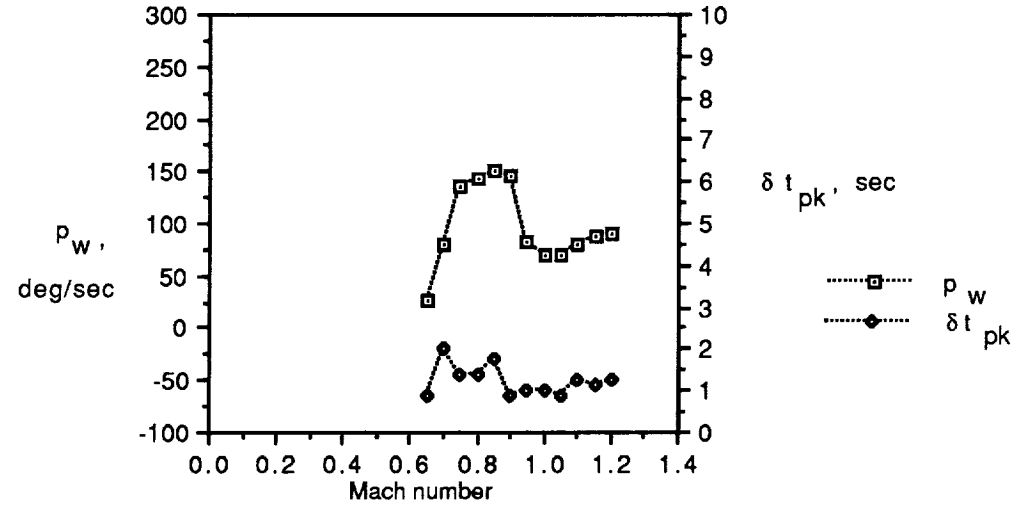

(b) Peak roll rate and time to peak.

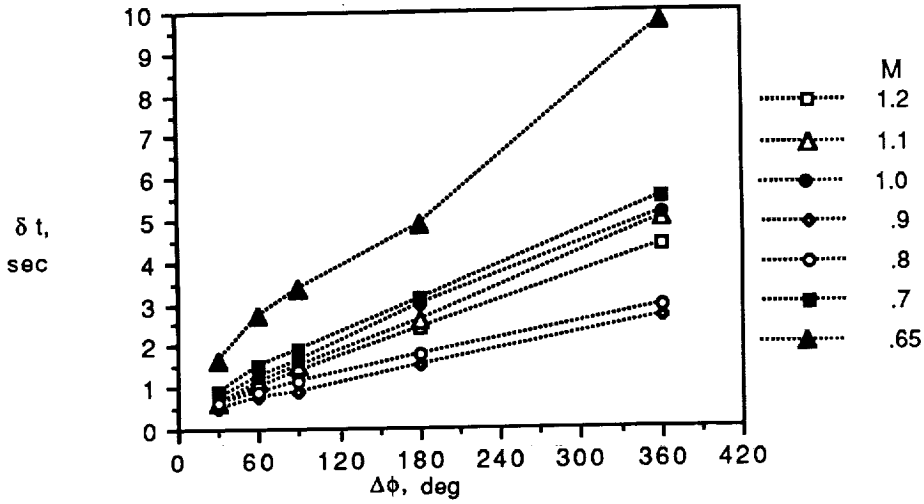

(c) Time to roll through $\Delta\phi$.

Figure A24. Wind-axis roll capability for flight load of $6g$ and $h = 15\,000$ ft.

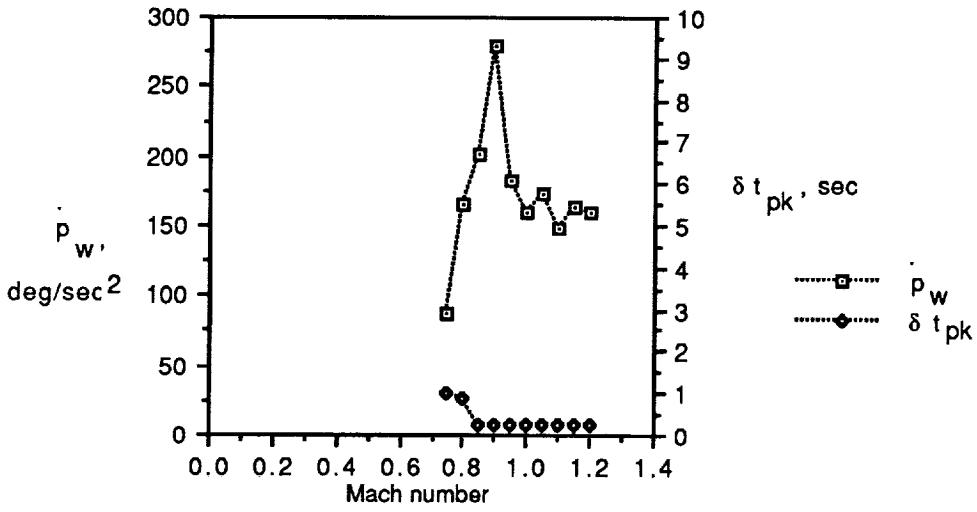

(a) Peak roll accel and time to peak.

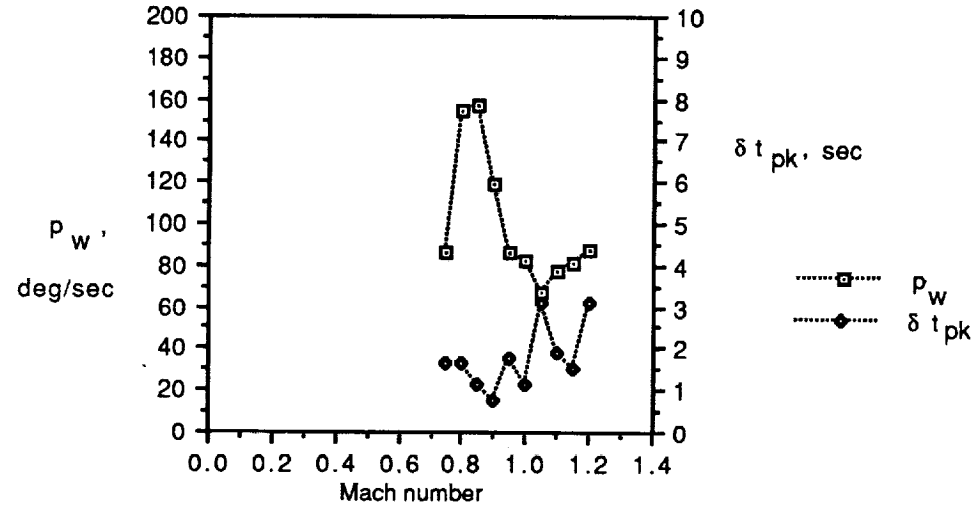

(b) Peak roll rate and time to peak.

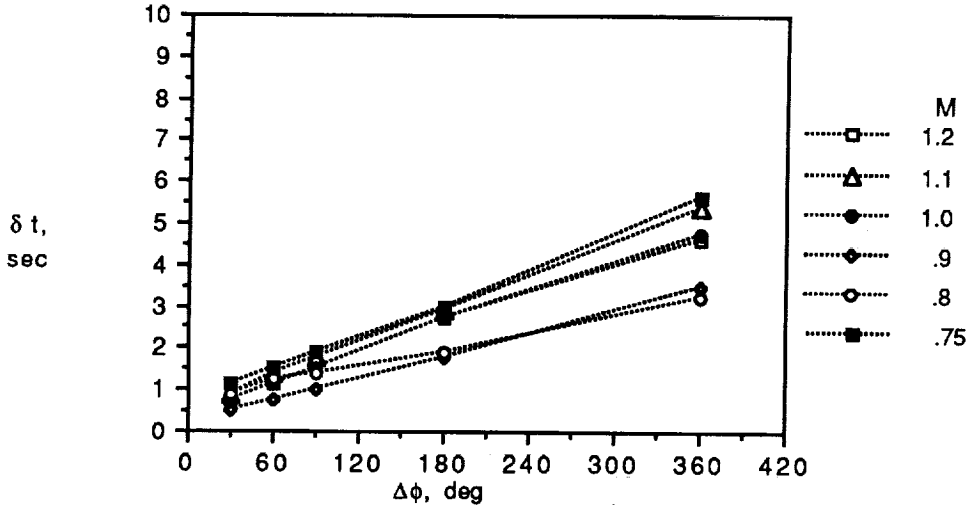

(c) Time to roll through $\Delta\phi$.

Figure A25. Wind-axis roll capability for flight load of $7.5g$ and $h = 15\,000$ ft.

References

1. *Military Standard—Flying Qualities of Piloted Aircraft.* MIL-STD-1797A, Jan. 30, 1990. (Supersedes MIL-STD-1797(USAF), Mar. 31, 1987.)
2. Foltyn, Robert W.; Skow, Andrew M.; Lynch, Urban H.; Lynch, Andrew M. P.; Laboy, Orlando J.; and Arand, Anthony J.: *Development of Innovative Air Combat Measures of Merit for Supermaneuverable Fighters.* AFWAL-TR-87-3073, U.S. Air Force, Oct. 1987.
3. Hodgkinson, J.; Skow, A.; Ettinger, R.; Lynch, U.; Laboy, O.; Chody, J.; and Cord, T. J.: Relationships Between Flying Qualities, Transient Agility, and Operational Effectiveness of Fighter Aircraft. AIAA-88-4329, Aug. 1988.
4. Phillips, William H.: *Analysis of Effects of Interceptor Roll Performance and Maneuverability on Success of Collision-Course Attacks.* NACA RM L58E27, 1958.
5. McAtee, Thomas P.: Agility in Demand. *Aerosp. America,* vol. 26, no. 5, May 1988, pp. 36–38.
6. Tamrat, B. F.: Fighter Aircraft Agility Assessment Concepts and Their Implication on Future Agile Fighter Design. AIAA-88-4400, Sept. 1988.
7. Skow, Andrew M.; Hamilton, William L.; and Taylor, John H.: Advanced Fighter Agility Metrics. AIAA-85-1779, Aug. 1985.
8. Taylor, John H.; Skow, Andrew M.; Parker, Robert W.; Malcolm, Gerald N.; and Foltyn, Robert W.: *Flight Test Validation of Advanced Agility Metrics for T-38 and F-4.* TR 86-212 (USAF Contract F33615-85-C-0120, P00001), Eidetics International, Inc., Sept. 1986.
9. Skow, Andrew M.; Foltyn, Robert W.; Taylor, John H.; and Parker, Robert W.: *Transient Performance and Maneuverability Measures of Merit for Fighter/Attack Aircraft.* TR 86-201 (USAF Contract F33615-85-C-0120), Eidetics International, Inc., Jan. 1986.
10. Schmidt, David K.; and Innocenti, Mario: *Pilot-Optimal Multivariable Control Synthesis by Output Feedback.* NASA CR-163112, 1981.
11. Bitten, R.: Qualitative and Quantitative Comparison of Government and Industry Agility Metrics. *A Collection of Technical Papers—AIAA Atmospheric Flight Mechanics Conference,* Aug. 1989, pp. 368–376. (Available as AIAA-89-3389-CP.)
12. Stucky, Paul R.: Instructional Text, F-15 Basic Fighter Maneuvers—Course F1500IDOPN, F-15. USAF Fighter Weapons School, Nellis Air Force Base, Nevada, Oct. 1982.
13. Pelikan, R. J.; and Swingle, R. L.: *F/A-18 Stability and Control Data Report. Volume I: Low Angle of Attack.* MDC A7247 (Contract No. N00019-75-C-0424), McDonnell Aircraft Co., Aug. 31, 1981. (Revised Nov. 15, 1982.)
14. Hobbs, C. R.: *F/A-18 Stability and Control Data Report. Volume II: High Angle of Attack.* MDC A7247 (Contract No. N00019-75-C-0424), McDonnell Aircraft Co., Aug. 31, 1981.
15. Groll, D. B.; Hess, R. K.; Hodges, W. D.; and Moomaw, R. F.: *F/A-18A Flight Control System Design Report. Volume I—System Description and Theory of Operation.* MDC A7813, Vol. I (Contract No. N00019-75-C-0424), McDonnell Aircraft Co., Dec. 23, 1982. (Revised Sept. 28, 1984.)
16. Moomaw, R. F.; Trame, L. W.; and Hess, R. K.: *F/A-18A Flight Control System Design Report. Volume II—Flight Control System Analysis—Inner Loops.* MDC A7813, Vol. II (Contract No. N00019-75-C-0424), McDonnell Aircraft Co., June 15, 1984. (Revised Aug. 30, 1985.)
17. Adams, William M., Jr.: *SPINEQ: A Program for Determining Aircraft Equilibrium Spin Characteristics Including Stability.* NASA TM-78759, 1978.
18. Etkin, Bernard: *Dynamics of Atmospheric Flight.* John Wiley & Sons, Inc., c.1972.
19. Herbst, W. B.: Dynamics of Air Combat. *J. Aircr.,* vol. 20, no. 7, July 1983, pp. 594–598.
20. Ziegler, J. G.; and Nichols, N. B.: Optimum Settings for Automatic Controllers. *Trans. A.S.M.E.,* vol. 64, no. 8, 1942, pp. 759–768.

Table I. Classic Point Performance Measures

[Data are for $h = 15\,000$ ft and 60 percent fuel unless otherwise indicated]

Weight, lb	32 366
Area, S, ft^2	400
Wing loading, W/S, lb/ft^2	81
Thrust (in afterburner at sea level), lbf	32 000
Thrust-to-weight ratio, T/W (sea level)	0.99
Thrust-to-weight ratio, T/W	0.52
Corner velocity, V_c (instantaneous)	Mach 0.62
Corner velocity, V_c (sustained)	Mach 0.80
Minimum horizontal turn radius at Mach 0.80, ft	3824
Minimum horizontal turn radius at Mach 0.25, ft	2135
Maximum horizontal turn rate at Mach 0.80, deg/sec	12.7
Maximum horizontal turn rate at Mach 0.62, deg/sec	31.2
Mach number, maximum	1.60
Mach number, minimum (for level flight)	0.20
Load factor (sustainable), g units	5.9
Load factor (control system limit), g units	7.5
Rate of climb ($M = 0.94$), ft/sec	590
Terminal Mach number (dive)	1.84

Table II. Transfer Function and Functional Agility for Pitch Metrics

$[M = 0.6]$

Metric	K, deg/sec	τ, sec	τ_d, sec	Peak, deg/sec	δt_{pk}, sec	m, deg/sec^2
q	47	0.40	0.23	47	0.76	118
q_w	16	.45	.42	16	1.37	36
$\dot{q}$	113	.30	.08	113	.38	377
$\dot{q}_w$	32	.24	.28	32	.52	133

Table III.Torsional Transfer Function and Functional Agility Metrics

$[M = 0.8]$

(a) Wind-axis roll rate						
N_z, g units	K, deg/sec	τ, sec	τ_d, sec	Peak, deg/sec^2	δt_{pk}, sec	m, deg/sec^2
1.0	219	0.42	0.10	219	0.73	521
2.0	218	.40	.14	218	.82	545
3.0	215	.41	.14	215	.87	524
4.0	184	.42	.14	184	.80	438
5.0	147	.32	.16	147	.94	459
6.0	140	.39	.12	140	1.22	359
7.5	147	.63	.15	147	1.40	233
(b) Wind-axis roll acceleration						
N_z, g units	K, deg/sec	τ, sec	τ_d, sec	Peak, deg/sec^2	δt_{pk}, sec	m, deg/sec^3
1.0	520	0.13	0.03	520	0.28	4000
2.0	510	.16	.03	510	.28	3188
3.0	495	.14	.05	495	.29	3536
4.0	470	.12	.07	470	.29	3917
5.0	430	.12	.07	430	.29	3583
6.0	375	.12	.06	375	.26	3125
7.5	188	.07	.08	188	.19	2686

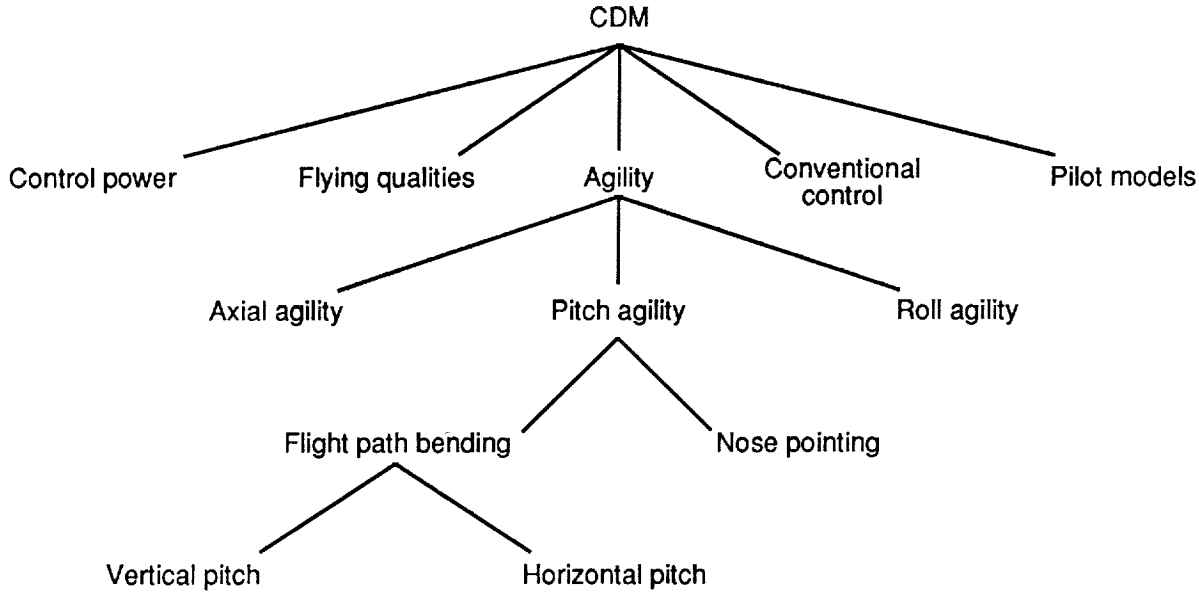

Figure 1. Metric categories.

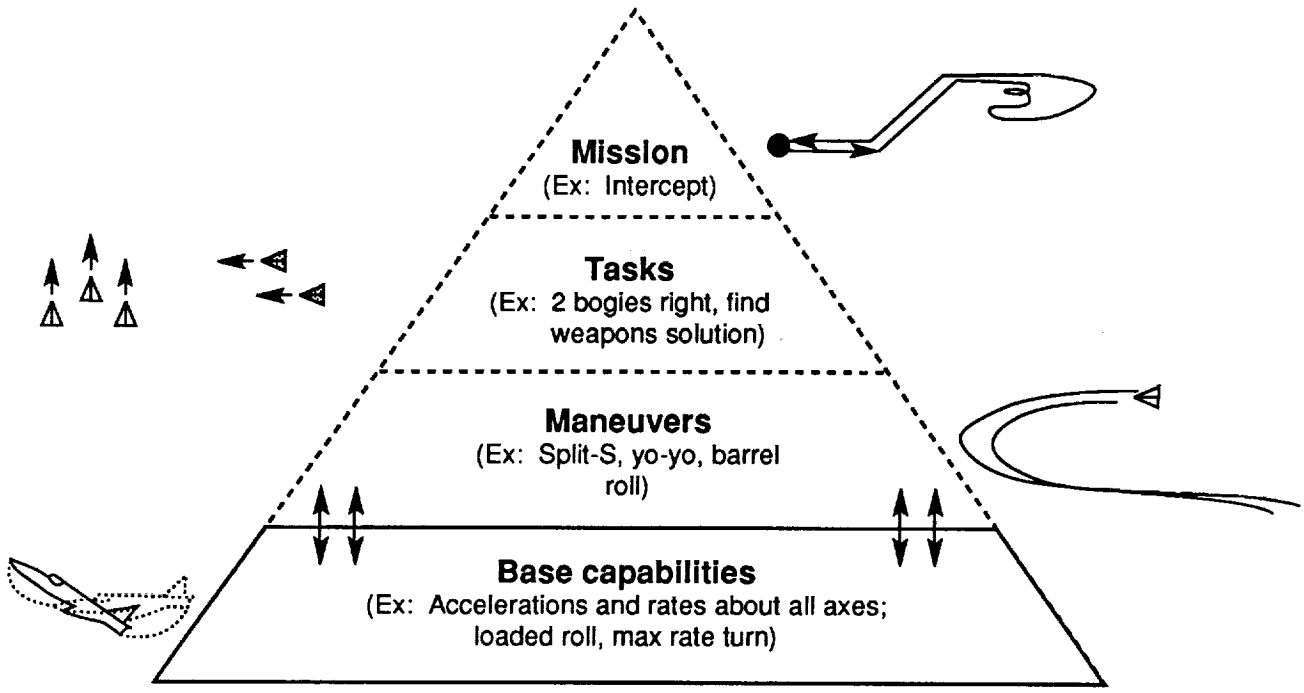

Figure 2. Design pyramid.

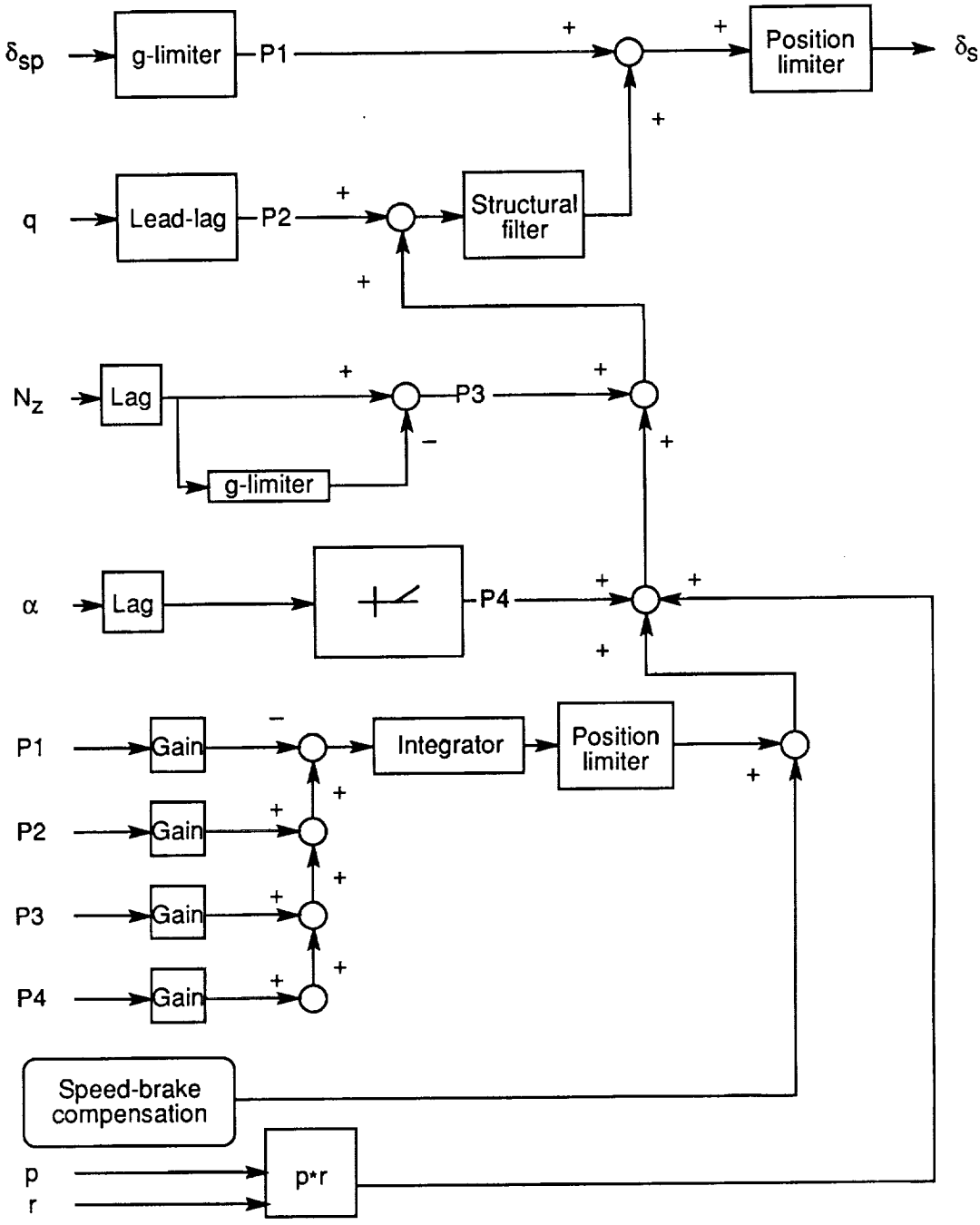

Figure 3. Longitudinal controller.

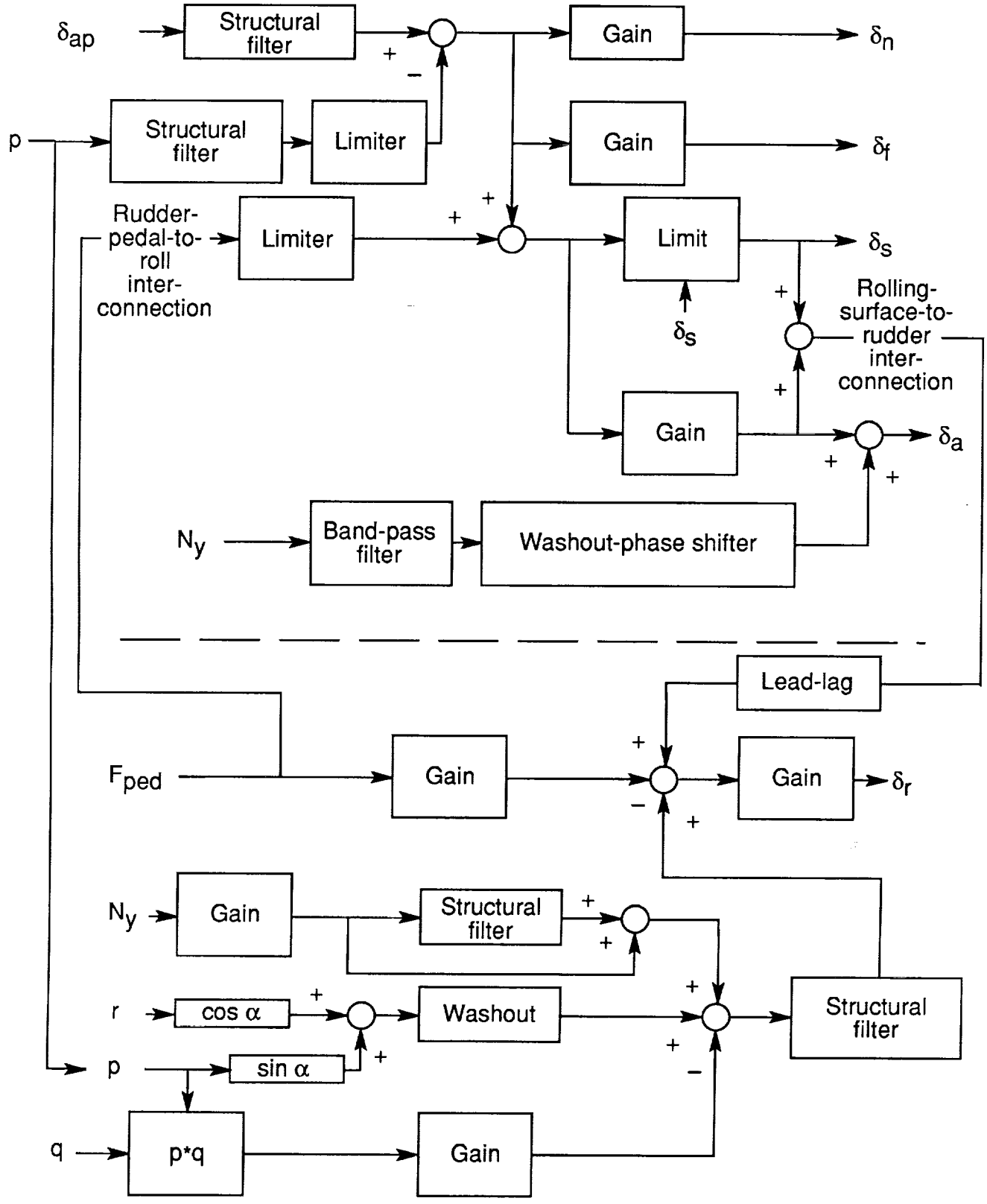

Figure 4. Lateral-directional controller.

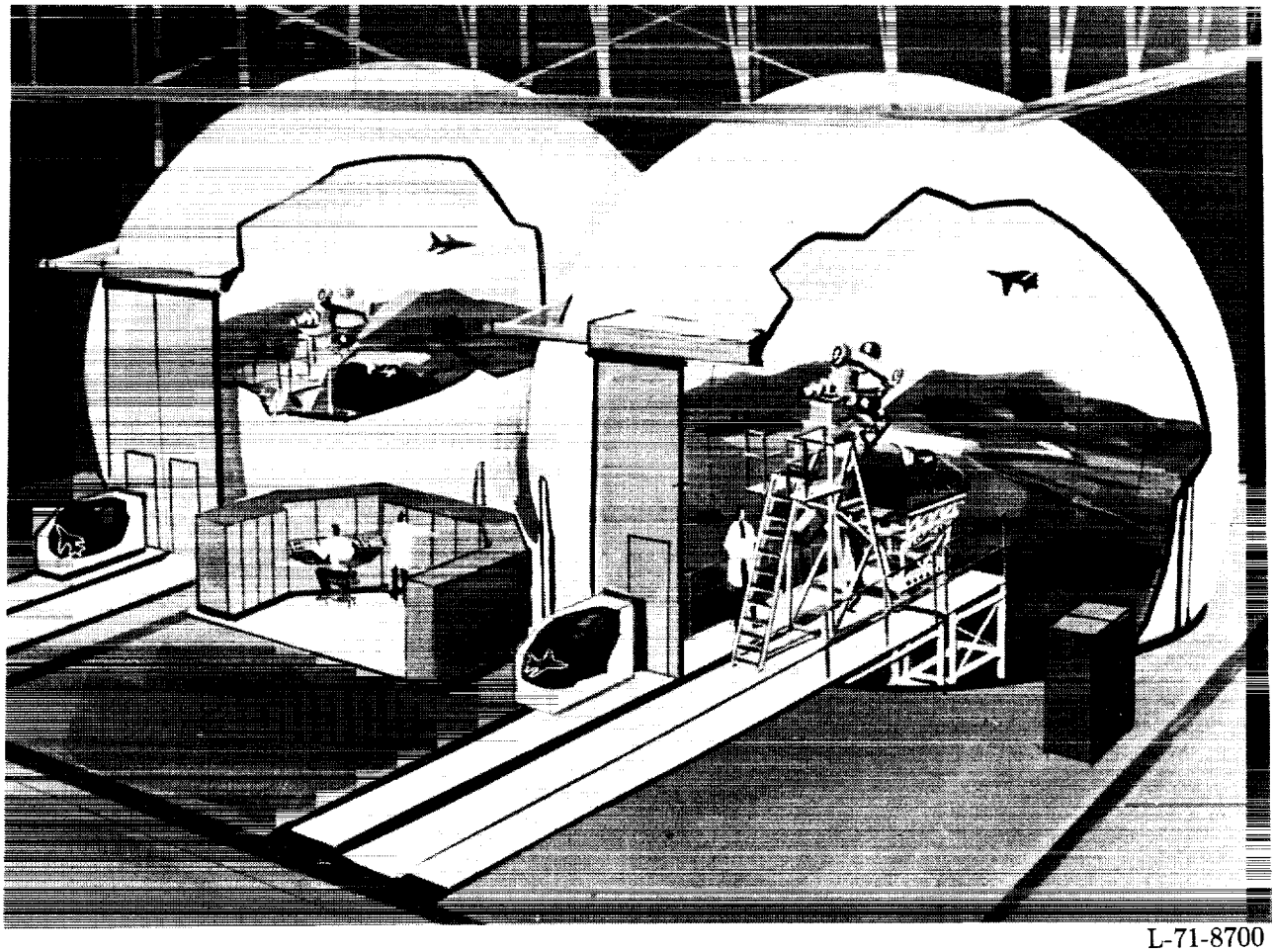

L-71-8700

Figure 5. Langley Differential Maneuvering Simulator.

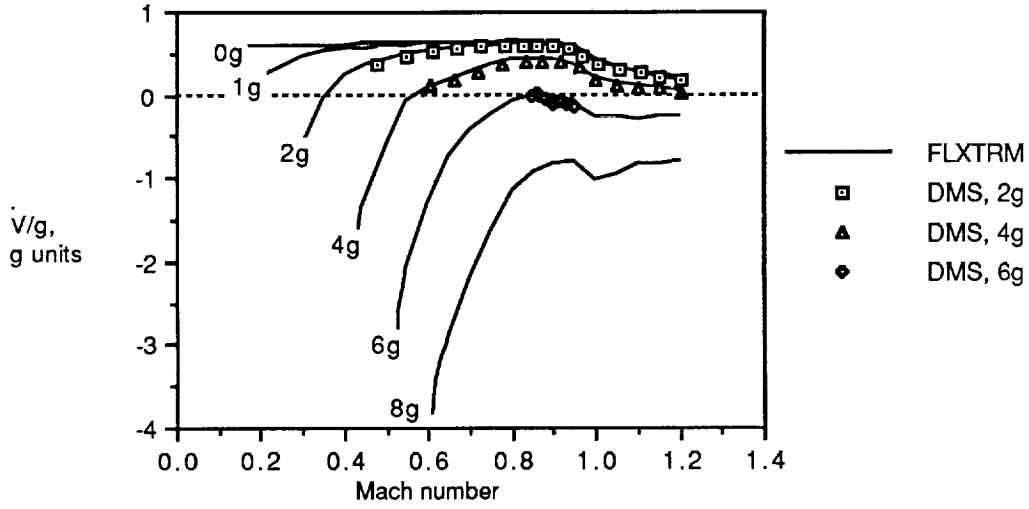

Figure 6. DMS and FLXTRM peak accelerations. $h = 15\,000$ ft.

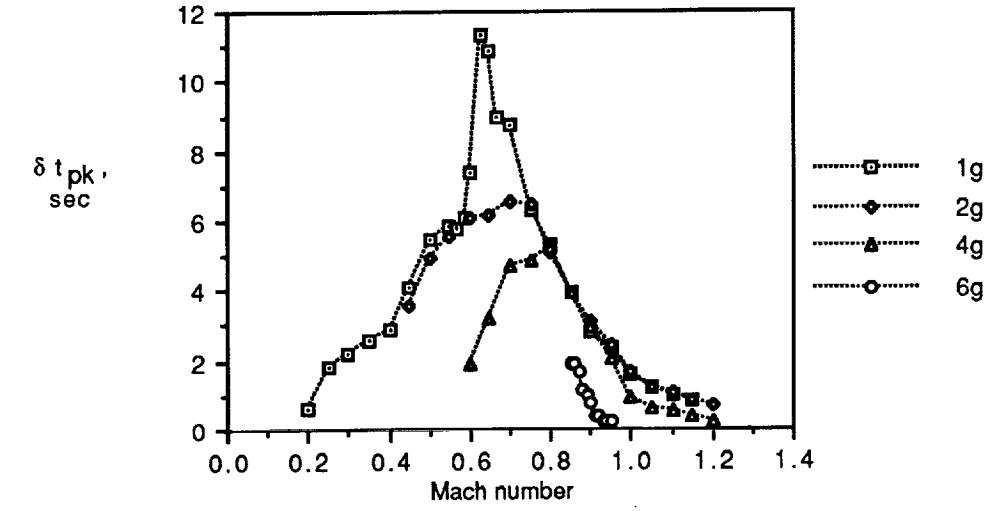

Figure 7. Time to peak acceleration from DMS.

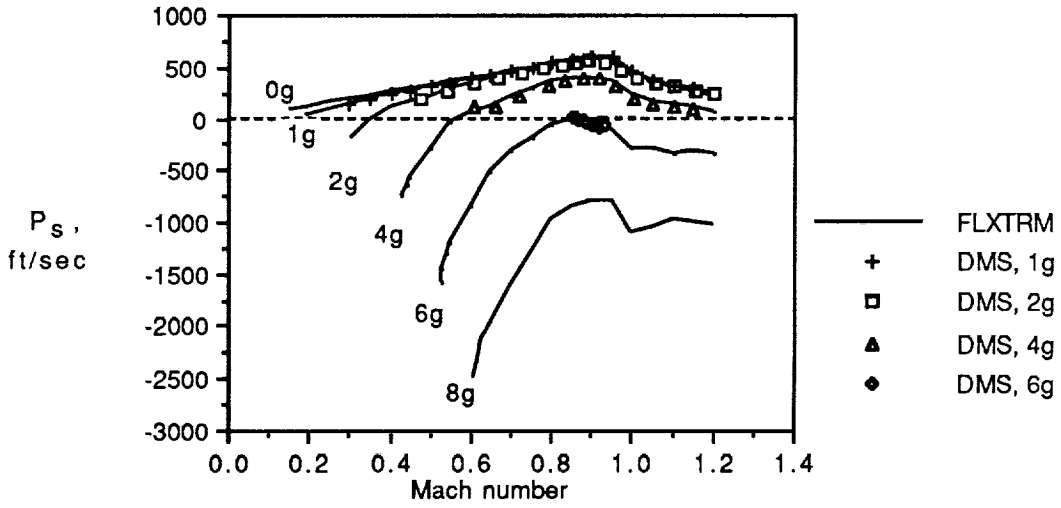

Figure 8. Specific excess power P_s from accels from DMS and FLXTRM.

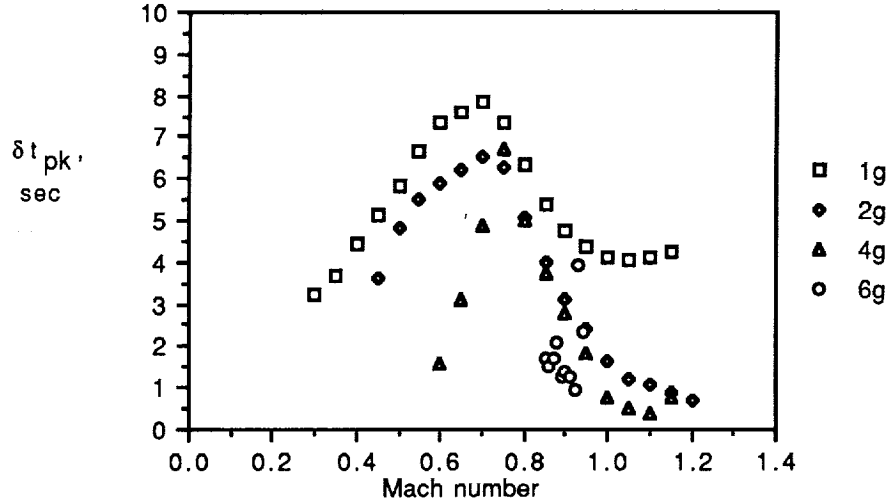

Figure 9. Time to peak P_s for accels.

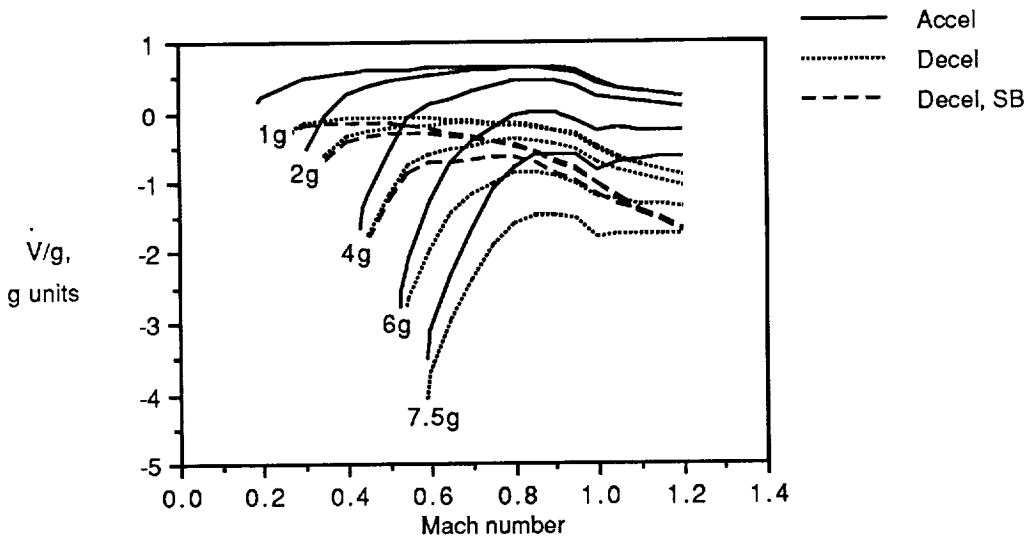

Figure 10. Accels and decels from FLXTRM data.

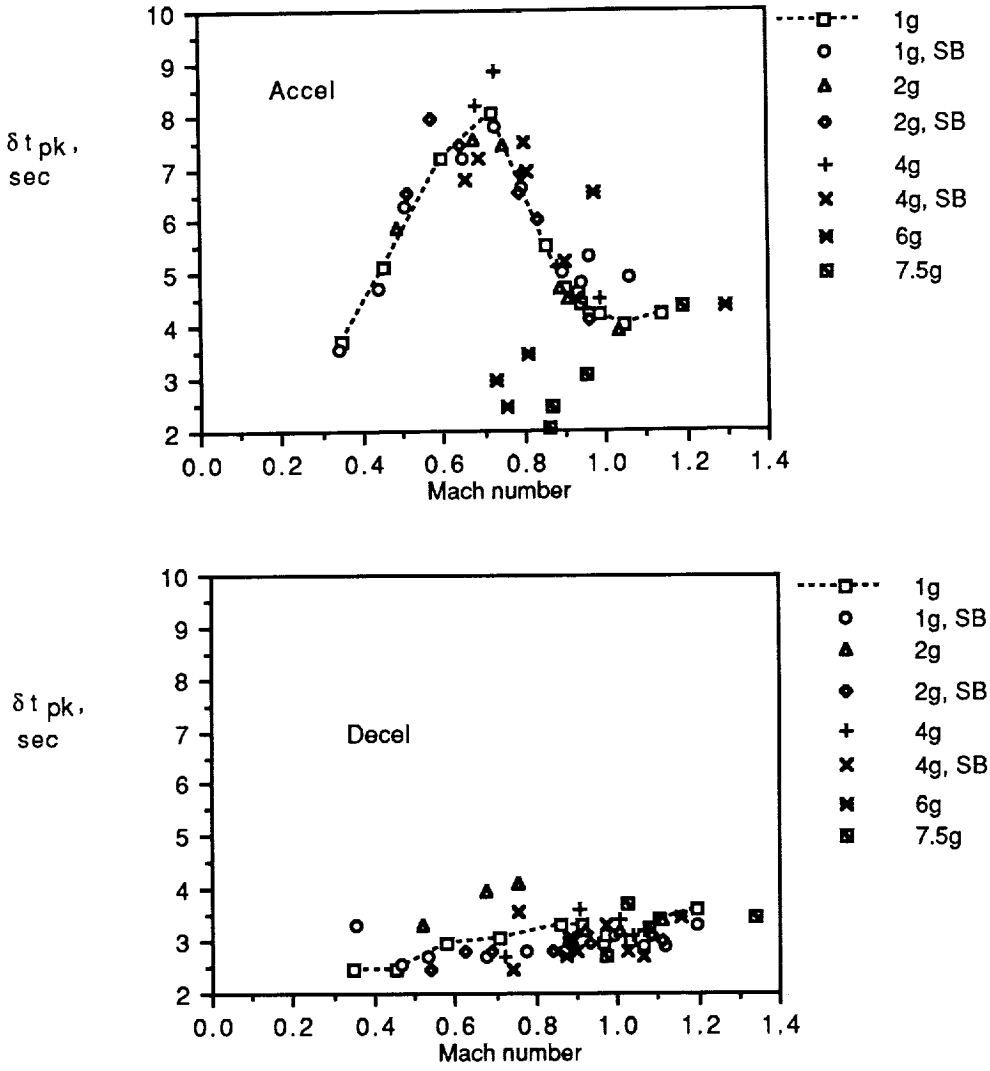

Figure 11. Time to peak accel and time from peak accel to peak decel (DMS data).

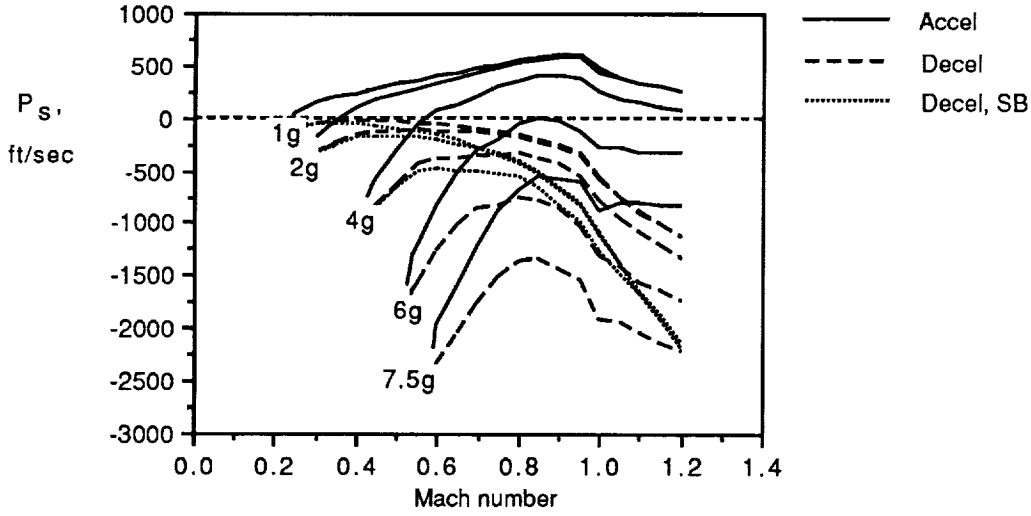

Figure 12. Specific excess power P_s for accel-decel (FLXTRM data).

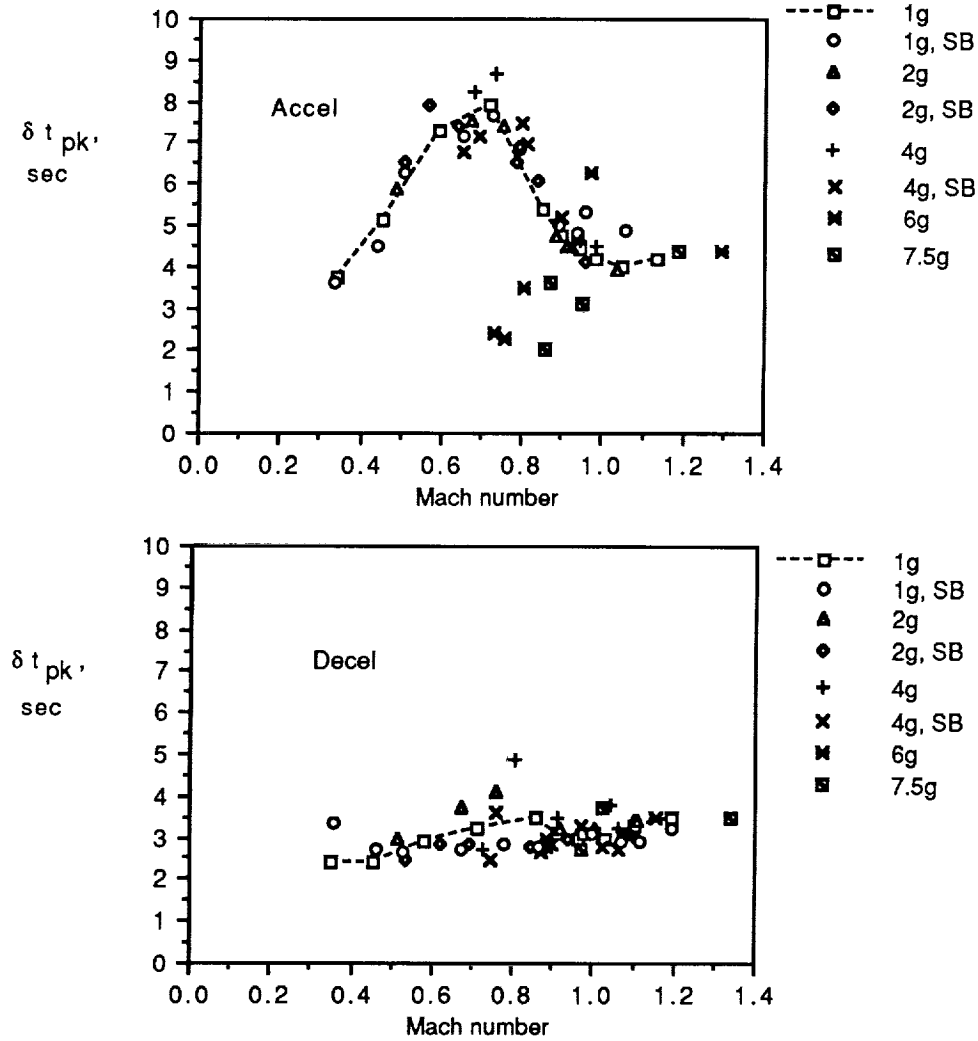

Figure 13. Time to peak P_s for accel-decel.

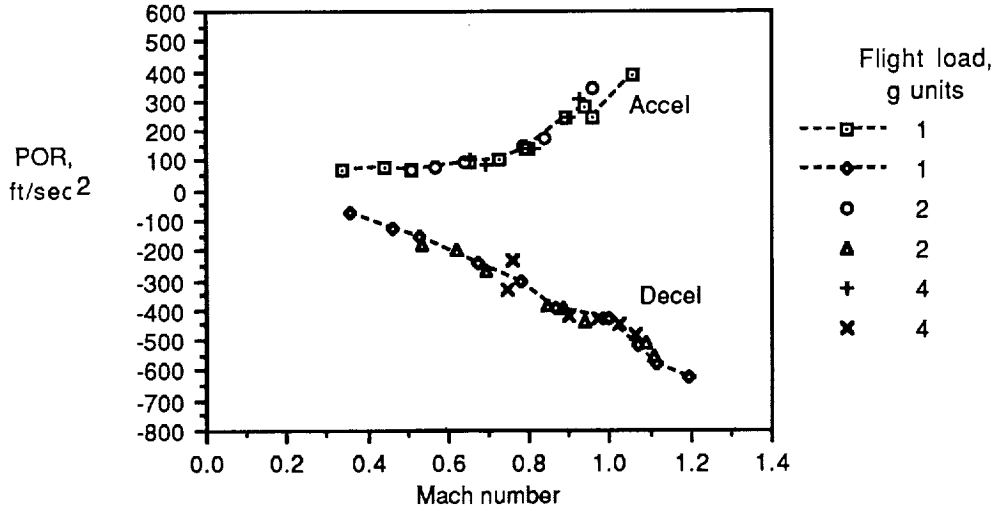

Figure 14. Power onset rate for accels-decels with speed brake.

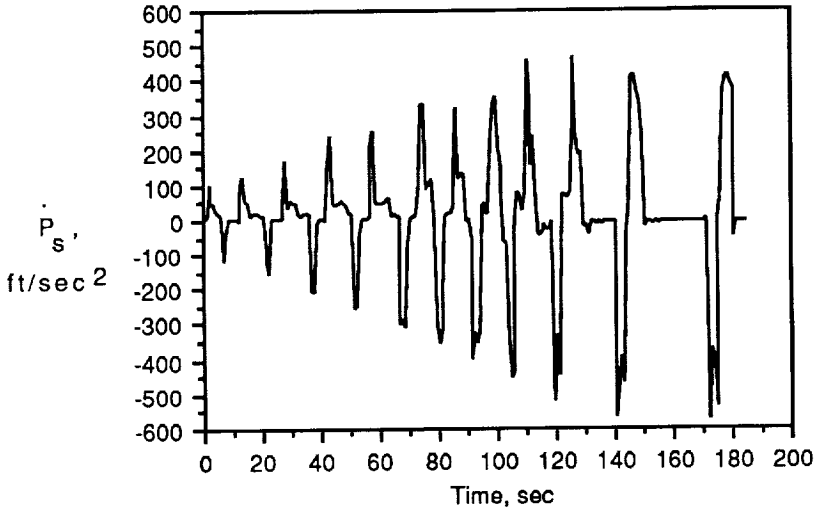

Figure 15. Time history of $\dot{P}_s$ for accel-decel BKM. Flight load, $1g$.

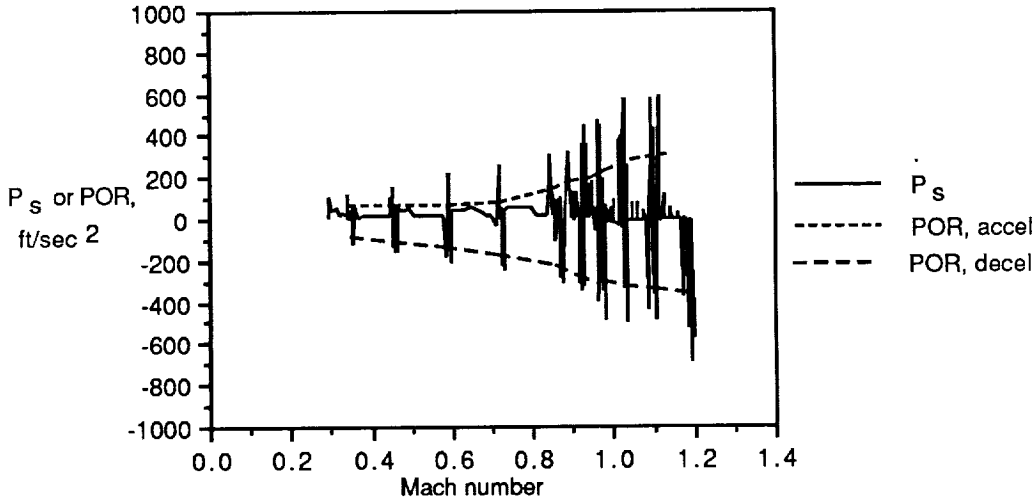

Figure 16. Values of $\dot{P}_s$ and POR for $1g$ accel-decel BKM.

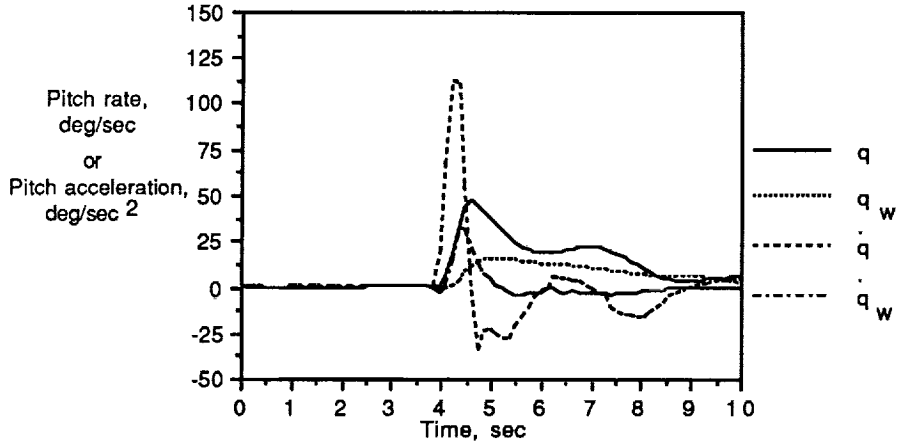

(a) Body- and wind-axis rates and accelerations.

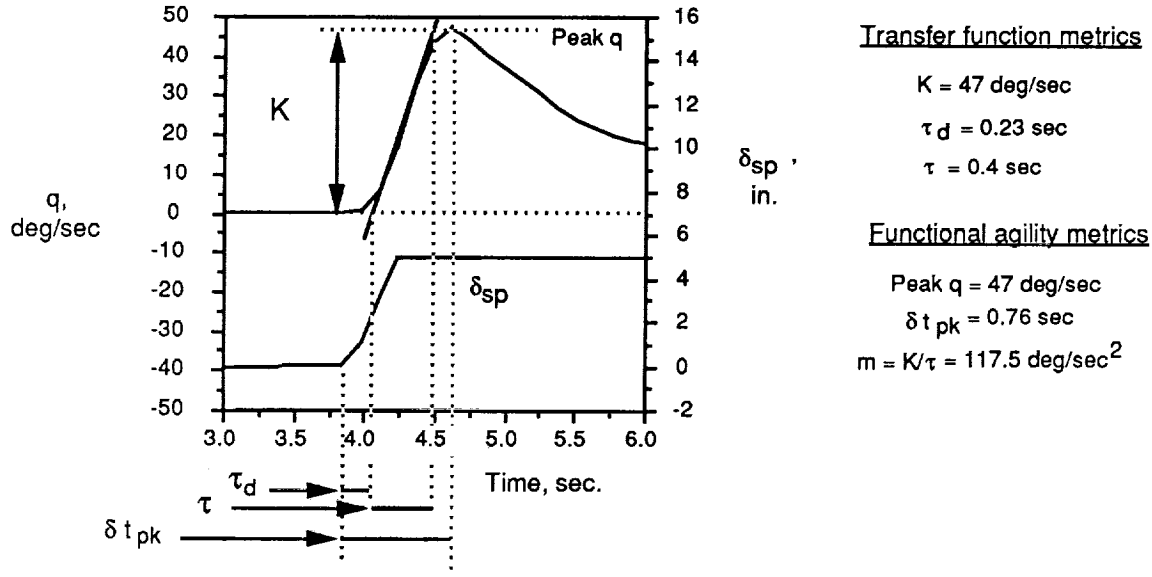

(b) Rate response to step input.

Figure 17. Typical pitch rate and acceleration responses to step input at Mach 0.6 and $h = 15\,000$ ft.

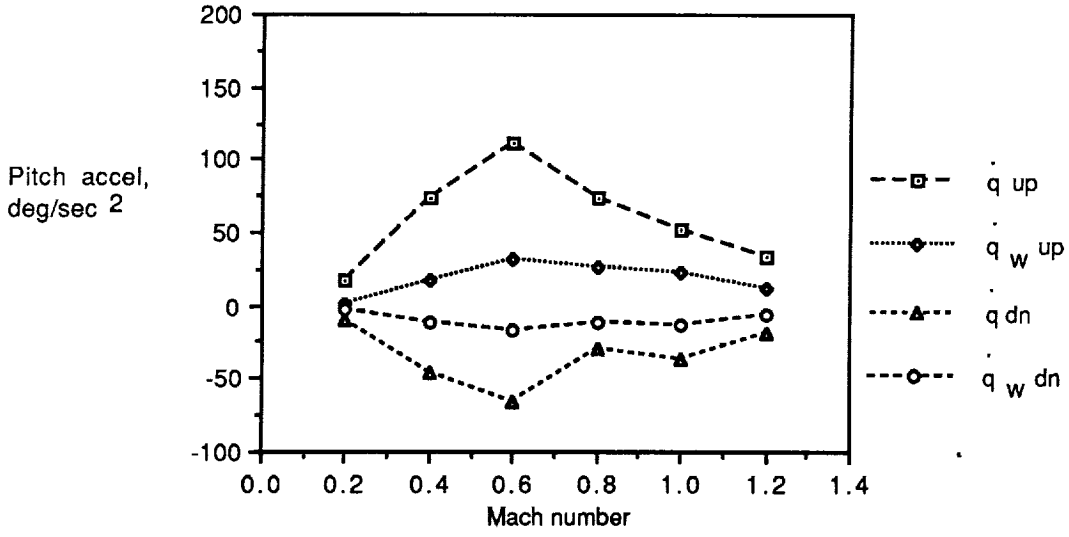

Figure 18. Peak pitch accel for wind- and body-axis systems.

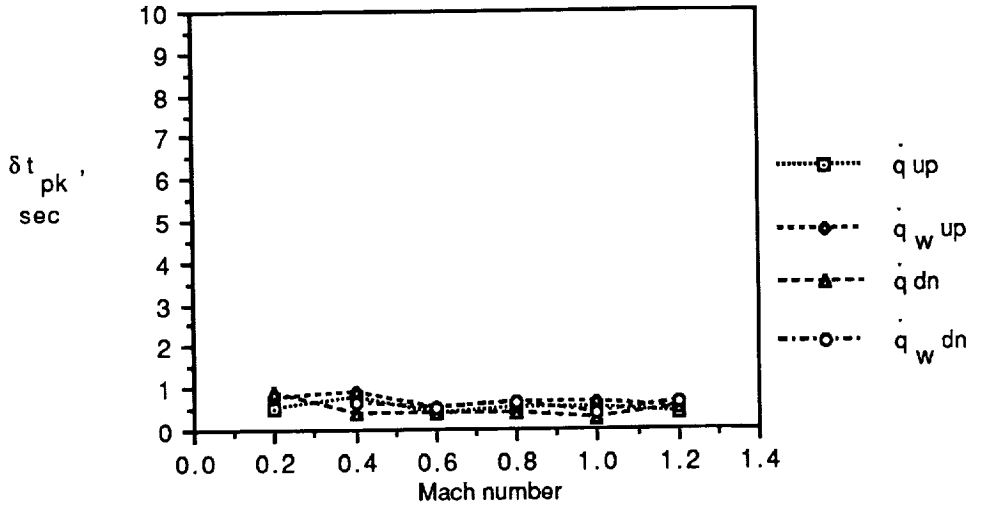

Figure 19. Time to peak pitch accelerations.

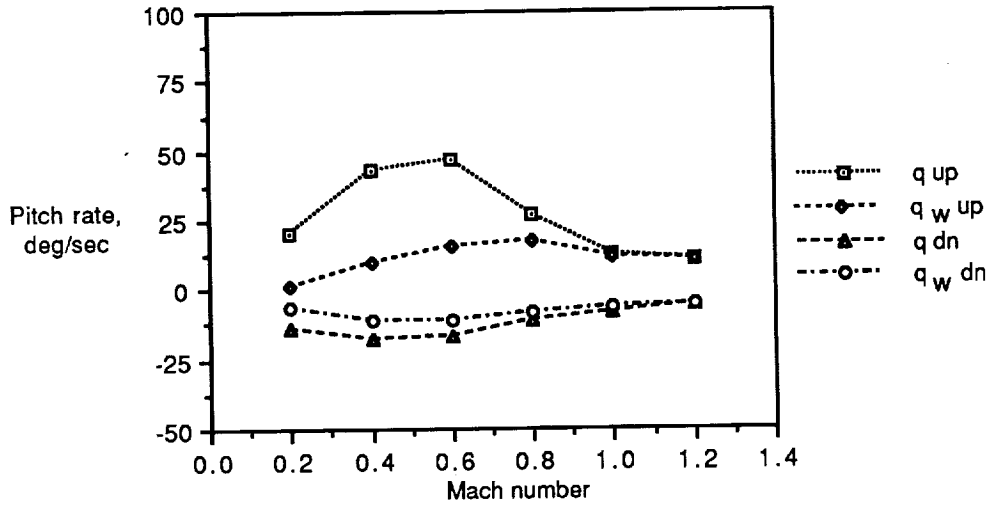

Figure 20. Peak pitch rates for wind- and body-axis systems.

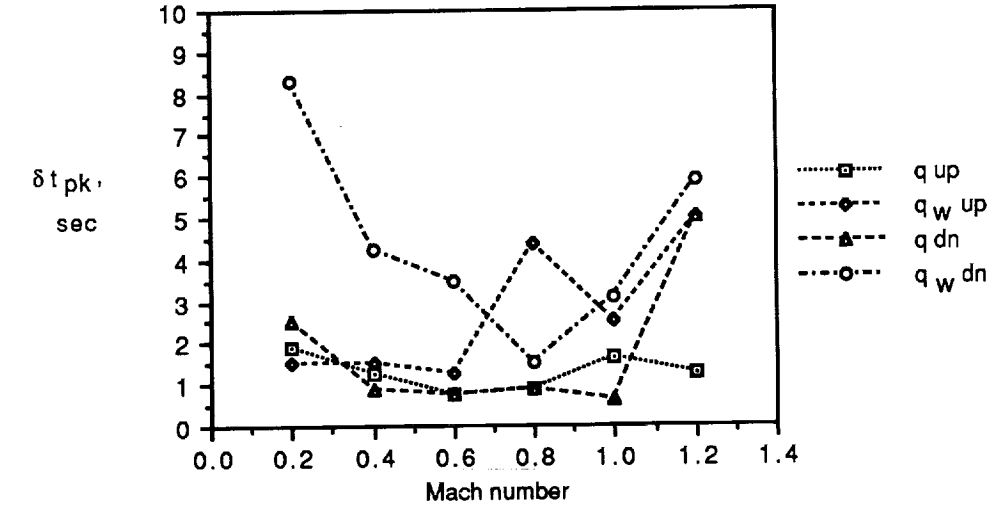

Figure 21. Time to peak pitch rates.

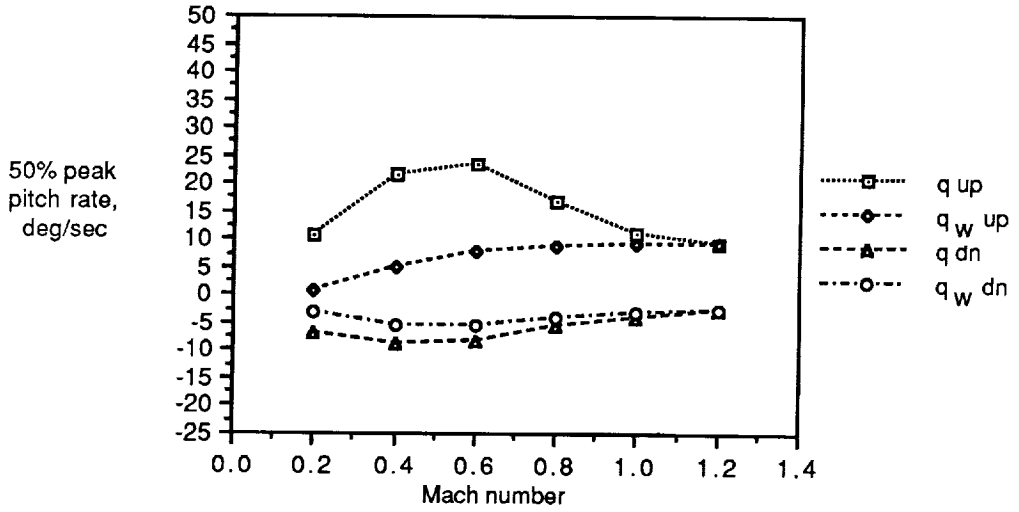

Figure 22. Fifty percent of peak pitch rates for wind- and body-axis systems.

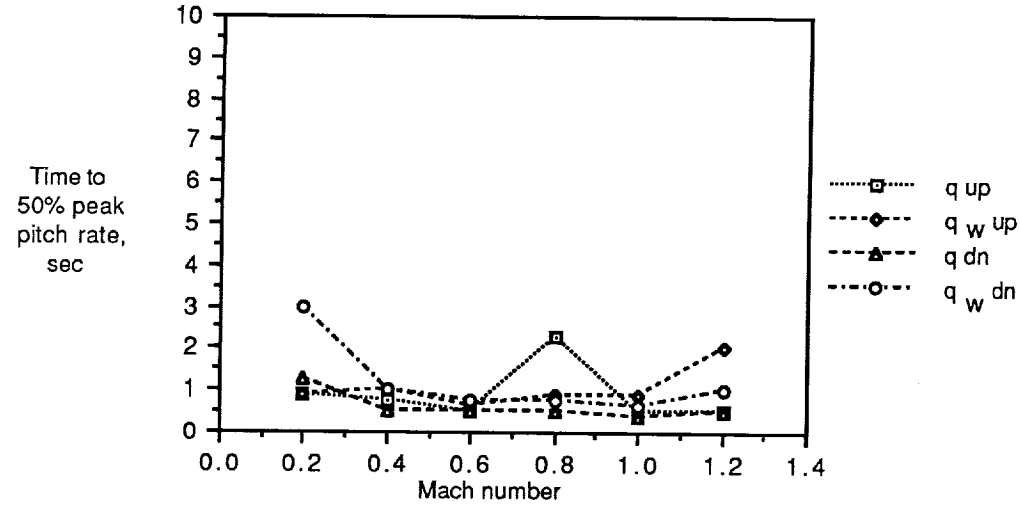

Figure 23. Time to 50 percent of peak pitch rate.

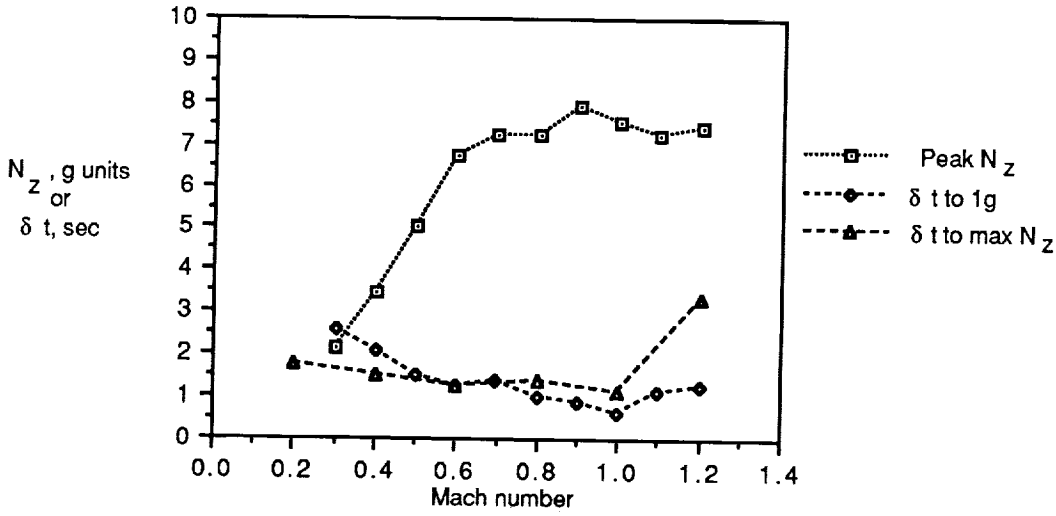

Figure 24. Maximum load factor and times to load and unload.

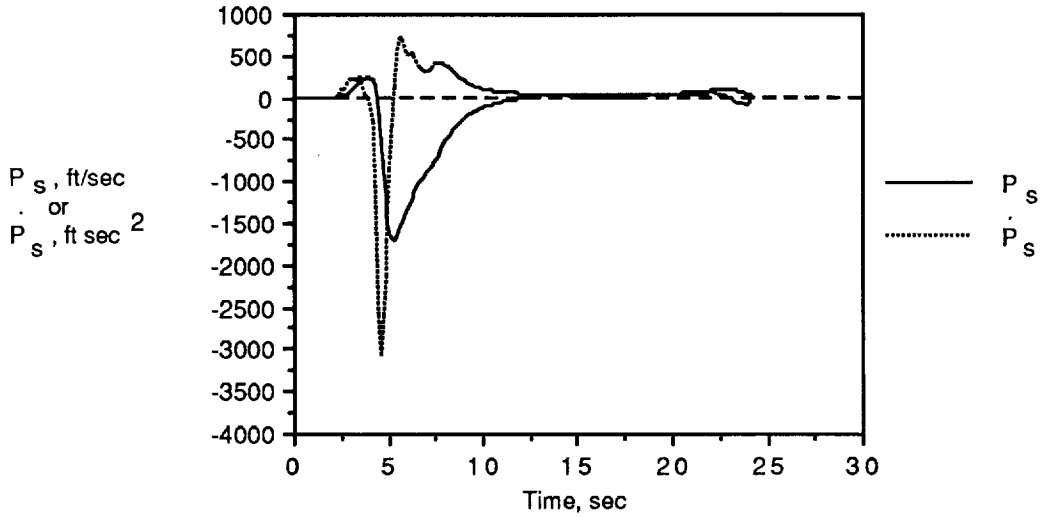

Figure 25. Specific excess power and power rate for pitching motion BKM.

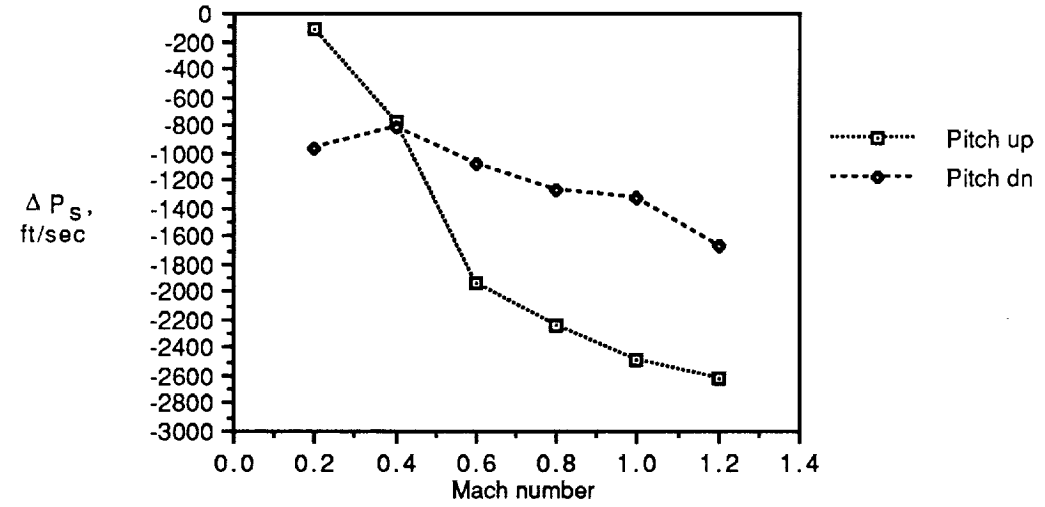

Figure 26. Peak change in P_s for pitching motion BKM.

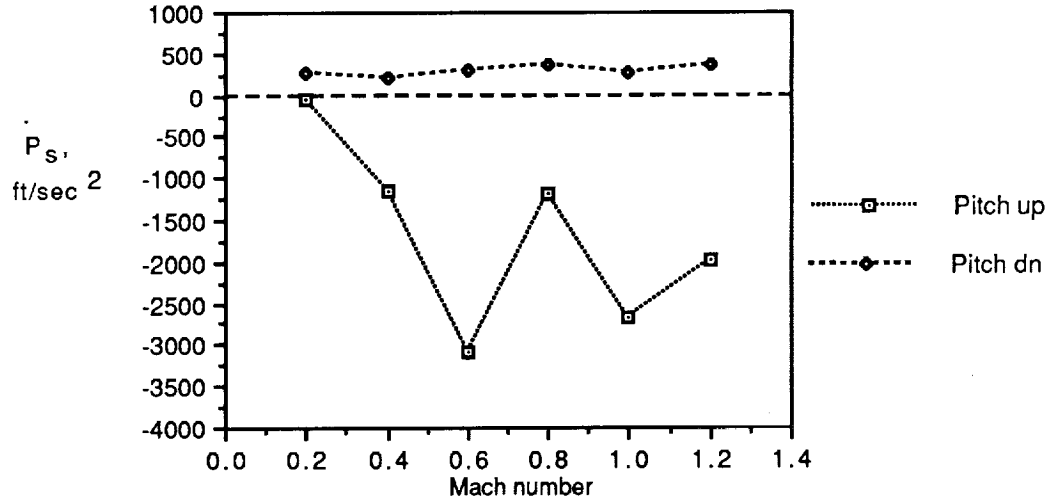

Figure 27. Peak $\dot{P}_s$ for pitching motion BKM.

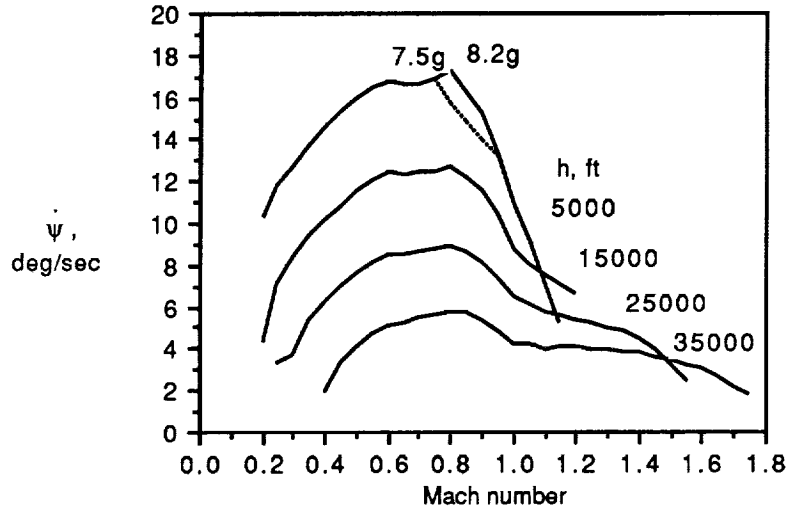

Figure 28. Maximum sustainable turn rates (FLXTRM data).

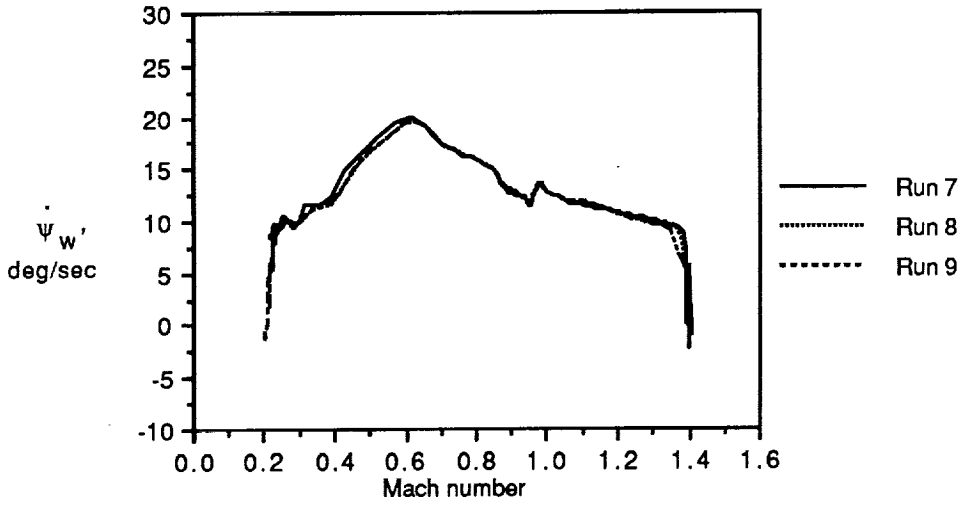

Figure 29. Maximum wind-axis instantaneous turn rate (DMS data).

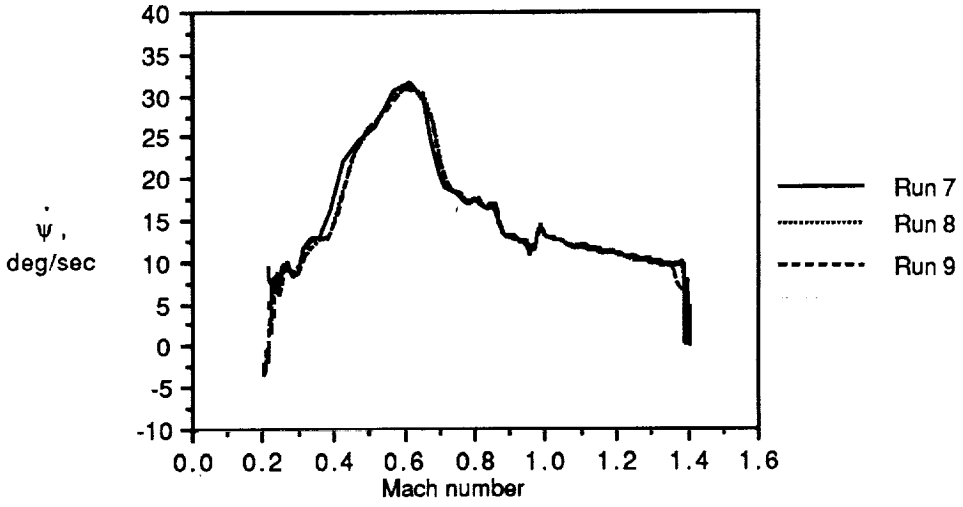

Figure 30. Maximum body-axis instantaneous turn rate (DMS data).

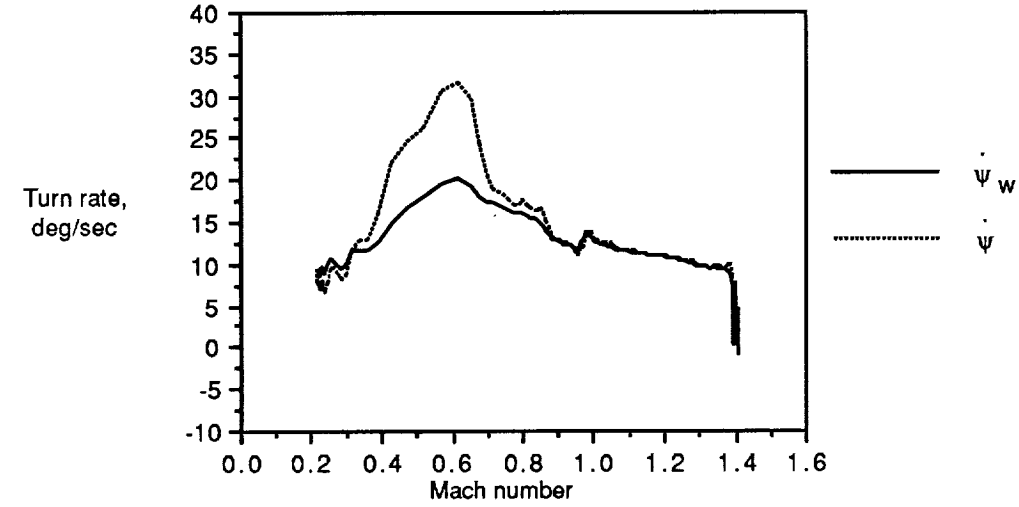

Figure 31. Wind- and body-axis instantaneous turn rates.

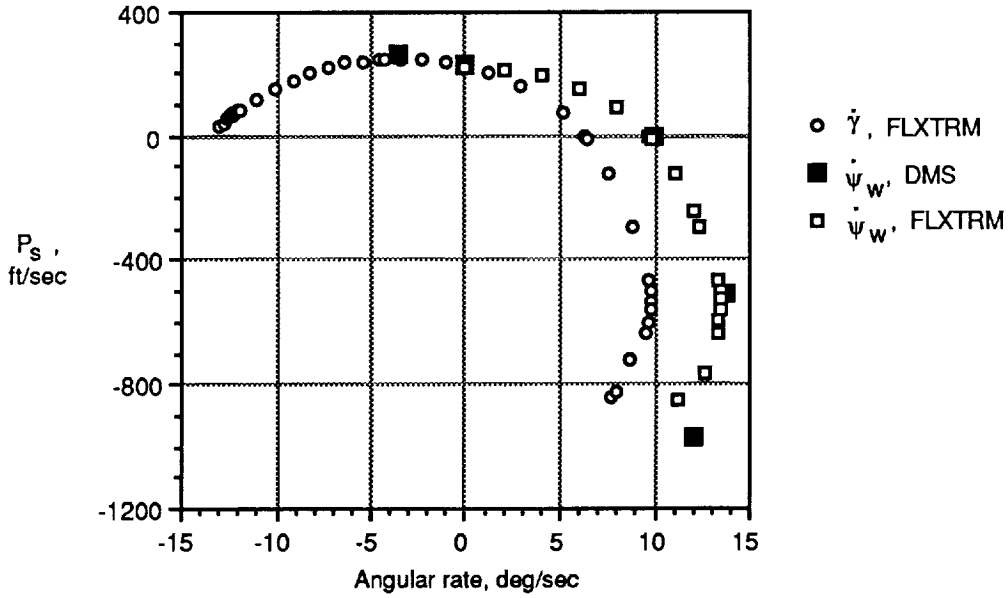

Figure 32. Specific excess power as function of wind-axis angular rates.

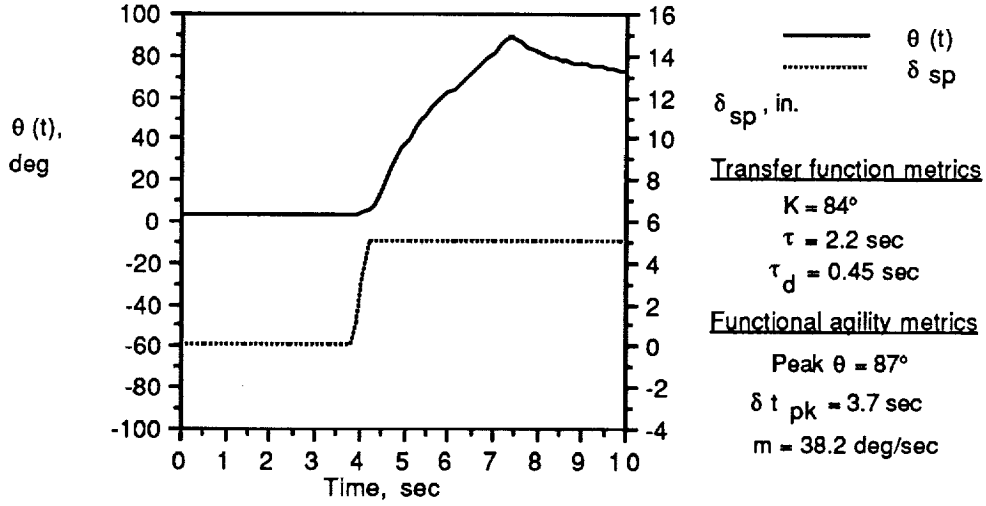

Figure 33. Response of $\theta(t)$ to pointing BKM at Mach 0.6 and $h = 15\,000$ ft.

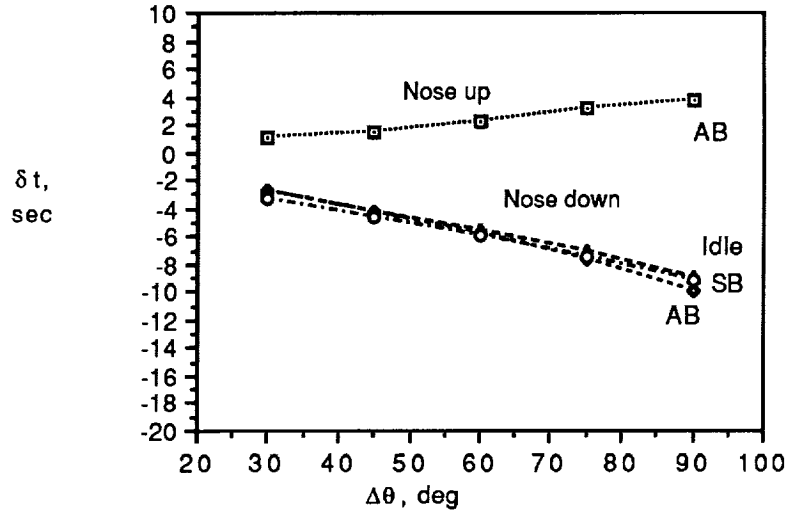

Figure 34. Time to achieve $\Delta\theta$ at Mach 0.6 and $h = 15\,000$ ft.

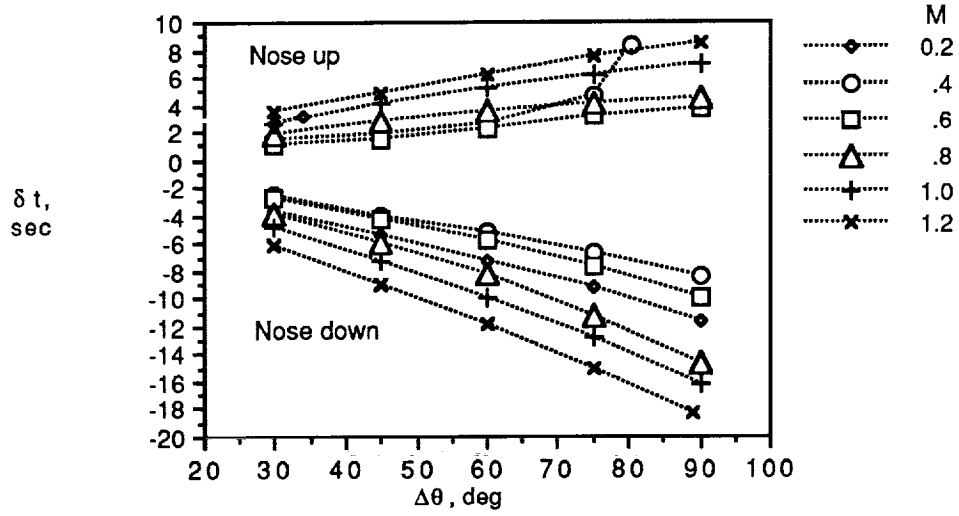

Figure 35. Time to achieve $\Delta\theta$ for indicated Mach numbers with maximum throttle.

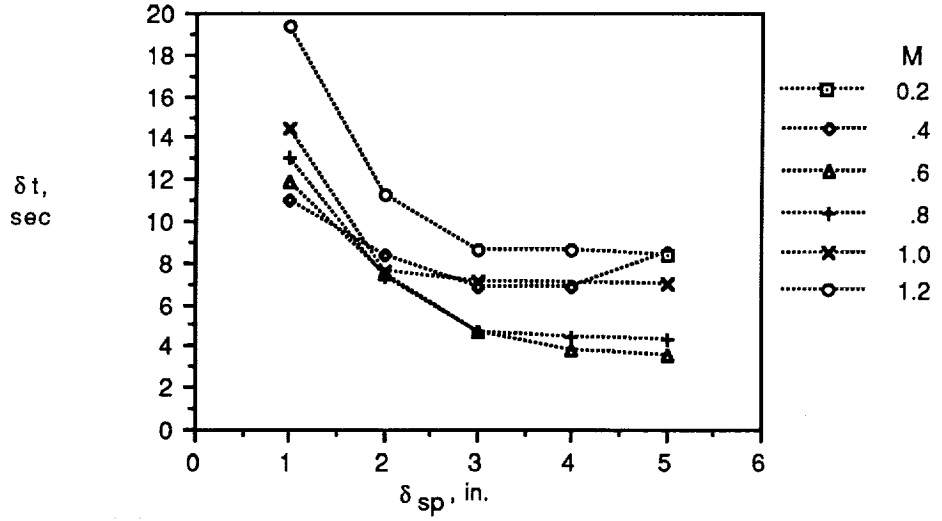

Figure 36. Time to pitch 90° with various stick deflections.

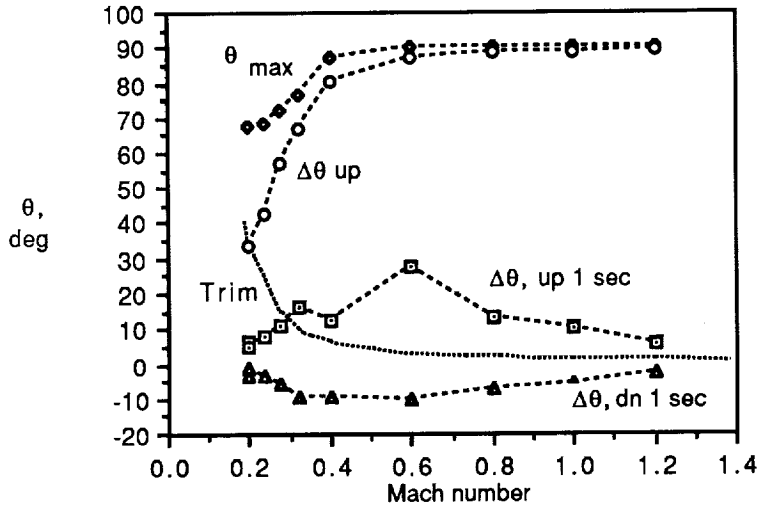

Figure 37. Pitch angle pointing envelope for body-axis system.

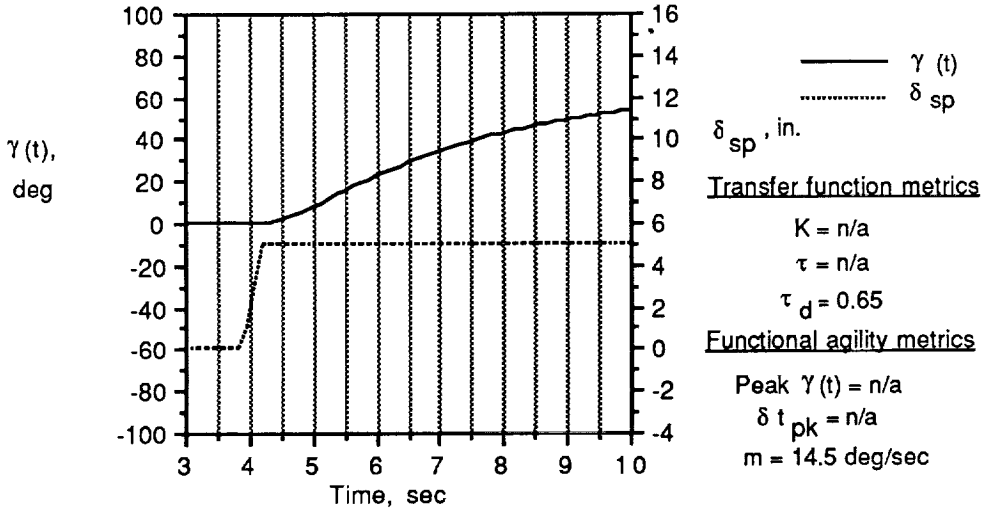

Figure 38. Response of $\gamma(t)$ to pitch-up BKM at Mach 0.6 and $h = 15\,000$ ft.

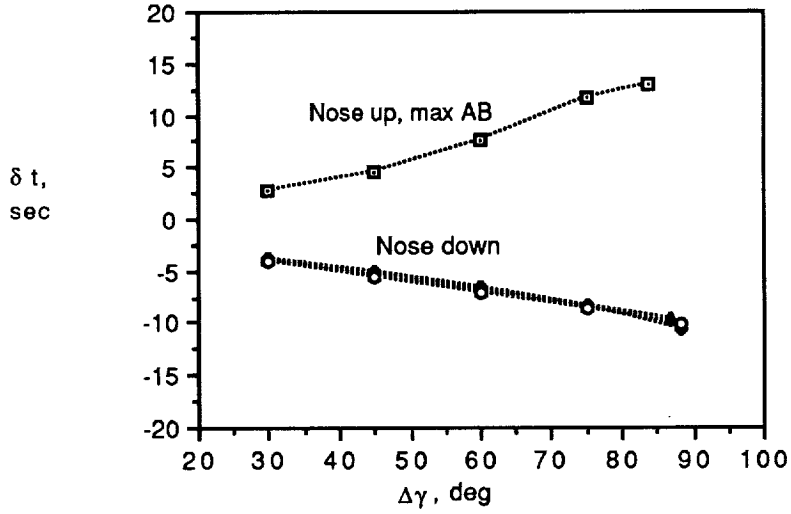

Figure 39. Time to achieve $\Delta\gamma$ at Mach 0.6 and $h = 15\,000$ ft.

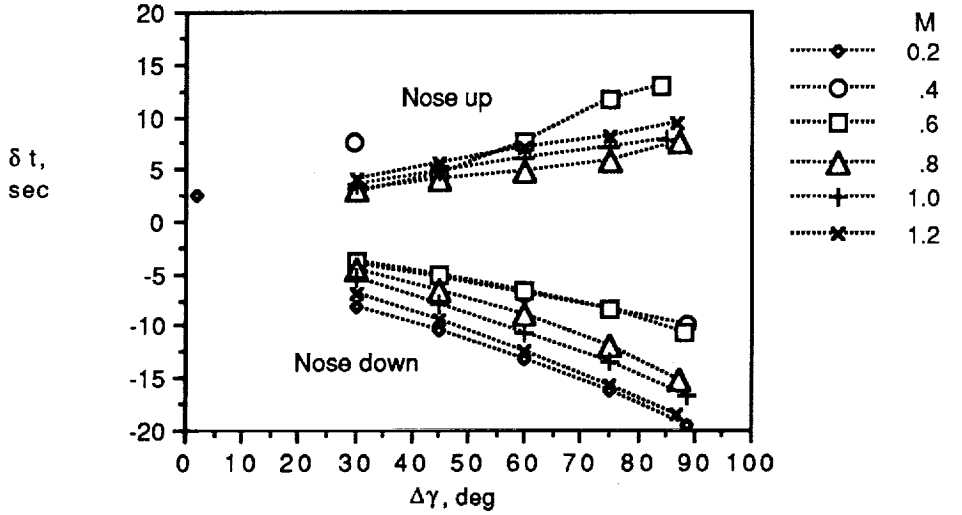

Figure 40. Time to achieve $\Delta\gamma$ for indicated Mach number at $h = 15\,000$ ft and full throttle.

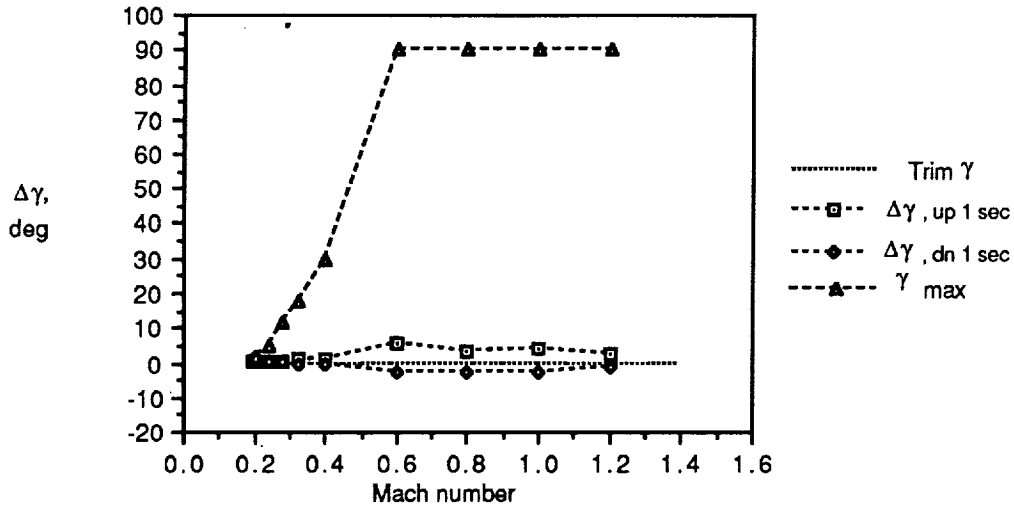

Figure 41. Pointing envelope for wind-axis system.

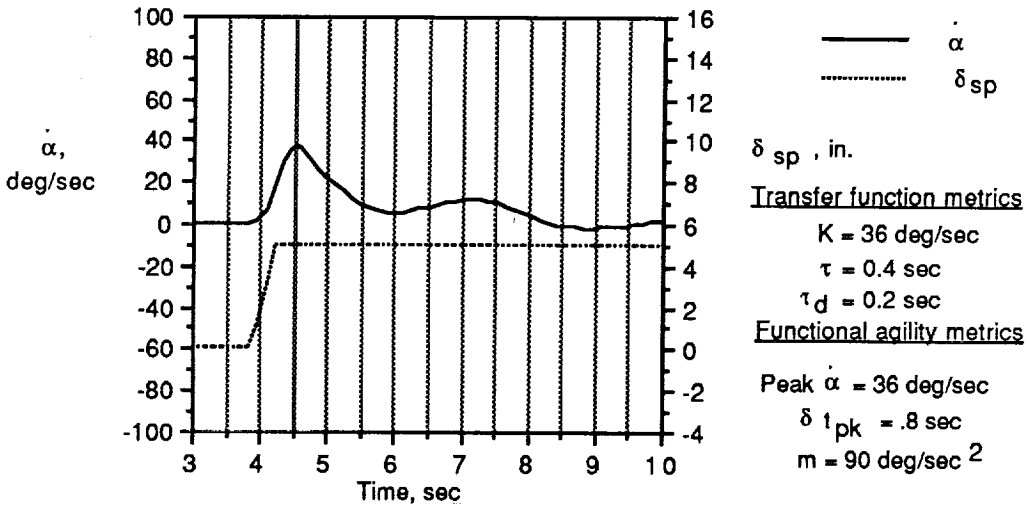

Figure 42. Response of $\dot{\alpha}(t)$ to pitch BKM at Mach 0.6 and $h = 15\,000$ ft.

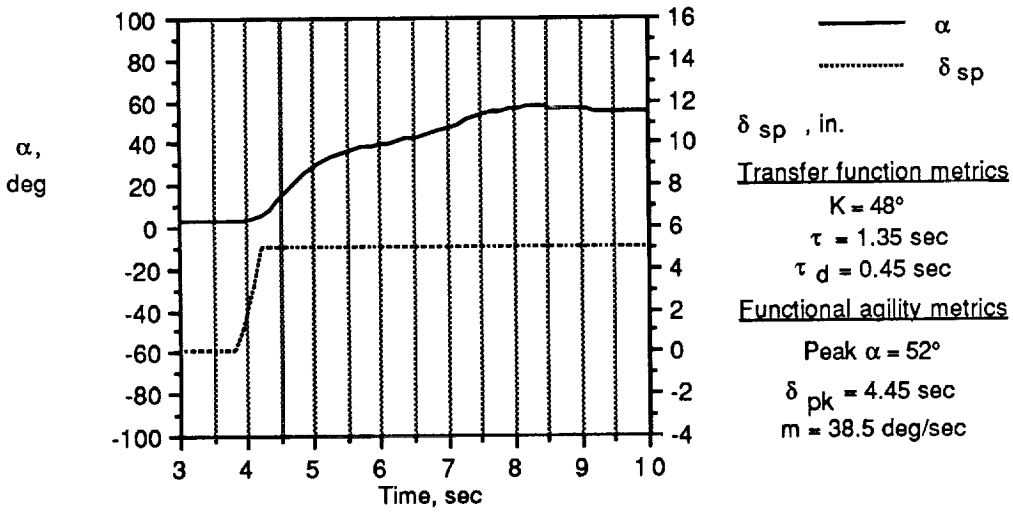

Figure 43. Response of $\alpha(t)$ to pitch BKM at Mach 0.6 and $h = 15\,000$ ft.

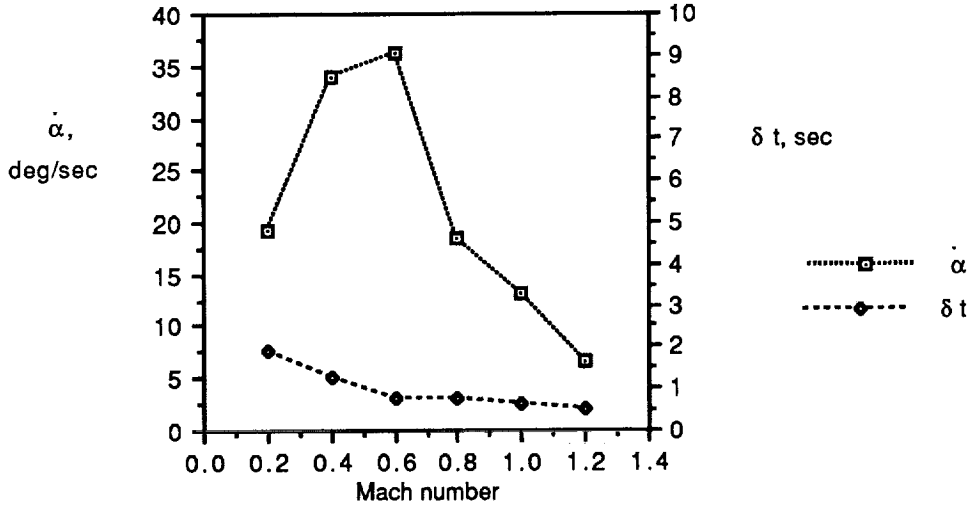

Figure 44. Peak and time to peak nose-up $\dot{\alpha}$.

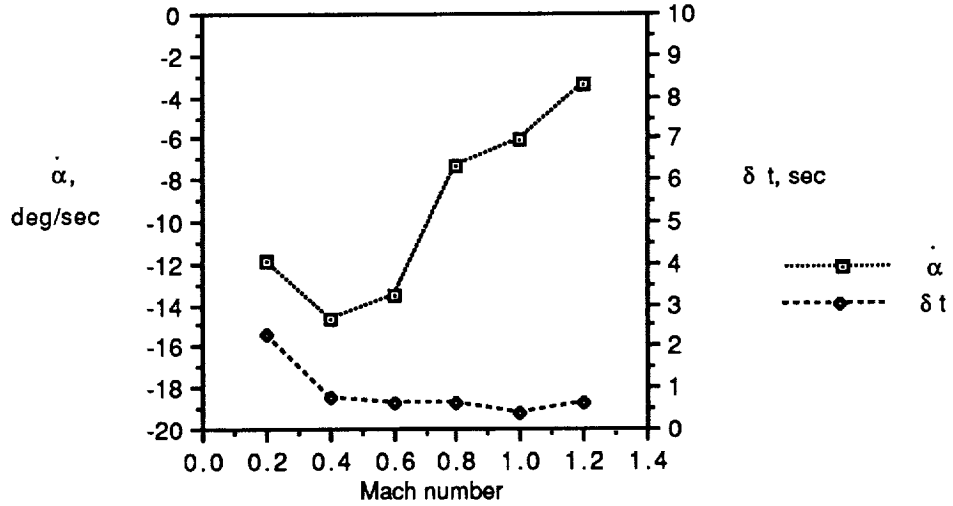

Figure 45. Peak and time to peak nose-down $\dot{\alpha}$.

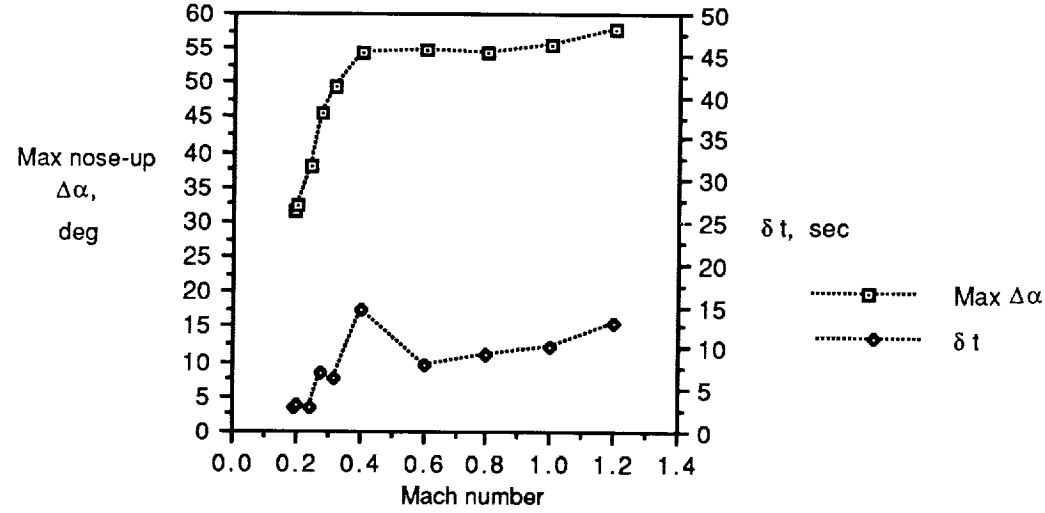

Figure 46. Maximum and time to maximum nose-up $\Delta\alpha$.

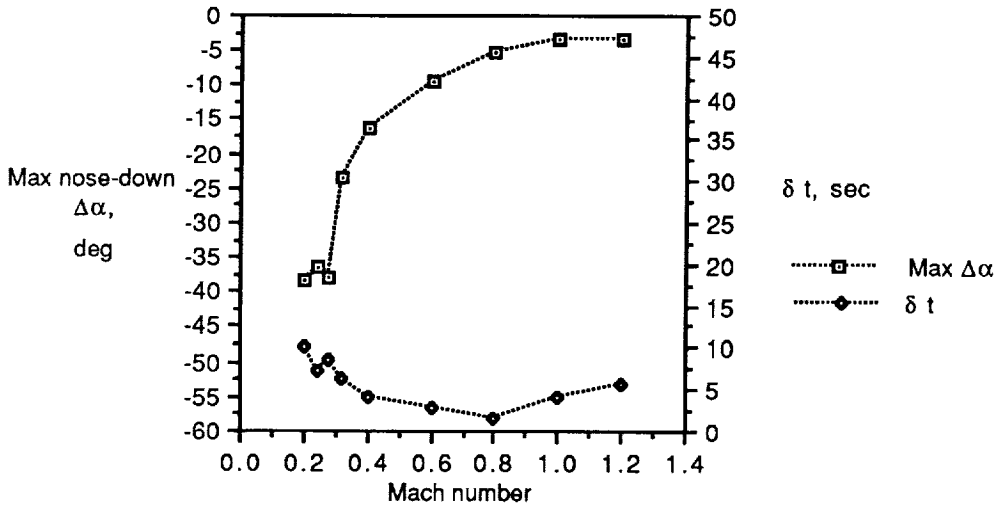

Figure 47. Maximum and time to maximum nose-down $\Delta\alpha$.

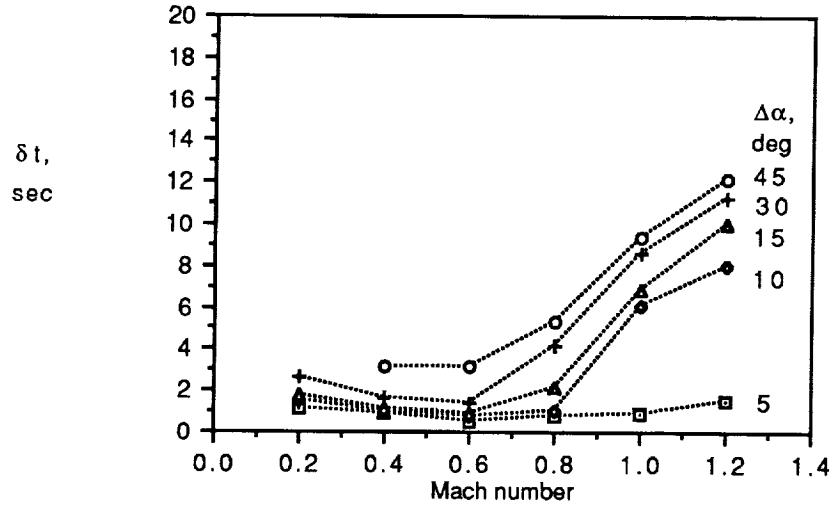

Figure 48. Time to achieve $\Delta\alpha$.

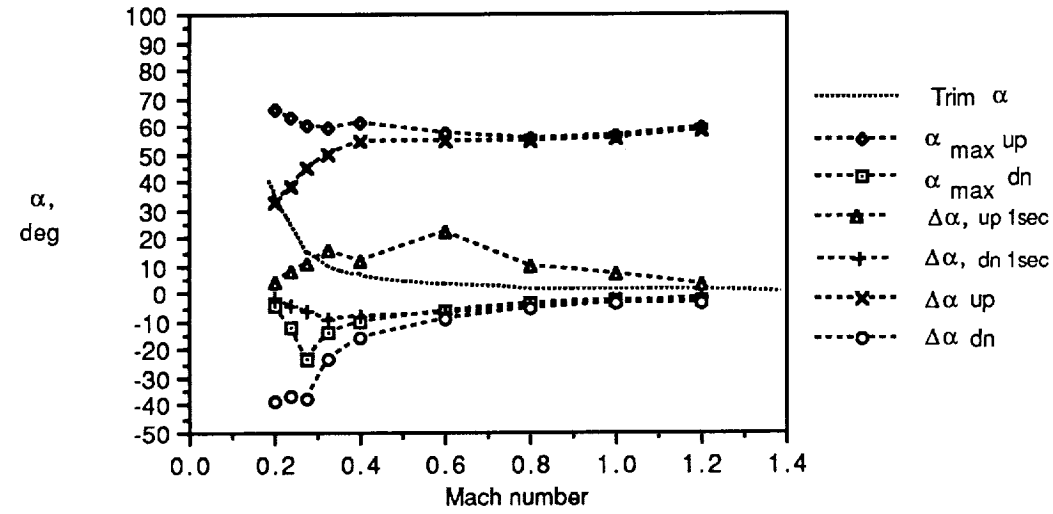

Figure 49. Angle-of-attack pointing envelope.

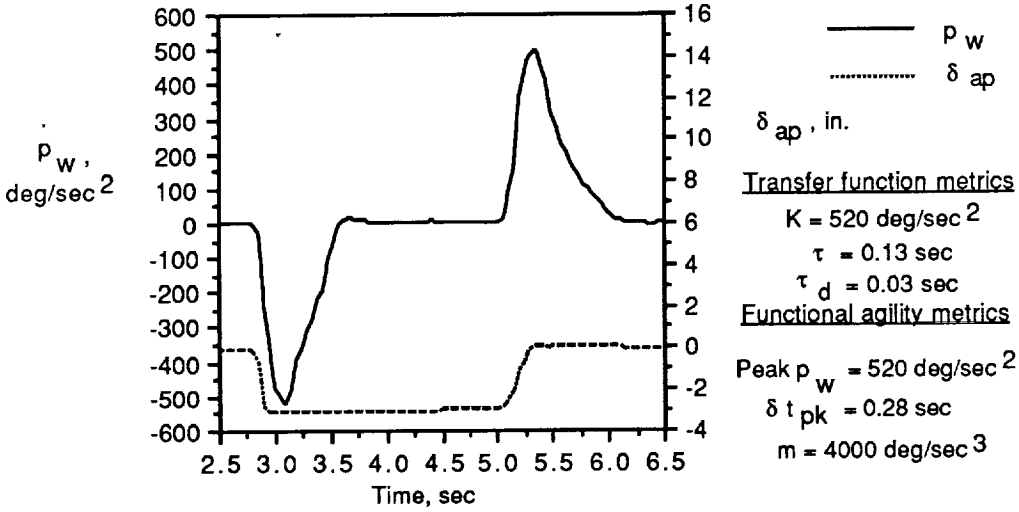

Figure 50. Wind-axis roll acceleration at Mach 0.8, $1g$, and $h = 15\,000$ ft.

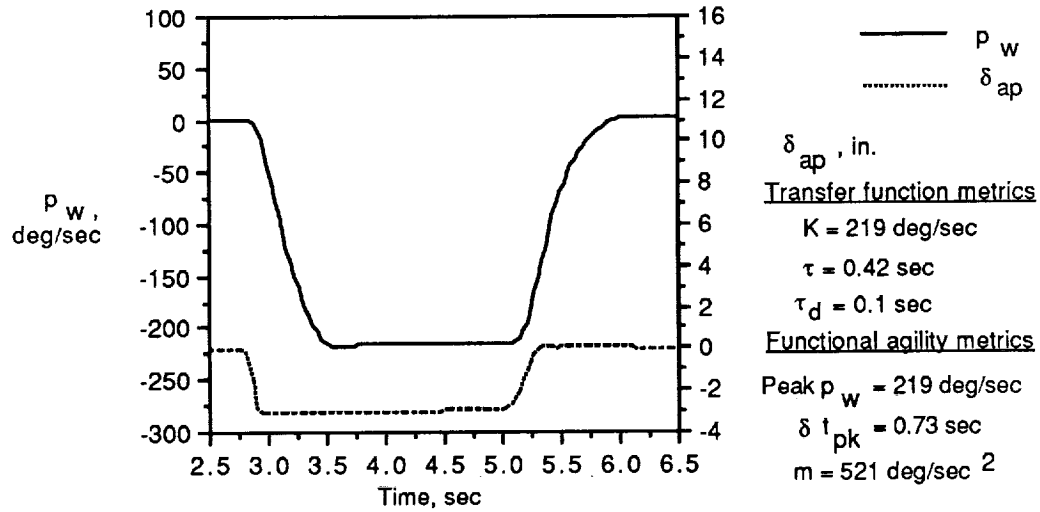

Figure 51. Wind-axis roll rate response at Mach 0.8, $1g$, and $h = 15\,000$ ft.

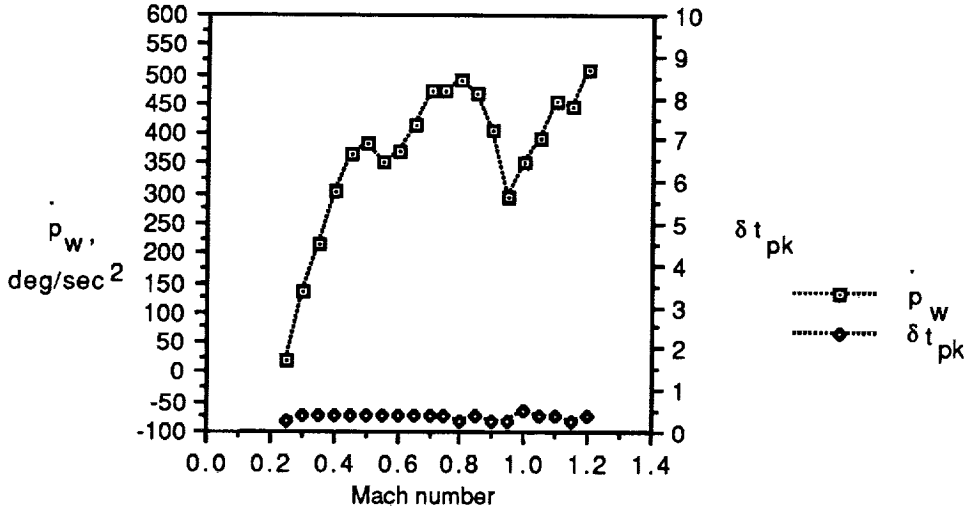

Figure 52. Peak roll acceleration and time to peak for $1g$ roll at $h = 15\,000$ ft.

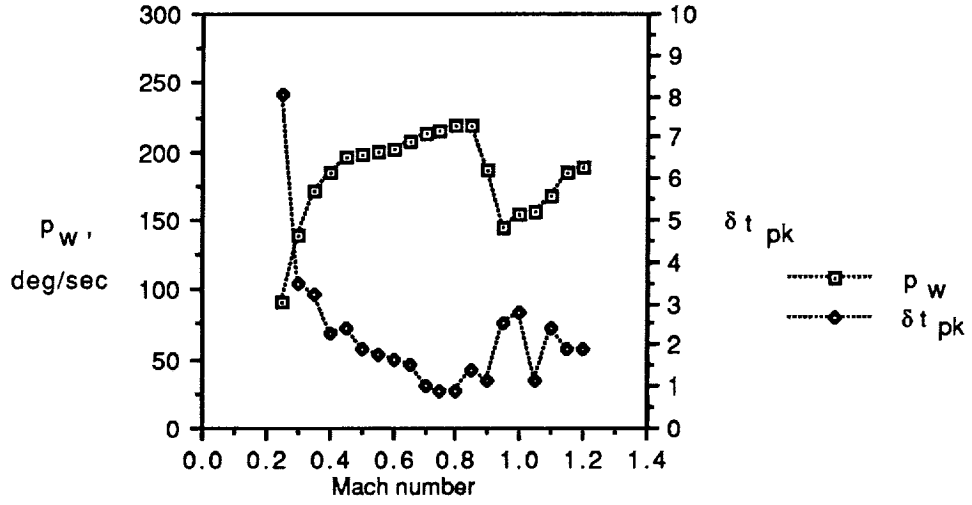

Figure 53. Peak wind-axis roll rate and time to peak for $1g$ roll at $h = 15\,000$ ft.

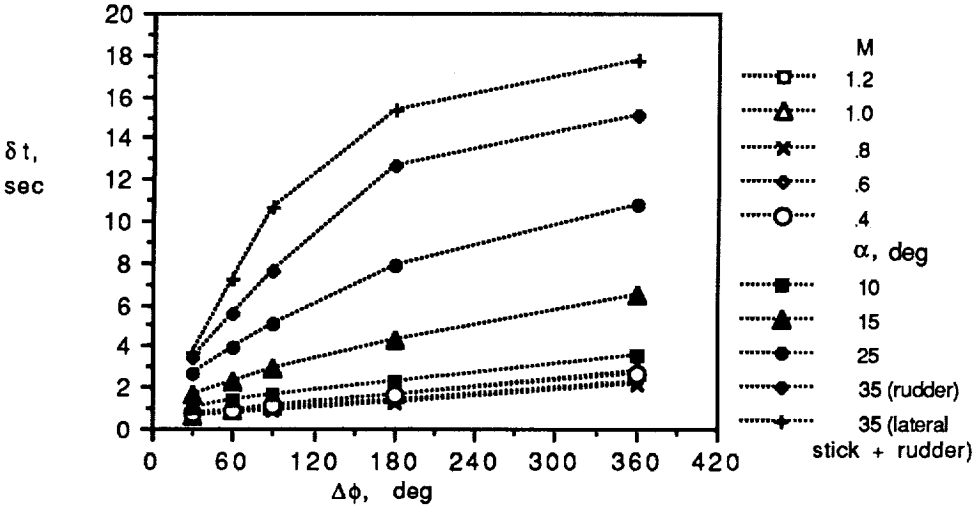

Figure 54. Time to roll through $\Delta\phi$ (wind axis) at $1g$ and $h = 15\,000$ ft.

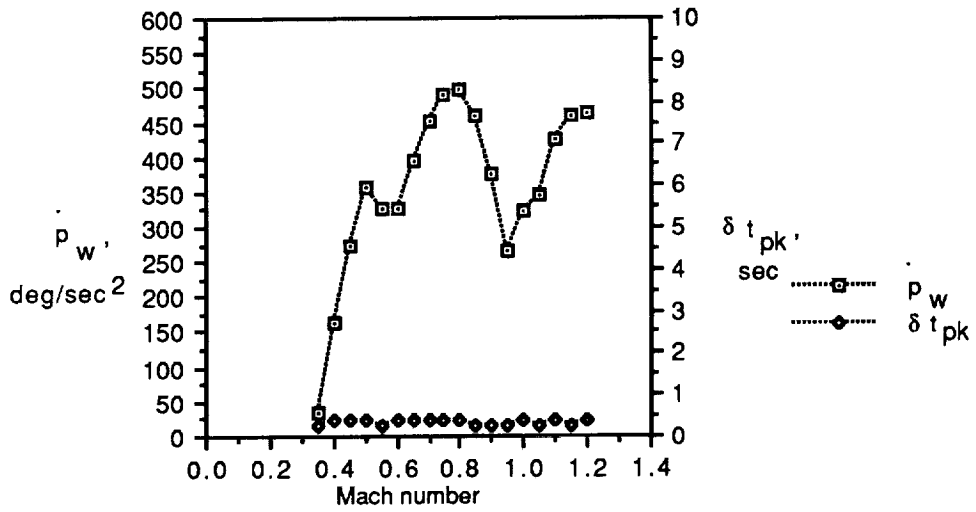

(a) Peak roll accel and time to peak.

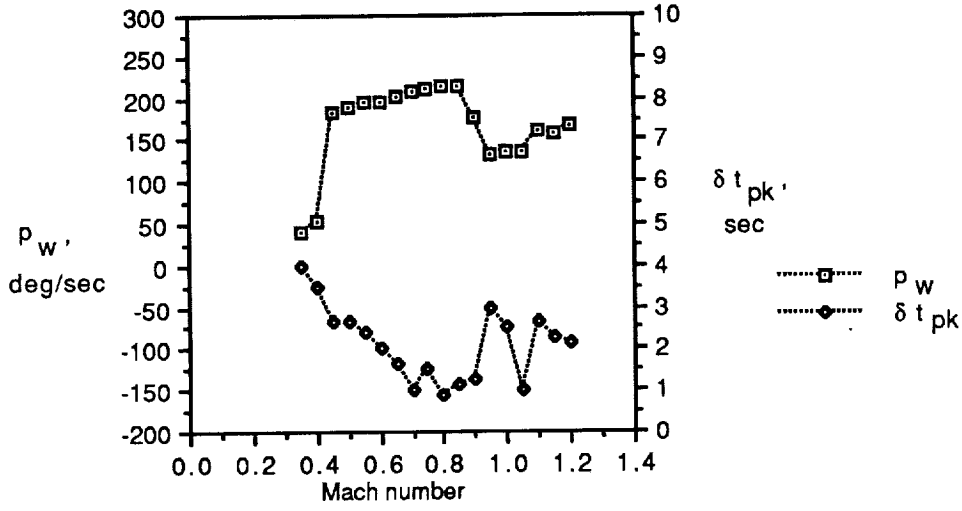

(b) Peak roll rate and time to peak.

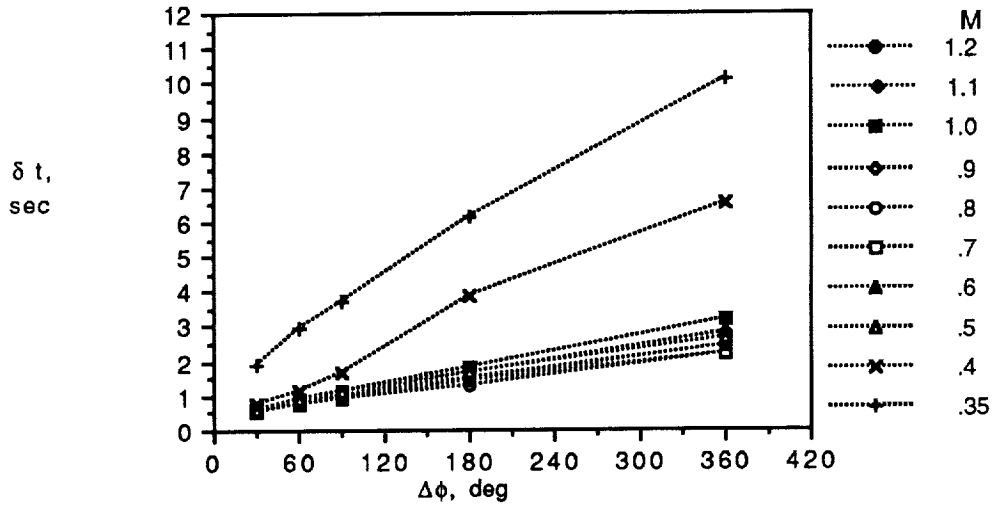

(c) Time to roll through $\Delta\phi$.

Figure 55. Wind-axis roll capability for flight load of $2g$ and $h = 15\,000$ ft.

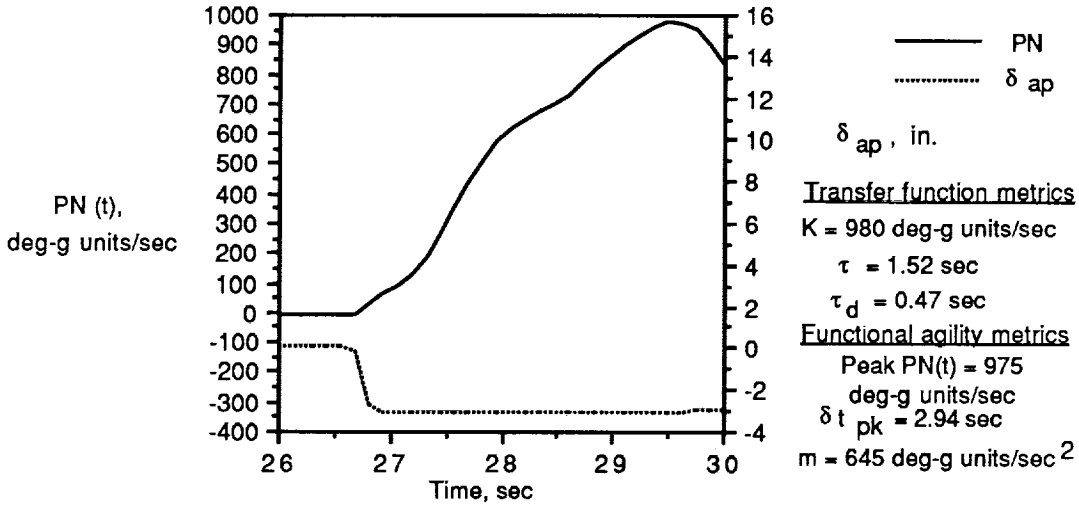

Figure 56. Loaded roll metric for maximum loaded roll ($7.5g$) at Mach 0.8 and $h = 15\,000$ ft.

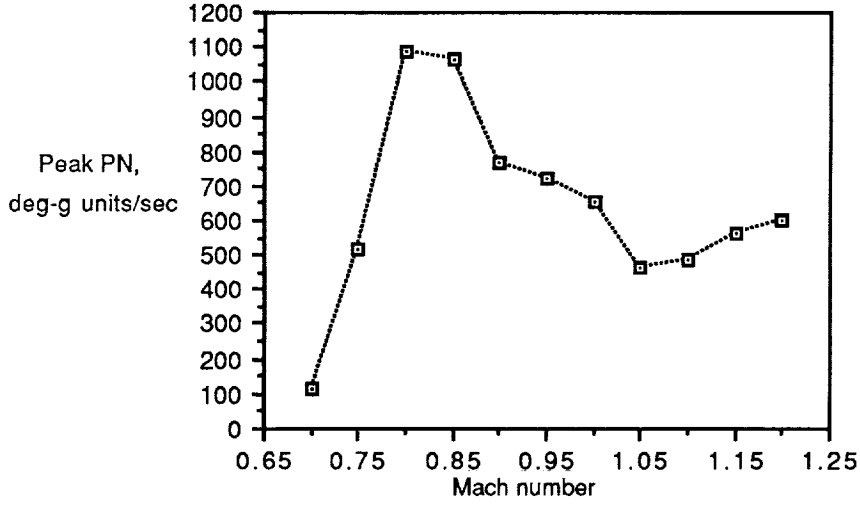

(a) Maximum loaded roll ($7.5g$).

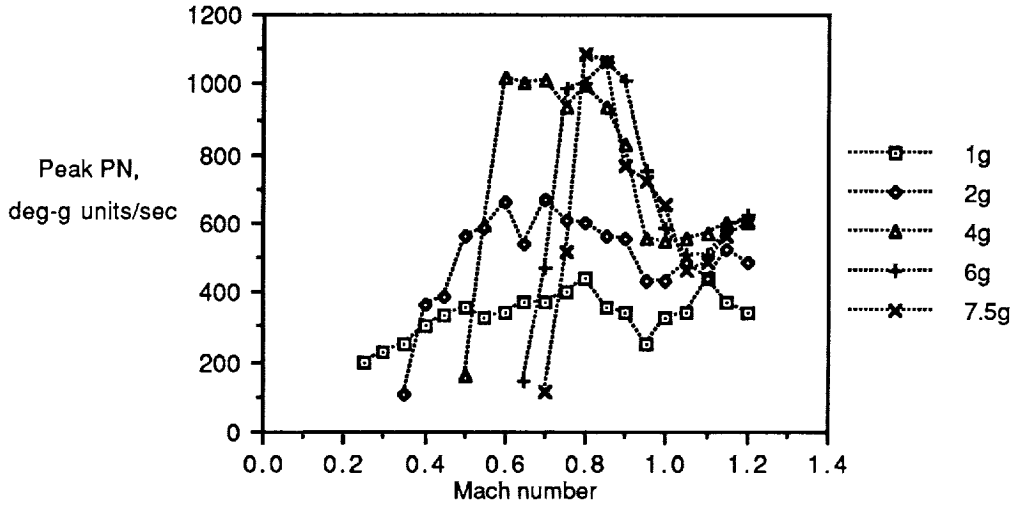

(b) Range of loaded rolls.

Figure 57. Peak PN at $h = 15\,000$ ft.

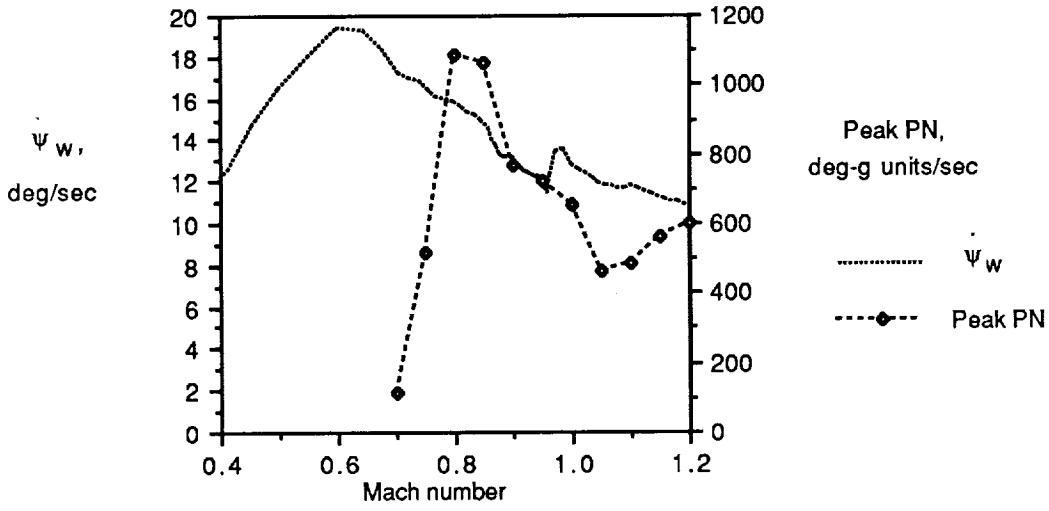

Figure 58. Maximum wind-axis turn rate and peak PN at $h = 15\,000$ ft.

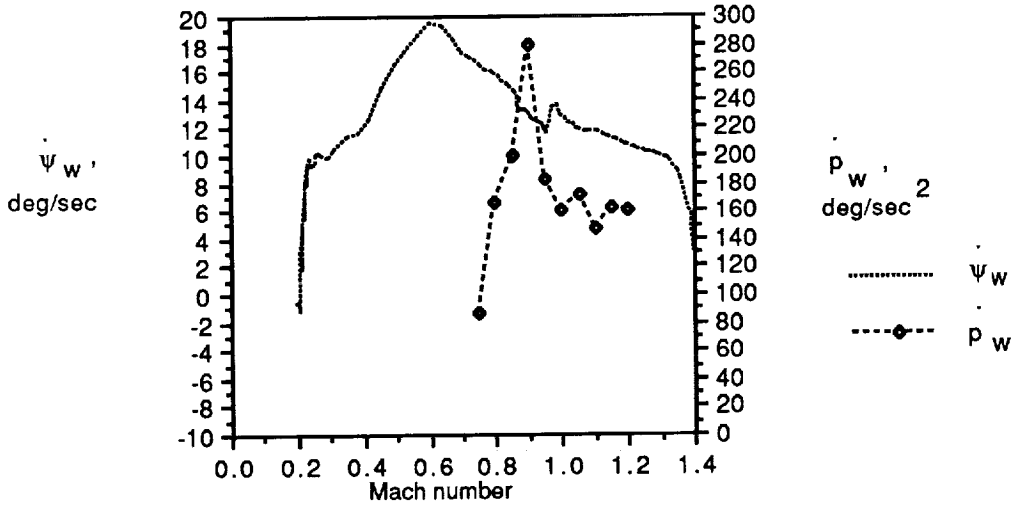

Figure 59. Maximum wind-axis turn rate and peak $\dot{p}_w$ at $h = 15\,000$ ft.

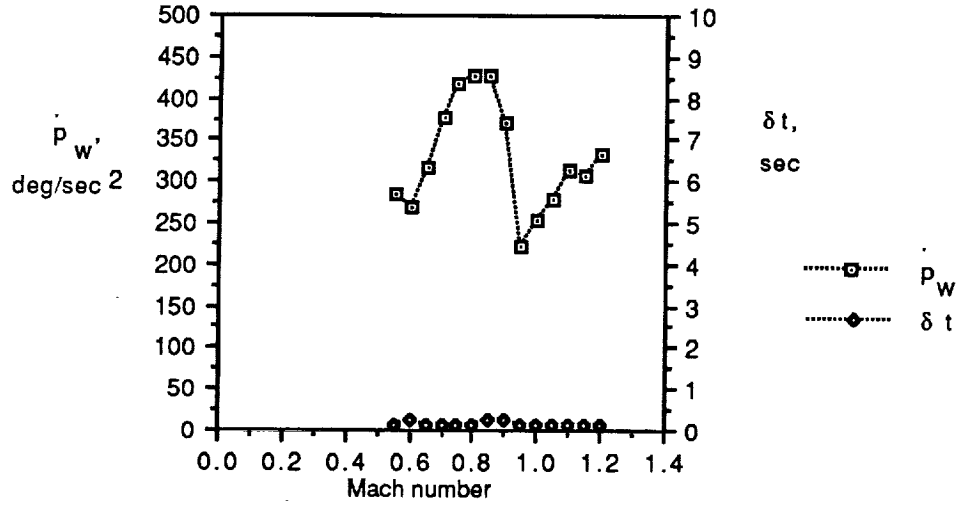

(a) Peak $\dot{p}_w$ and time to achieve $\dot{p}_w$.

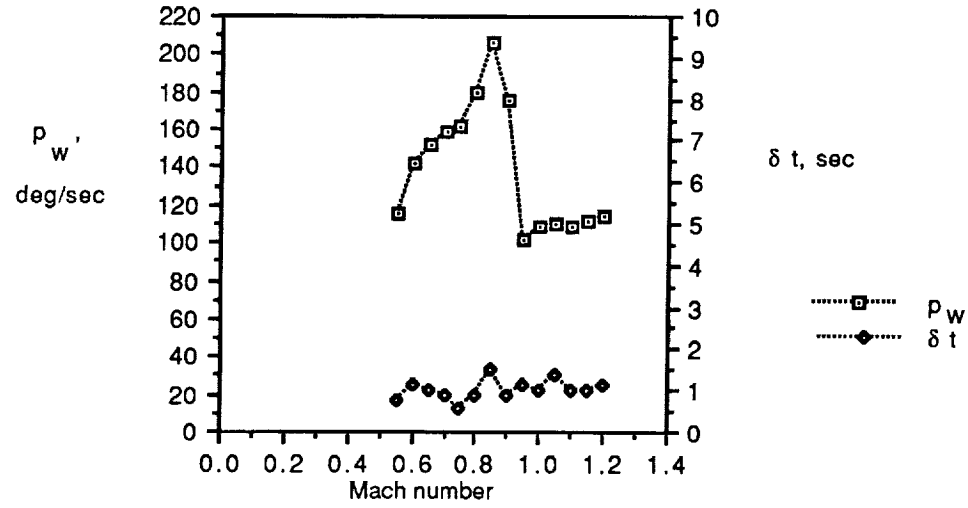

(b) Peak p_w and time to achieve p_w.

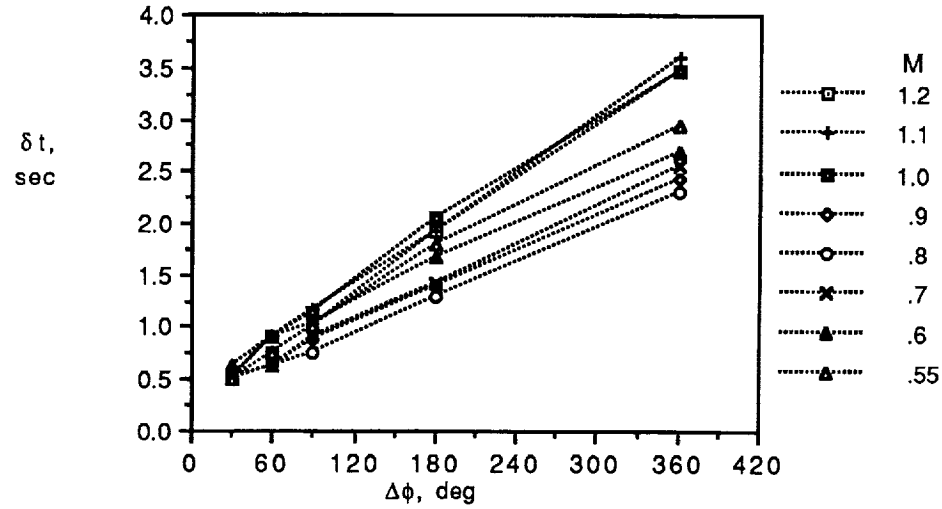

(c) Time to roll through $\Delta\phi$.

Figure 60. Capability to perform hold-α loaded roll at $4g$ and $h = 15\,000$ ft.

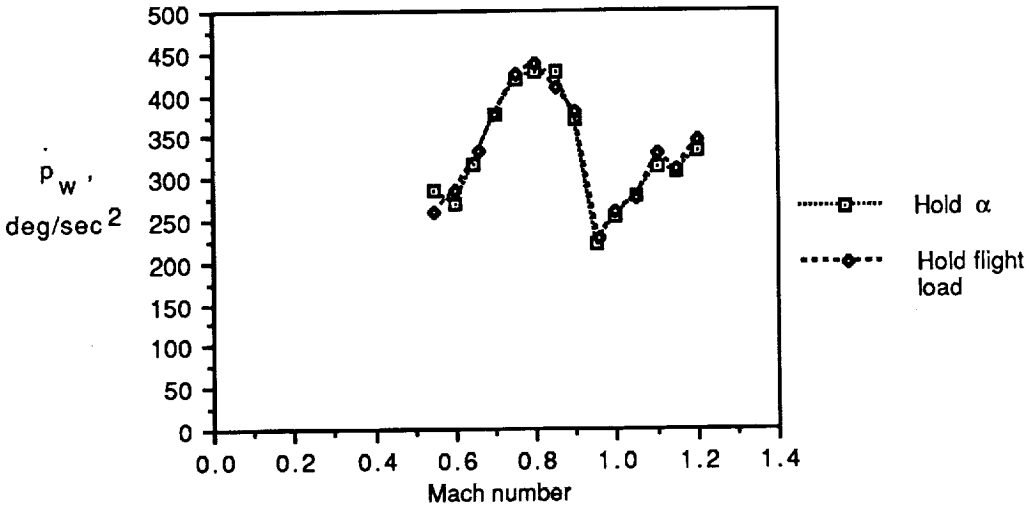

Figure 61. Peak $\dot{p}_w$ for hold-α and hold-flight-load BKM at $4g$ and $h = 15\,000$ ft.

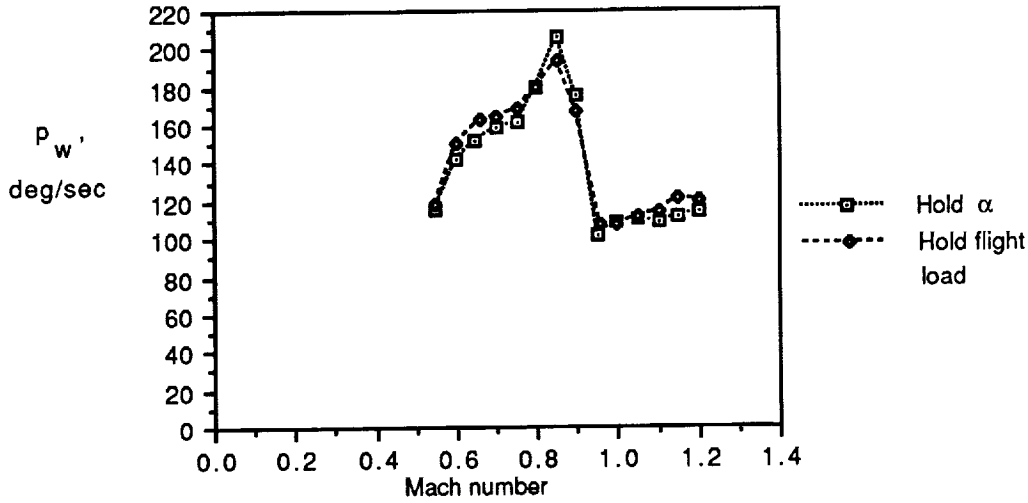

Figure 62. Peak p_w for hold-α and hold-flight-load BKM at $4g$ and $h = 15\,000$ ft.

NASA
National Aeronautics and Space Administration

Report Documentation Page

1. Report No.	2. Government Accession No.	3. Recipient's Catalog No.
NASA TM-4238		

4. Title and Subtitle	5. Report Date
Candidate Control Design Metrics for an Agile Fighter	March 1991
	6. Performing Organization Code
7. Author(s)	8. Performing Organization Report No.
Patrick C. Murphy, Melvin L. Bailey, and Aaron J. Ostroff	L-16766
9. Performing Organization Name and Address	10. Work Unit No.
NASA Langley Research Center Hampton, VA 23665-5225	505-66-71-03
	11. Contract or Grant No.
12. Sponsoring Agency Name and Address	13. Type of Report and Period Covered
National Aeronautics and Space Administration Washington, DC 20546-0001	Technical Memorandum
	14. Sponsoring Agency Code

15. Supplementary Notes

Patrick C. Murphy and Aaron J. Ostroff: Langley Research Center, Hampton, Virginia.
Melvin L. Bailey: Lockheed Engineering & Sciences Company, Hampton, Virginia.

16. Abstract

Success in future fighter combat will require increased capabilities from aircraft technology. These capabilities, in the form of superagility and supermaneuverability, require special design techniques that translate advanced air combat maneuvering requirements into design criteria. Control design metrics can provide some of these techniques for control designers. This study presents an overview of control design metrics and investigates metrics for advanced fighter agility. The objectives of various metric users, such as airframe designers and pilots, are differentiated from the objectives of the control designer. Metric values are documented over a portion of the flight envelope through piloted simulation. These values provide a baseline against which future control system improvements can be compared and against which a control design methodology can be developed. Agility is measured for axial, pitch, and roll axes. Axial metrics highlight acceleration and deceleration capabilities under different flight loads and include specific excess power measurements to characterize energy maneuverability. Pitch metrics cover both body-axis and wind-axis pitch rates and accelerations. Included are nose pointing metrics that highlight displacement capabilities between the nose and the velocity vectors. Roll metrics (or torsional metrics) focus on rotational capability about the wind axis.

17. Key Words (Suggested by Authors(s))	18. Distribution Statement
Flight controls Control design metrics Agility Fighter aircraft	Unclassified—Unlimited Subject Category 08

19. Security Classif. (of this report)	20. Security Classif. (of this page)	21. No. of Pages	22. Price
Unclassified	Unclassified	62	A04

NASA FORM 1626 OCT 86
NASA-Langley, 1991
For sale by the National Technical Information Service, Springfield, Virginia 22161-2171